Supporting Information

for

Catalytic Hydroboration of α,β-Unsaturated Ketones Using β-Diketiminate Magnesium Hydride and Mechanistic Insights

Anubhab Das, Sayantan Mukhopadhyay, Sagrika Rajput, Sharanappa Nembenna*

School of Chemical Sciences, National Institute of Science Education and Research (NISER), HBNI, Bhubaneswar, 752 050, India. Email: snembenna@niser.ac.in

Contents

1. Stoichiometric Experiments and Mechanistic Studies

(i) Stoichiometric reaction of Mg-1 and 1a

Synthesis of *[LMg–OCH(CH$_3$)C≡C–Ph]$_2$* (Mg-2): [NMR Scale] 7.5μL (0.051 mmol, 1.0 equiv.) of 4-phenyl-3-butyn-2-one (**1a**) was added to a solution of **Mg-1** (20 mg, 0.026 mmol, 0.5 equiv.) in C_6D_6 (~ 0.3 mL) in a J. Young valve NMR tube, affording the intermediate **Mg-2** within 10 minutes at room temperature. Single crystals suitable for X-ray diffraction were grown inside the glovebox via slow evaporation of C_6D_6. NMR conversion > 99%. **^{1}H NMR** (400 MHz, C_6D_6, 298 K) δ = 7.41 (d, *J* = 1.9 Hz, 4H, Ar-*H*), 7.26 (dd, *J* = 8.0, 4.2 Hz, 12H, Ar-*H*), 6.93 (brs, 6H, Ar-*H*), 4.53 (q, *J* = 6.6 Hz, 2H, OC*H*), 4.31 (s, 2H, γ-C*H*), 2.87 – 2.76 (m, 8H, C*H*$_2$CH$_3$), 2.44 – 2.38 (m, 2H, C*H*$_2$CH$_3$), 2.30 (dd, *J* = 15.1, 7.6 Hz, 2H, C*H*$_2$CH$_3$), 2.17 (dd, *J* = 15.4, 7.7 Hz, 2H, C*H*$_2$CH$_3$), 2.07 (dd, *J* = 15.1, 7.5 Hz, 2H, C*H*$_2$CH$_3$), 1.42 (s, 6H, CC*H*$_3$), 1.40 (s, 6H, CC*H*$_3$), 1.36 (d, *J* = 6.4 Hz, 6H, OCHC*H*$_3$), 1.25 (t, *J* = 3.8 Hz, 6H, CH$_2$C*H*$_3$), 1.20 (t, *J* = 7.5 Hz, 18H, CH$_2$C*H*$_3$). **^{13}C{^{1}H} NMR** (101 MHz, C_6D_6, 298 K) δ = 168.5, 168.1, 148.3, 148.1, 148.0, 137.9, 137.5, 132.4, 128.0, 126.5, 126.1, 126.0, 125.3, 124.6, 124.4, 124.3, 97.7, 94.7, 83.0, 58.8, 28.2, 28.1, 24.7, 24.4, 24.3, 24.0, 23.7, 23.2, 23.1, 14.6, 14.3, 14.1, 13.9. Despite several attempts, we were unable to produce HRMS data of a proper intensity ratio.

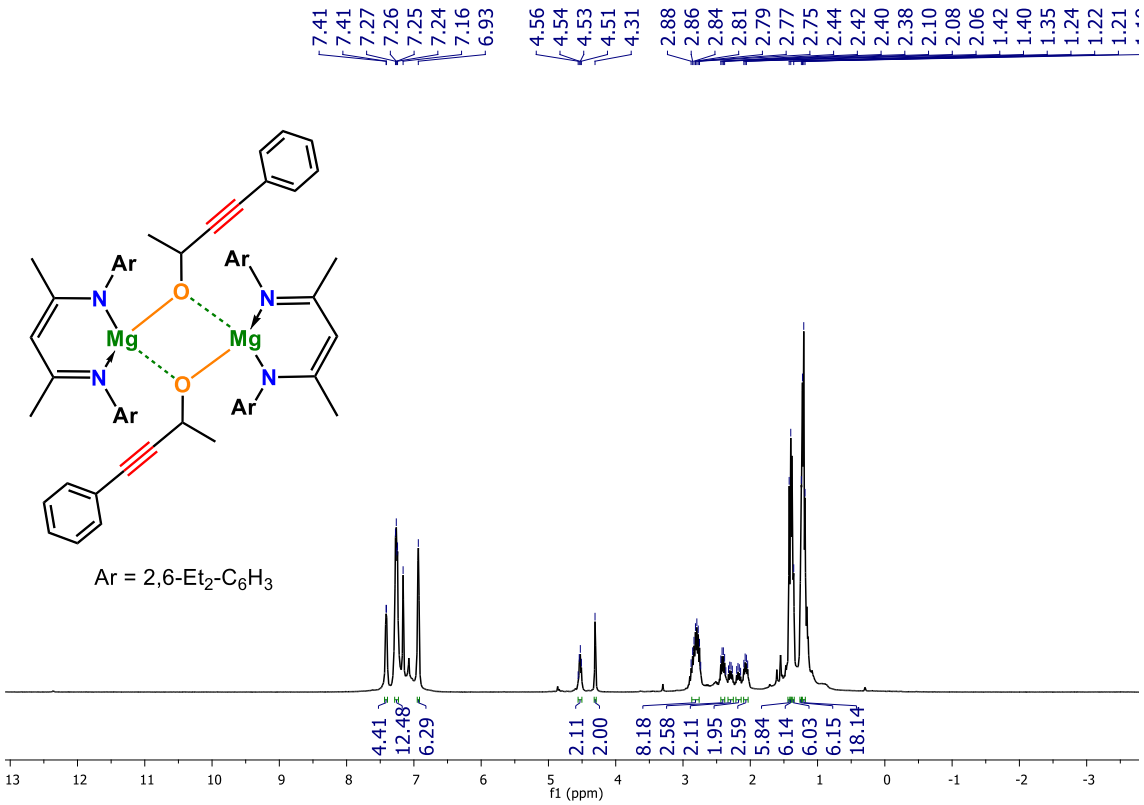

Figure S1. ^{1}H NMR spectrum of **Mg-2** (400 MHz, C_6D_6, 298K).

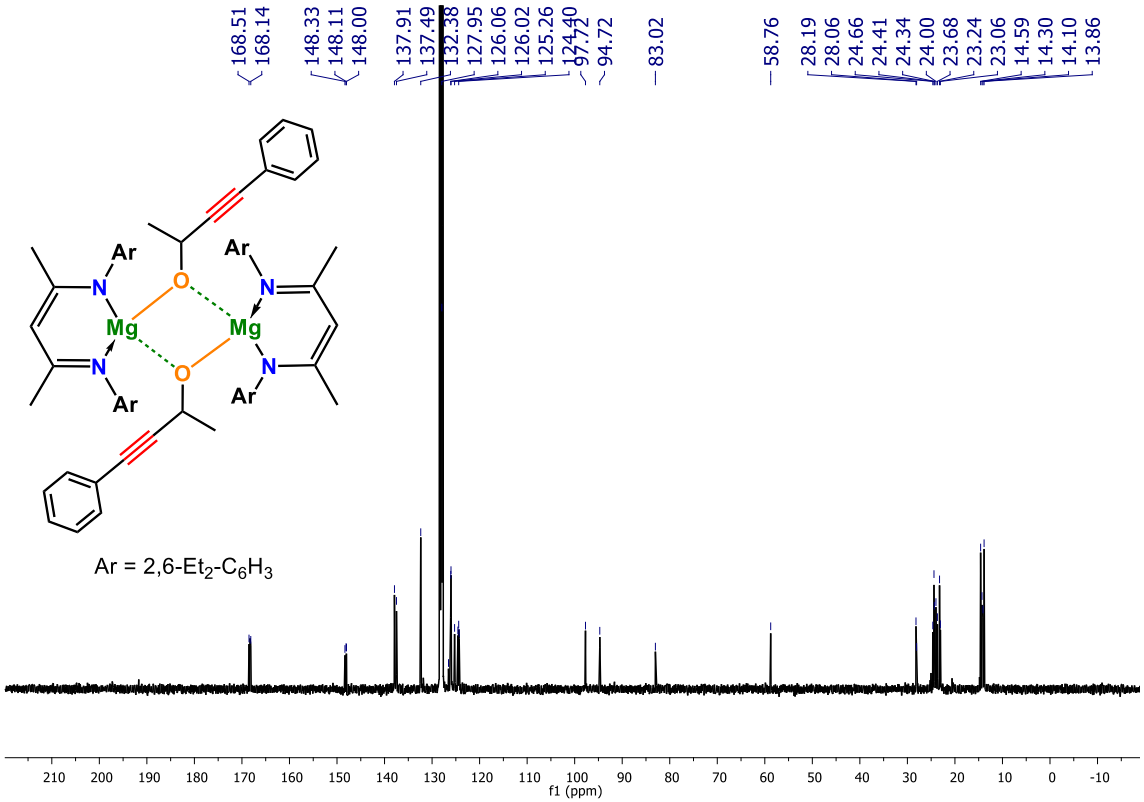

Figure S2. ^{13}C{^{1}H} NMR spectrum of **Mg-2** (101 MHz, C_6D_6, 298K).

(ii) Reaction of Mg-2 with HBpin

[NMR Scale] 7.5μL of HBpin (0.051 mmol, 2.0 equiv.) was added to a solution of **Mg-2** (0.026 mmol, 1.0 equiv.) in C_6D_6 (~ 0.3 mL) in a J. Young valve NMR tube and kept at room temperature for 2 hours. The ^{1}H and ^{11}B NMR spectroscopic analyses revealed no observable changes, indicating that no reaction occurred under the standard reaction conditions. **^{1}H NMR** (400 MHz, C_6D_6, 298 K) δ = 7.40 (s, 4H), 7.29 – 7.23 (m, 12H), 6.93 (s, 6H), 4.53 (q, *J* = 6.3 Hz, 2H), 4.30 (s, 2H), 2.80 (td, *J* = 16.3, 7.9 Hz, 8H), 2.41 (dd, *J* = 15.1, 7.5 Hz, 2H), 2.29 (dd, *J* = 15.1, 7.6 Hz, 2H), 2.17 (dd, *J* = 15.4, 7.7 Hz, 2H), 2.06 (dd, *J* = 15.0, 7.5 Hz, 2H), 1.42 (s, 6H), 1.40 (s, 6H), 1.36 (d, *J* = 7.1 Hz, 6H), 1.26 – 1.24 (m, 6H), 1.20 – 1.16 (m, 18H), 0.99 (s, 24H). **^{11}B NMR** (128 MHz, C_6D_6, 298 K) δ = 28.50 (d, *J* = 174.7 Hz).

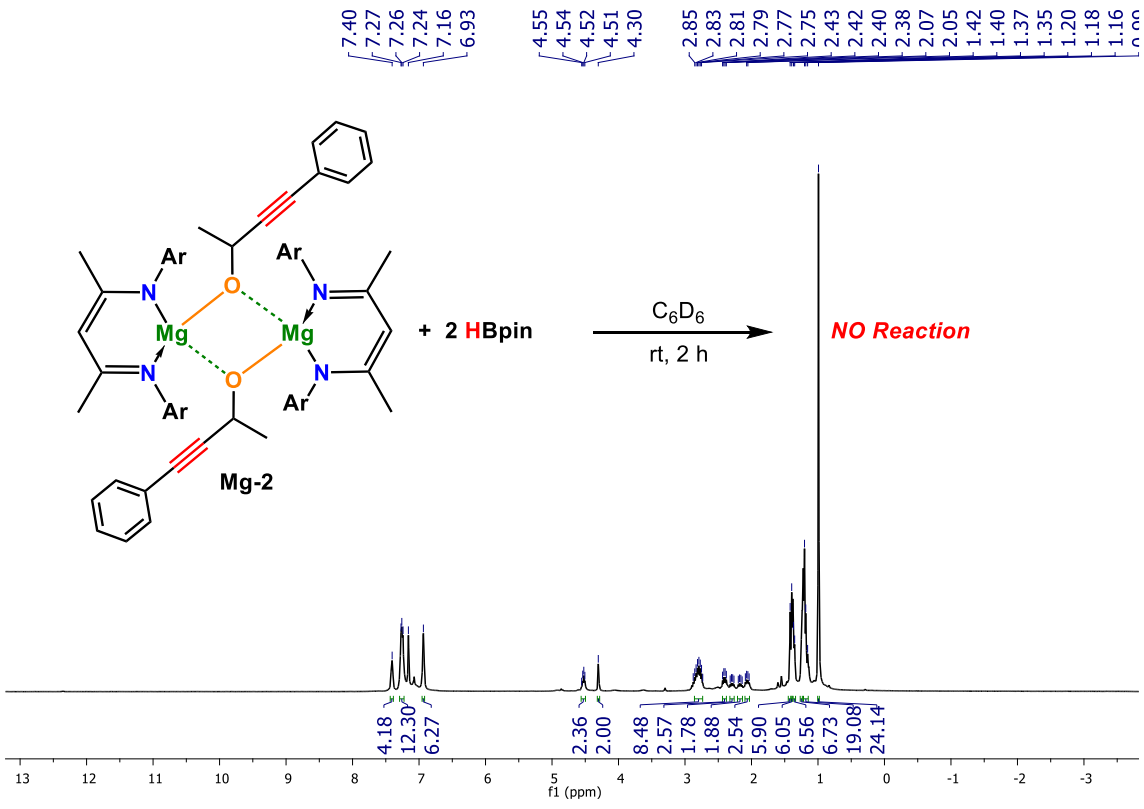

Figure S3. ^{1}H NMR (400 MHz, 298 K) spectrum for the reaction of **Mg-2** with **HBpin** in C_6D_6.

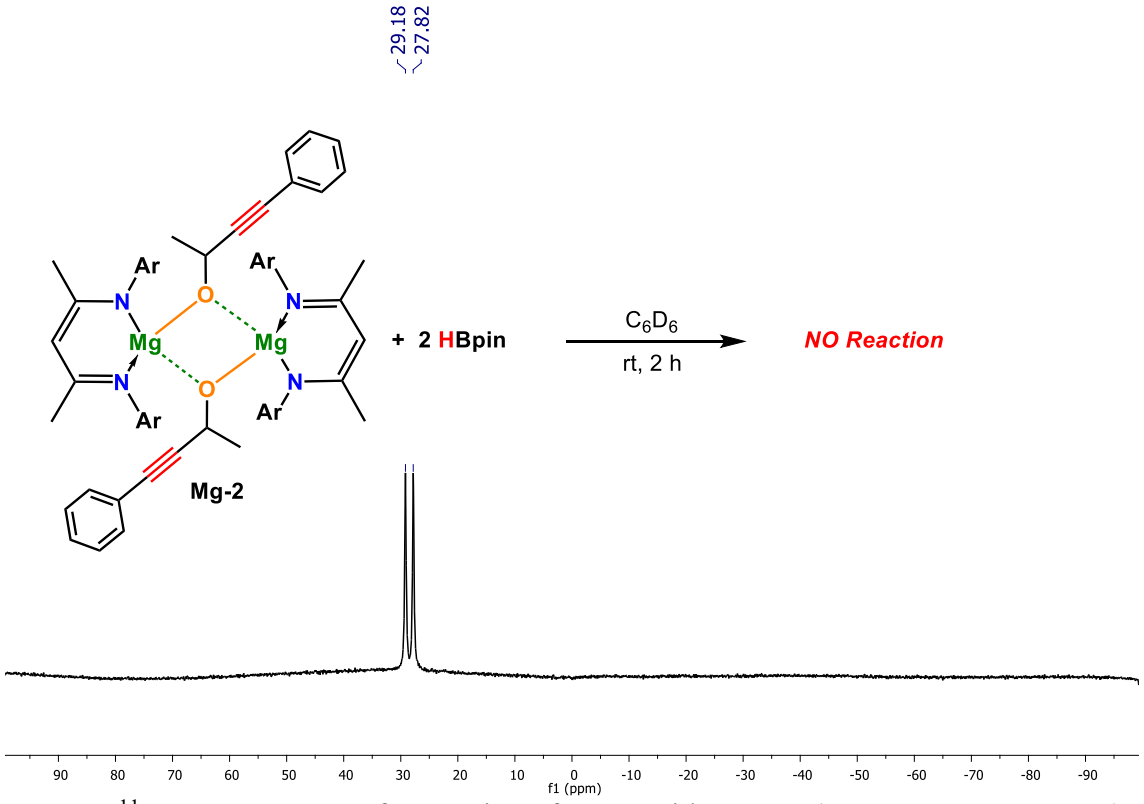

Figure S4. ^{11}B NMR spectrum for reaction of **Mg-2** with **HBpin** (128 MHz, C_6D_6, 298K).

(iii) Reaction of Mg-2 and HBpin with 1a

[NMR Scale] To the above reaction mixture, 7.5μL (0.051 mmol, 1.0 equiv.) of 4-phenyl-3-butyn-2-one (**1a**) was added, and the solution was analysed by NMR spectroscopy after 15 min. The ^{1}H and ^{11}B NMR spectra indicated complete conversion to the boronate ester product **2a**, along with **Mg-2**. NMR conversion > 99%. **^{1}H NMR** (400 MHz, C_6D_6, 298 K) δ 7.40 (s, 8H), 7.28 – 7.23 (m, 12H), 6.94 (s, 12H), 5.30 (q, *J* = 6.4 Hz, 2H), 4.53 (q, *J* = 6.1 Hz, 2H), 4.30 (s, 2H), 2.80 (td, *J* = 16.9, 8.4 Hz, 8H), 2.41 (dd, *J* = 14.9, 7.5 Hz, 2H), 2.29 (dd, *J* = 15.1, 7.6 Hz, 2H), 2.17 (dd, *J* = 15.3, 7.6 Hz, 2H), 2.06 (dd, *J* = 15.0, 7.5 Hz, 2H), 1.52 (d, *J* = 6.5 Hz, 6H), 1.42 (s, 6H), 1.39 (s, 6H), 1.35 (s, 6H), 1.26 – 1.24 (m, 6H), 1.20 – 1.15 (m, 18H), 1.06 (s, 12H), 1.04 (s, 12H). **^{11}B NMR** (128 MHz, C_6D_6, 298 K) δ = 22.61.

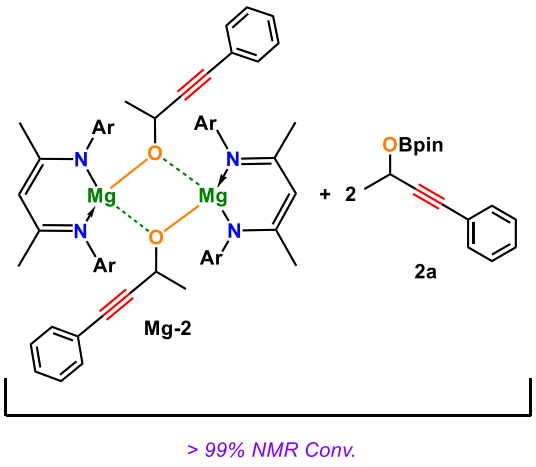

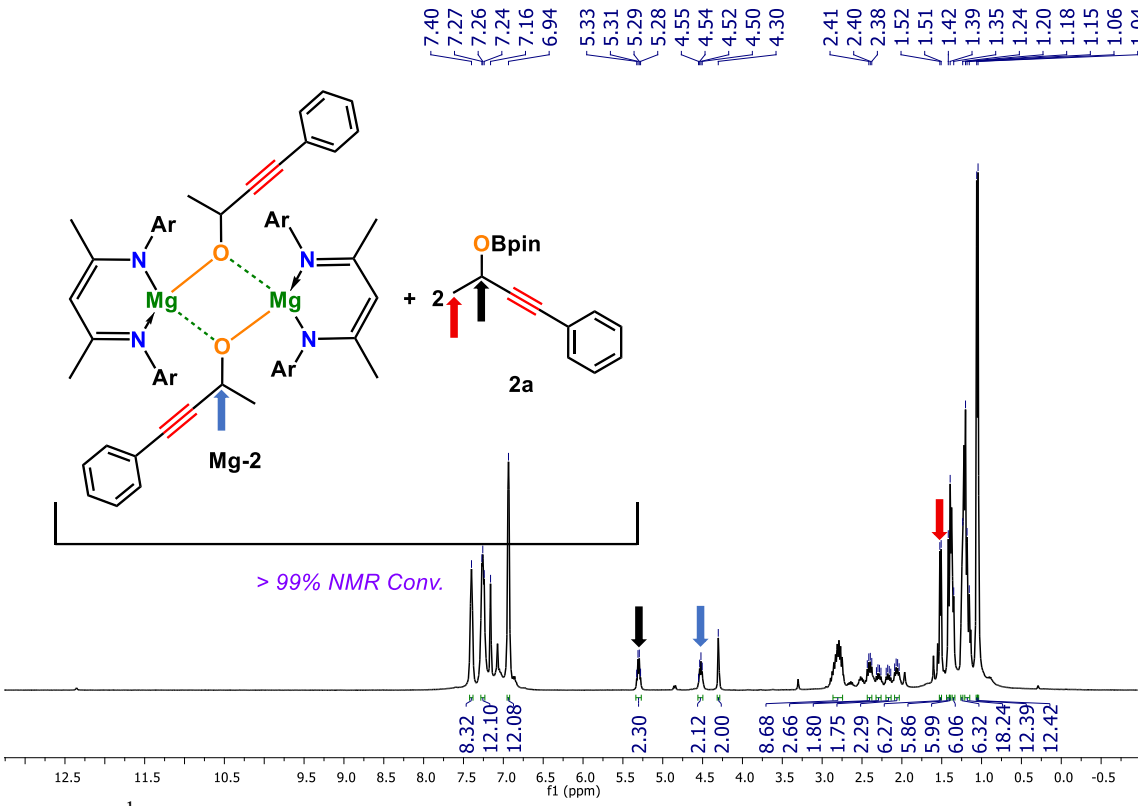

Figure S5. ^{1}H NMR spectrum for reaction of **Mg-2** and **HBpin** with **1a** (400 MHz, C_6D_6, 298K).

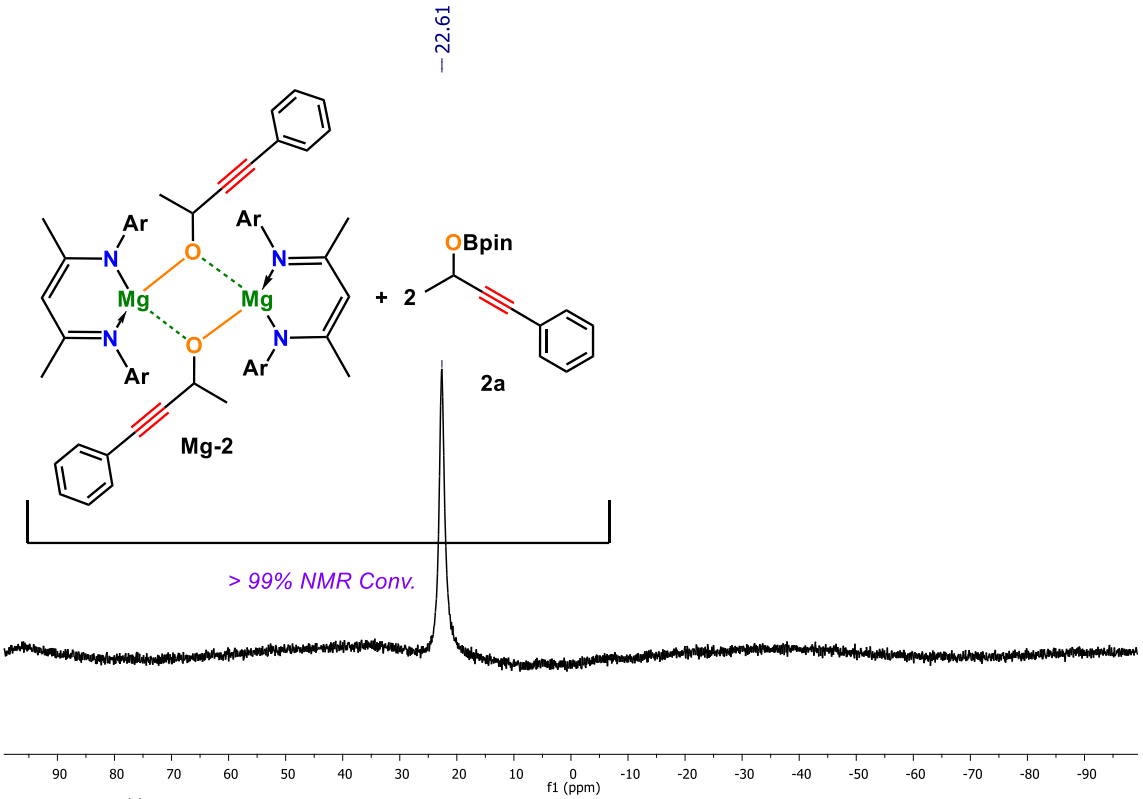

Figure S6. ^{11}B NMR spectrum for reaction of **Mg-2** and **HBpin** with **1a** (128 MHz, C_6D_6, 298K).

(iv) Reaction of Mg-1 with HBpin

In a 50 mL Schlenk flask equipped with a magnetic stir bar, HBpin (1 mmol, 1.0 equiv.) and **Mg-1** (0.1 mmol) were combined under neat conditions and stirred at room temperature for 2 h. After completion of the reaction, the ^{11}B NMR spectrum was recorded in C_6D_6, which showed no evidence for the formation of BH_3.

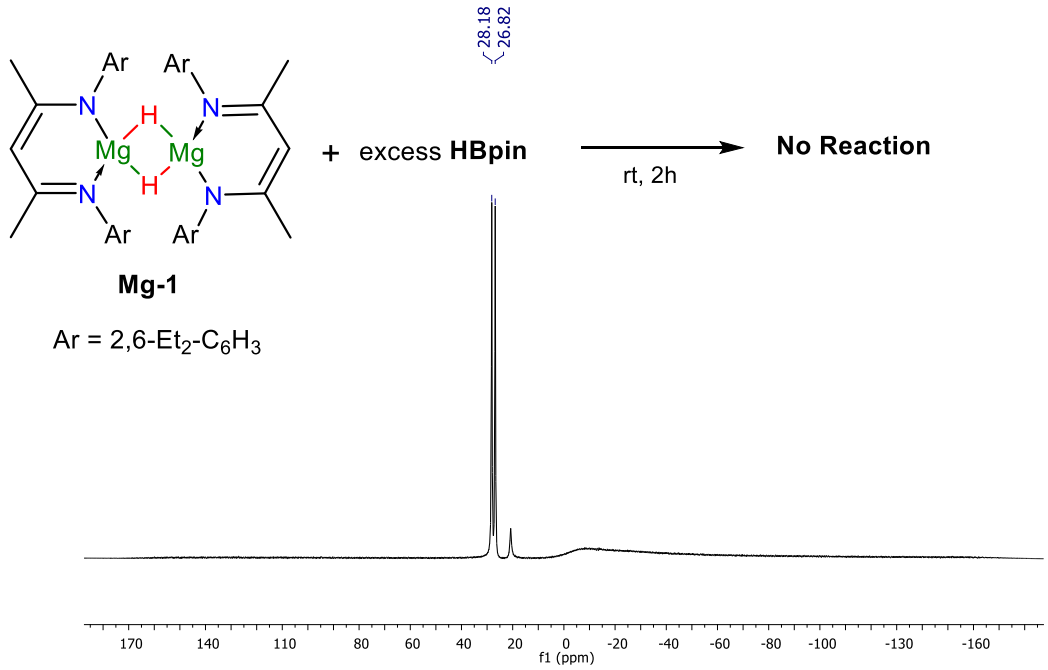

Figure S7. ^{11}B NMR spectrum for reaction of **Mg-1** and **HBpin** (128 MHz, C_6D_6, 298K).

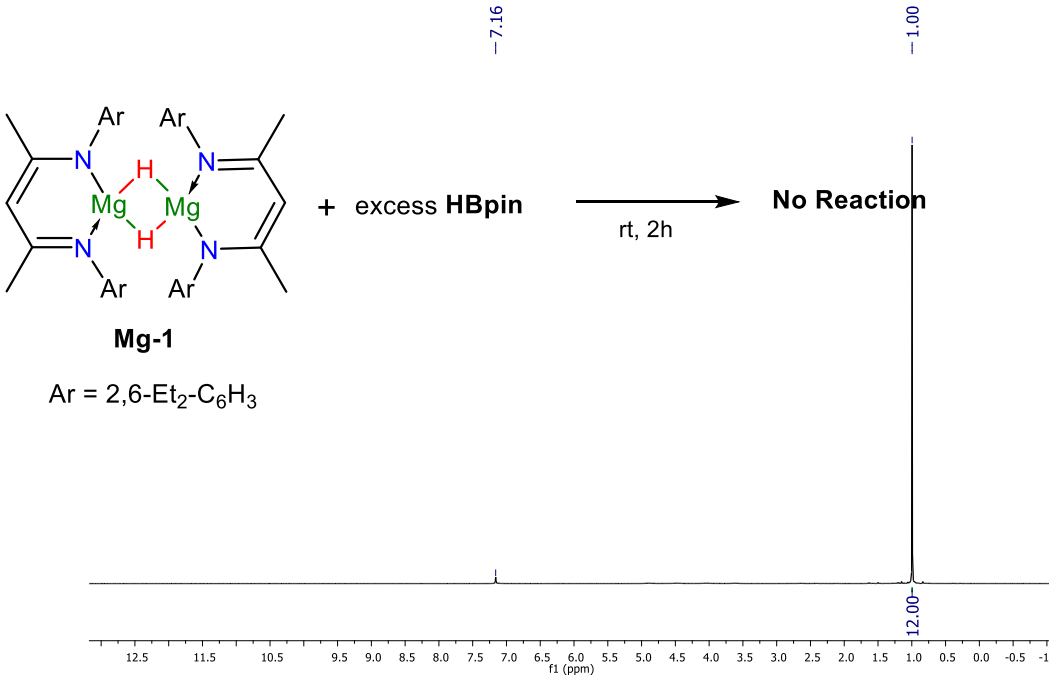

Figure S8. ^{1}H NMR spectrum for reaction of **Mg-1** and **HBpin** (400 MHz, C_6D_6, 298K).

(v) The study of the effect of BH_3 on the hydroboration reaction of 1a

In a 10 mL reaction vial, the catalyst and ynone **1a** (0.1 mmol, 1.0 equiv.) were combined, followed by the addition of HBpin (14.5 µL, 0.1 mmol, 1.0 equiv.) under neat conditions inside the glovebox. The reaction mixture was stirred at room temperature for 2 h. The ^{1}H NMR spectrum (in $CDCl_3$) confirmed complete consumption of ynone **1a** and the appearance of a characteristic OC*H* resonance, consistent with the formation of the corresponding boronate ester product **2a**. In the presence of TMEDA, full conversion (>99%) was achieved, whereas no noticeable conversion was observed when $BH_3.SMe_2$ was employed as the catalyst.

Table S1. The hydroboration of **1a** with HBpin in the presence of different catalysts.

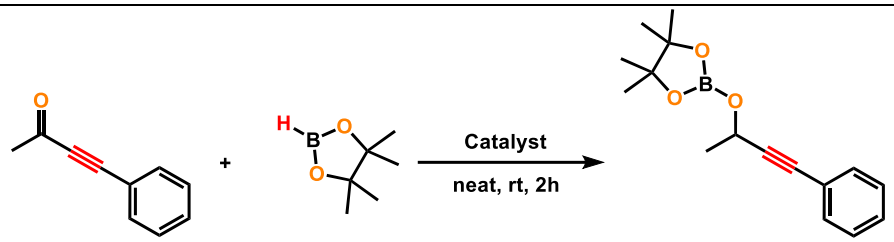

Catalyst	NMR Conv. (%)
Mg-1 (0.5 mol%)	> 99%
Mg-1 (0.5 mol%) + TMEDA (1 mol%)	> 99%
$BH_3.SMe_2$ (0.5 mol%)	0%

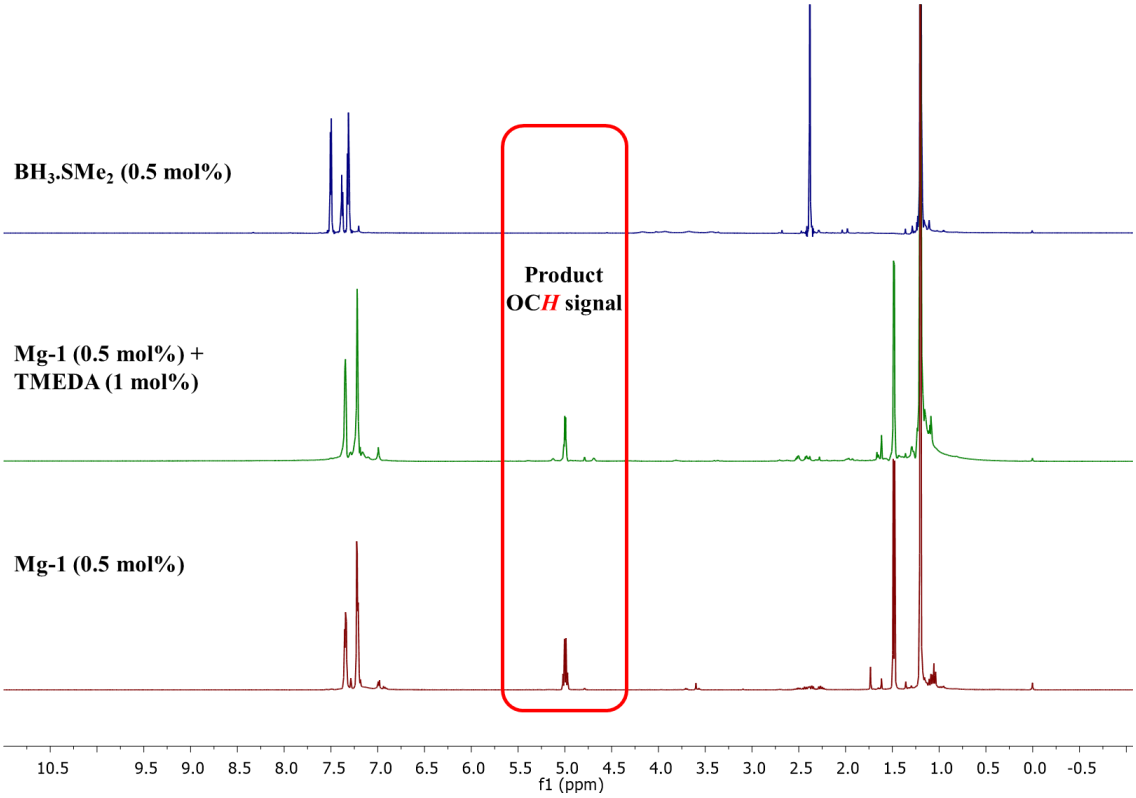

Figure S9. The hydroboration of **1a** with HBpin in the presence of different catalysts.

2. ^{1}H, $^{13}C\{^{1}H\}$ and ^{11}B Spectra of Boronate Ester Products

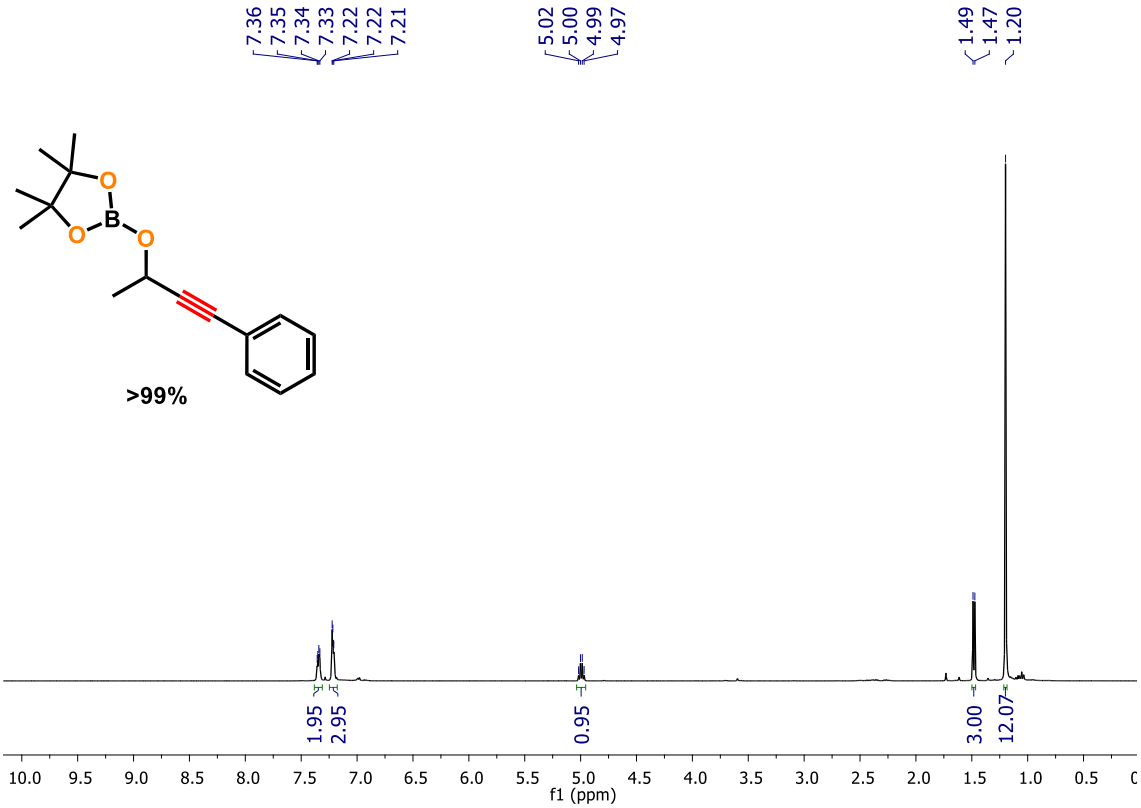

Figure S10. ^{1}H NMR spectrum of **2a** (400 MHz, $CDCl_3$, 298K).

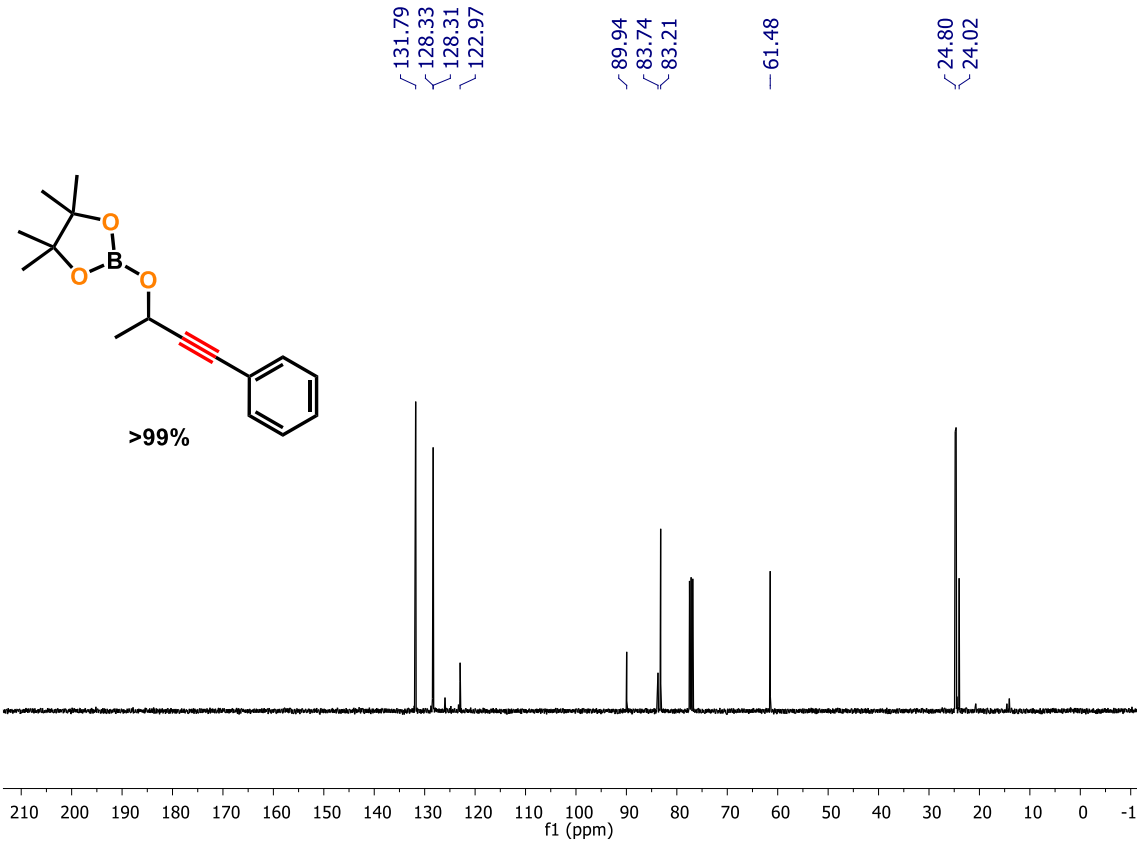

Figure S11. $^{13}C\{^{1}H\}$ NMR spectrum of **2a** (101 MHz, $CDCl_3$, 298K).

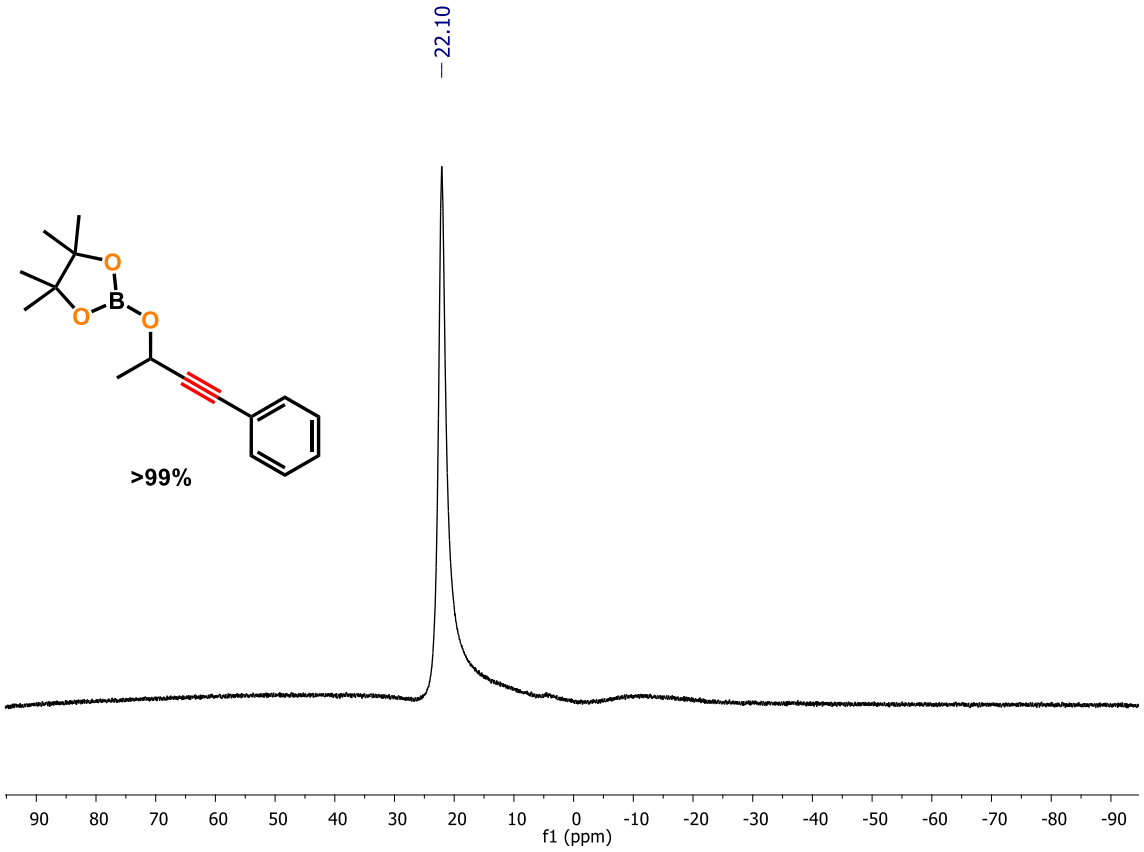

Figure S12. ^{11}B NMR spectrum of **2a** (128 MHz, $CDCl_3$, 298K).

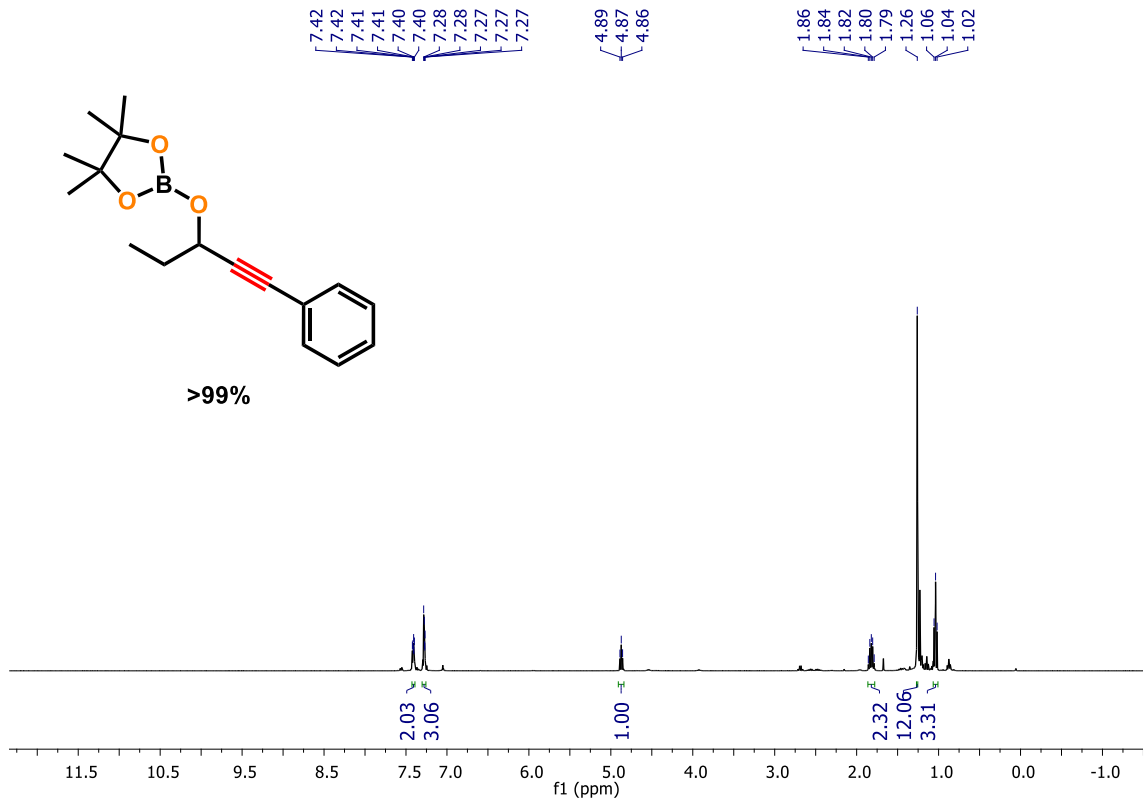

Figure S13. ^{1}H NMR spectrum of **2b** (400 MHz, $CDCl_3$, 298K).

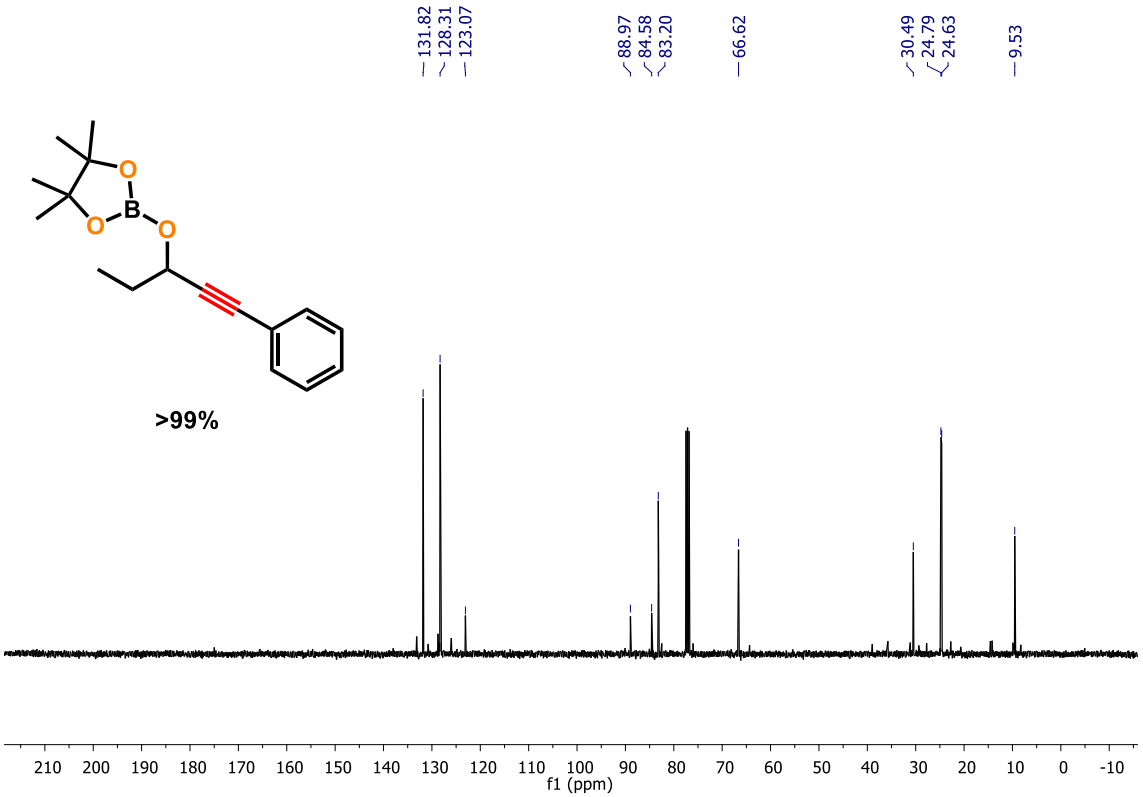

Figure S14. $^{13}C\{^{1}H\}$ NMR spectrum of **2b** (101 MHz, $CDCl_3$, 298K).

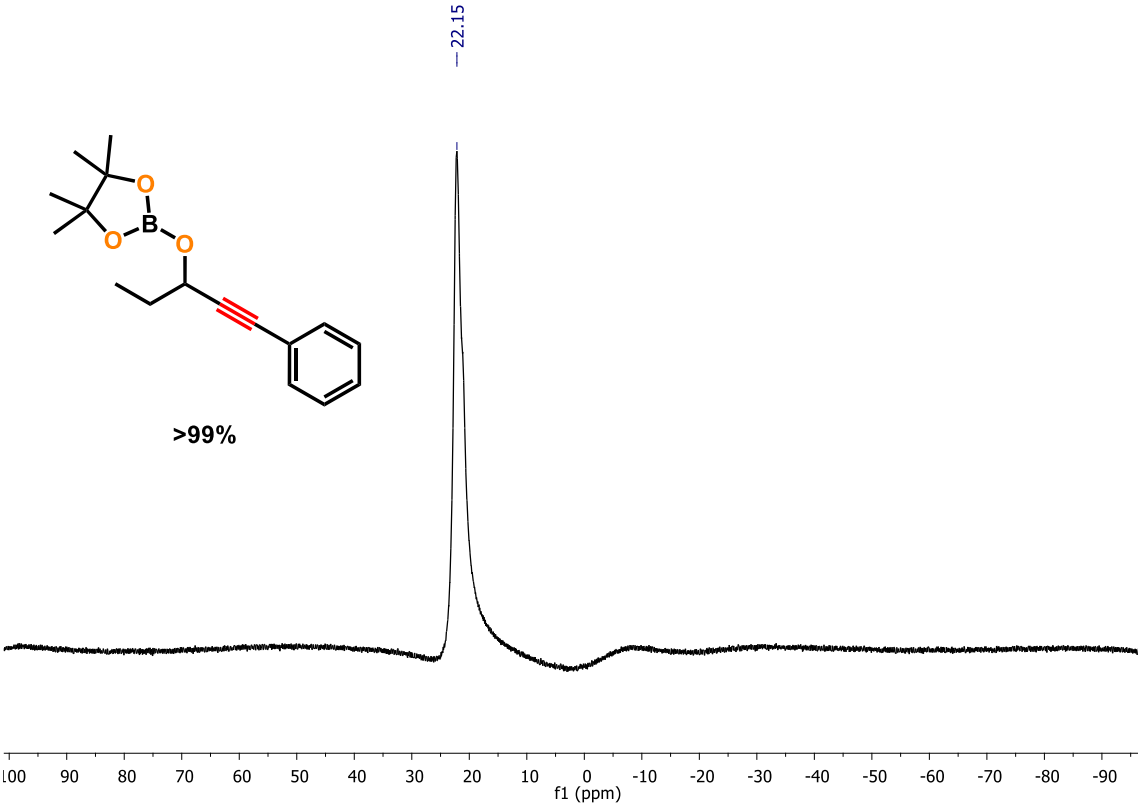

Figure S15. ^{11}B NMR spectrum of **2b** (128 MHz, $CDCl_3$, 298K).

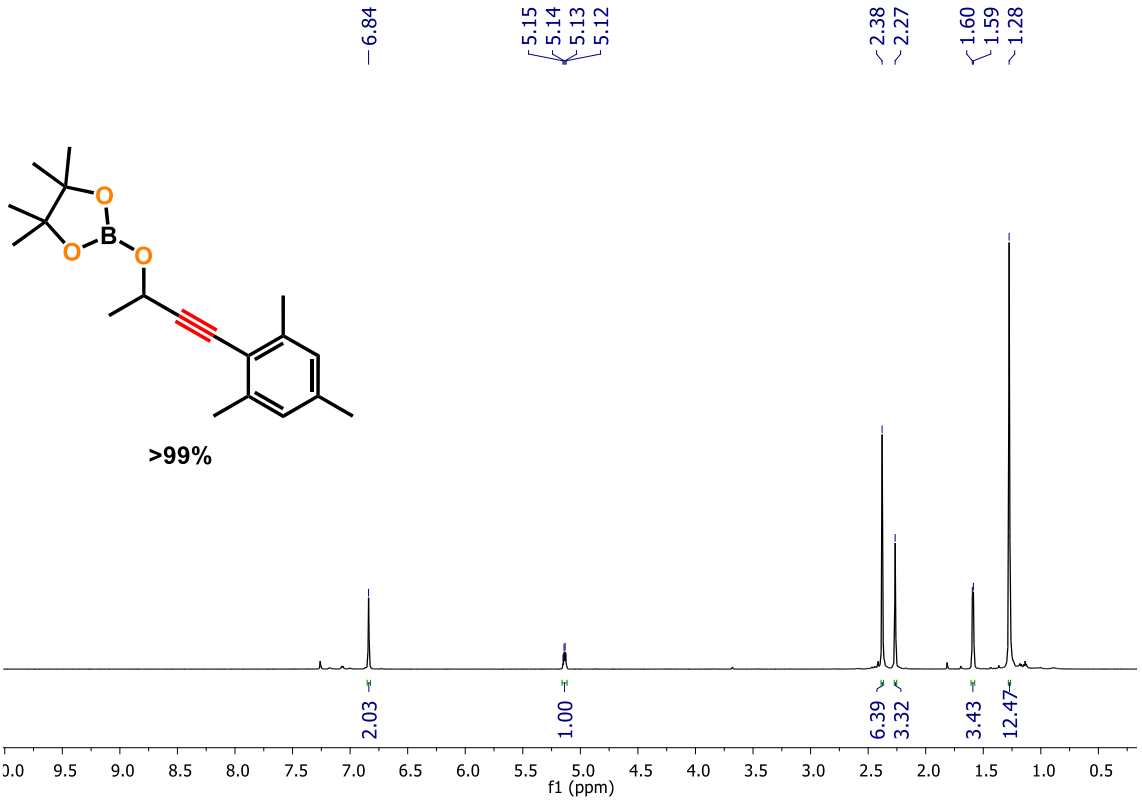

Figure S16. ^{1}H NMR spectrum of **2c** (700 MHz, $CDCl_3$, 298K).

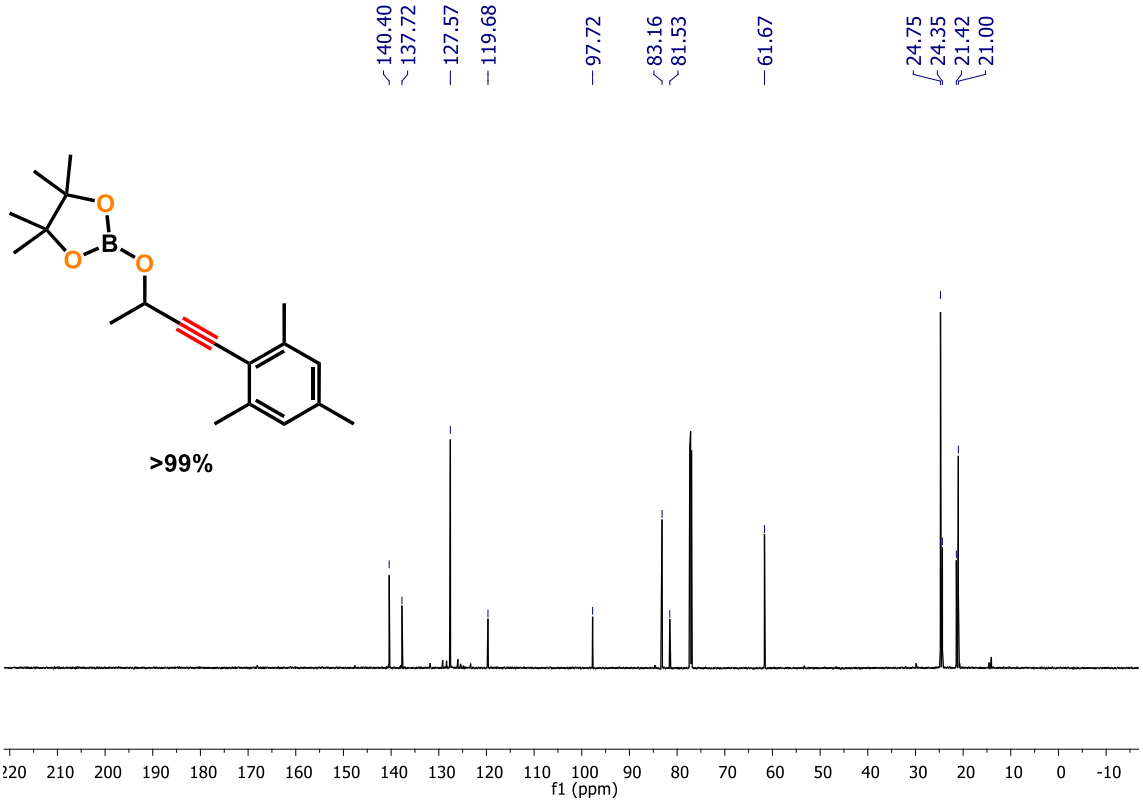

Figure S17. $^{13}C\{^{1}H\}$ NMR spectrum of **2c** (176 MHz, $CDCl_3$, 298K).

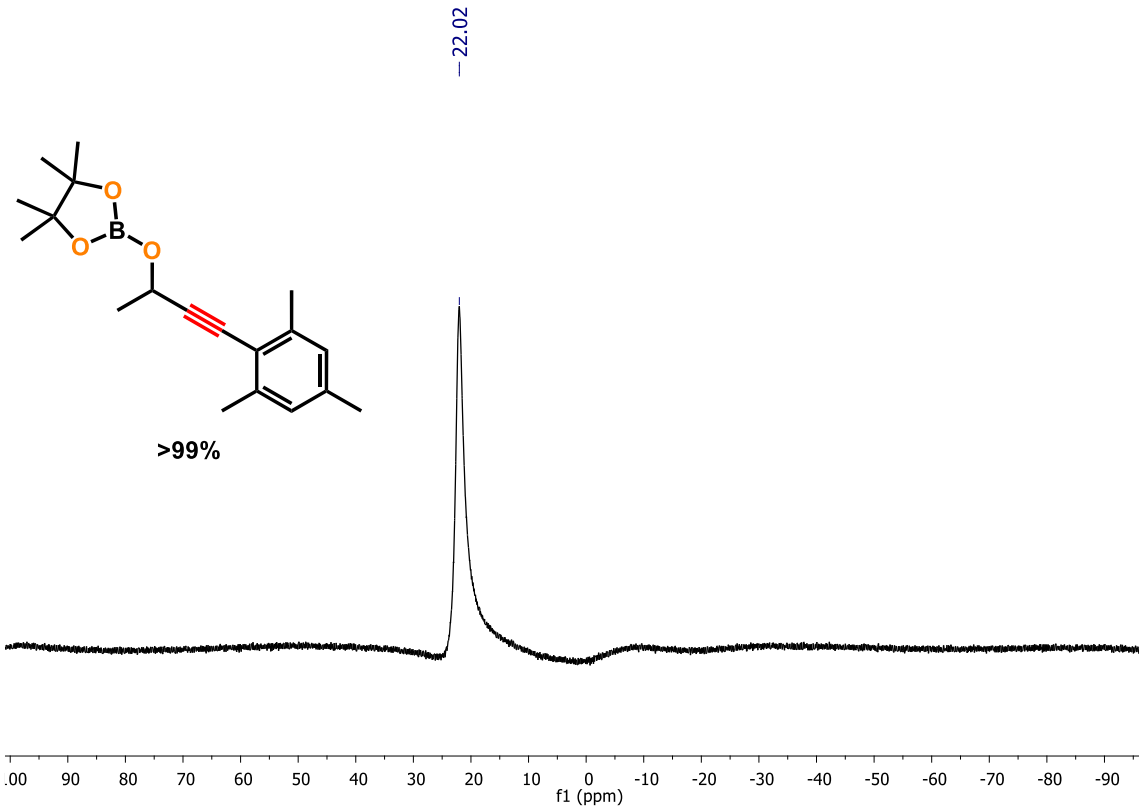

Figure S18. ^{11}B NMR spectrum of **2c** (128 MHz, $CDCl_3$, 298K).

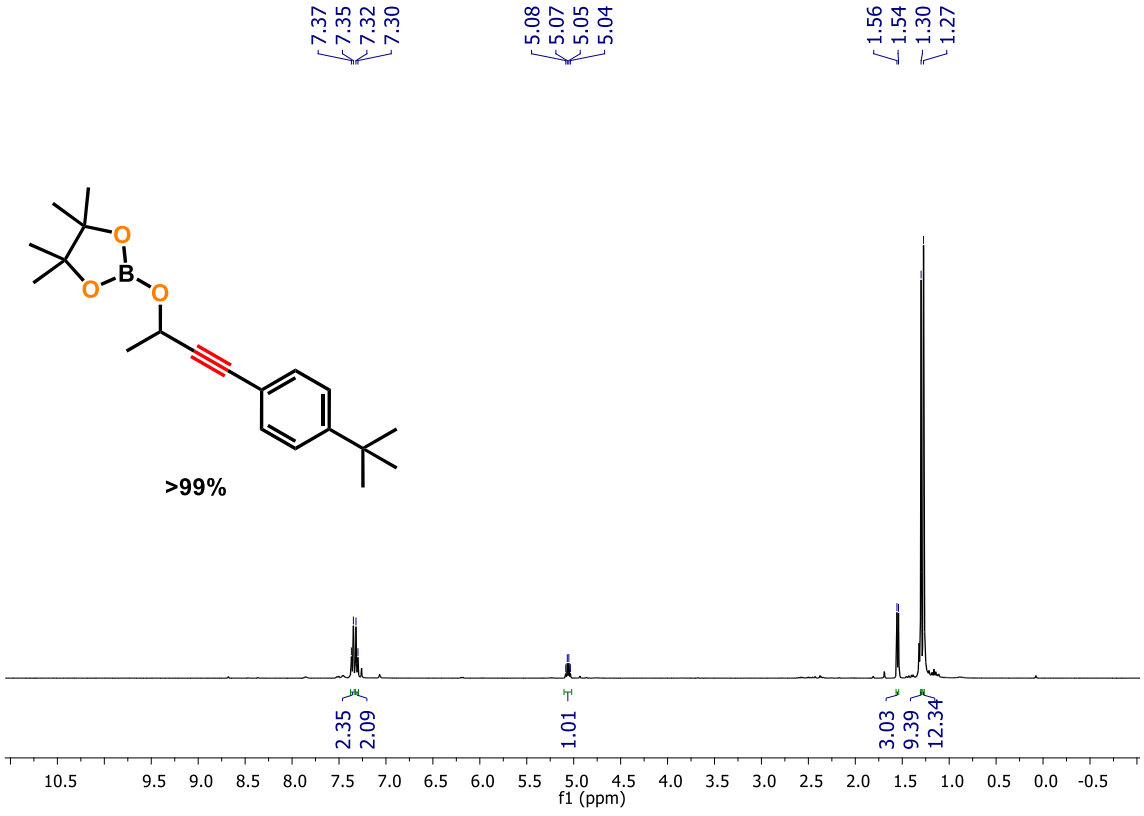

Figure S19. ^{1}H NMR spectrum of **2d** (400 MHz, $CDCl_3$, 298K).

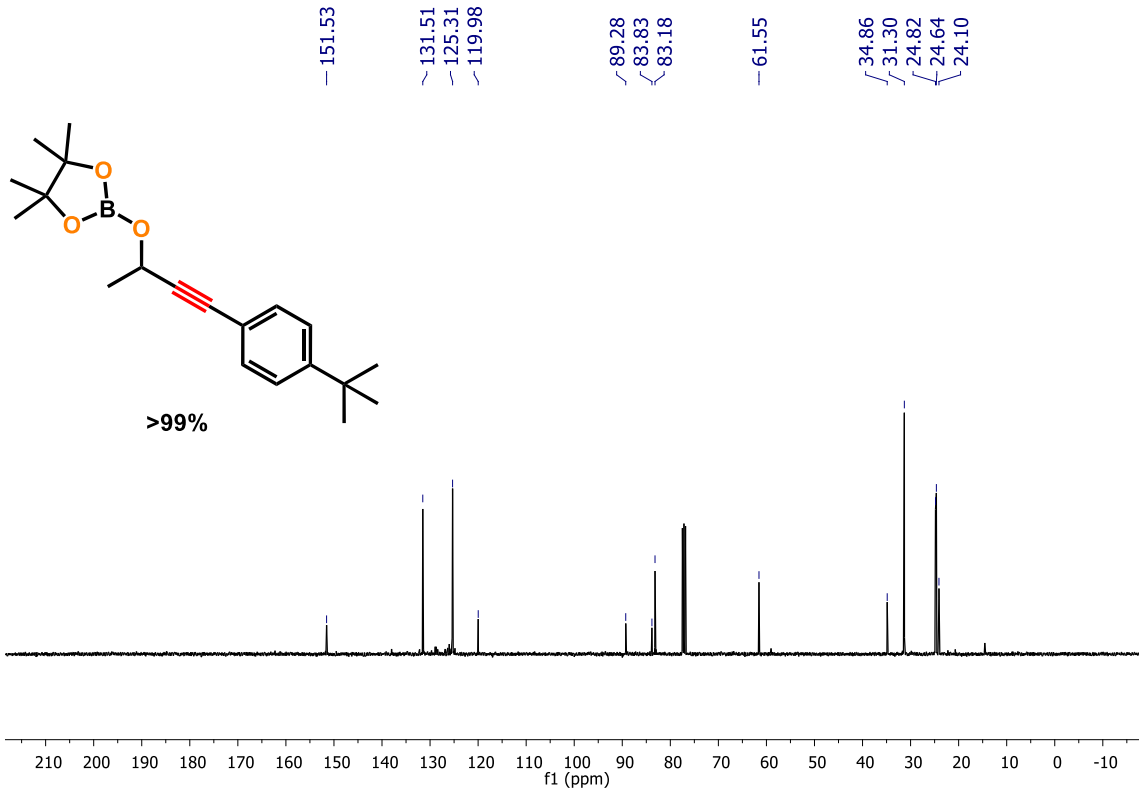

Figure S20. $^{13}C\{^{1}H\}$ NMR spectrum of **2d** (101 MHz, $CDCl_3$, 298K).

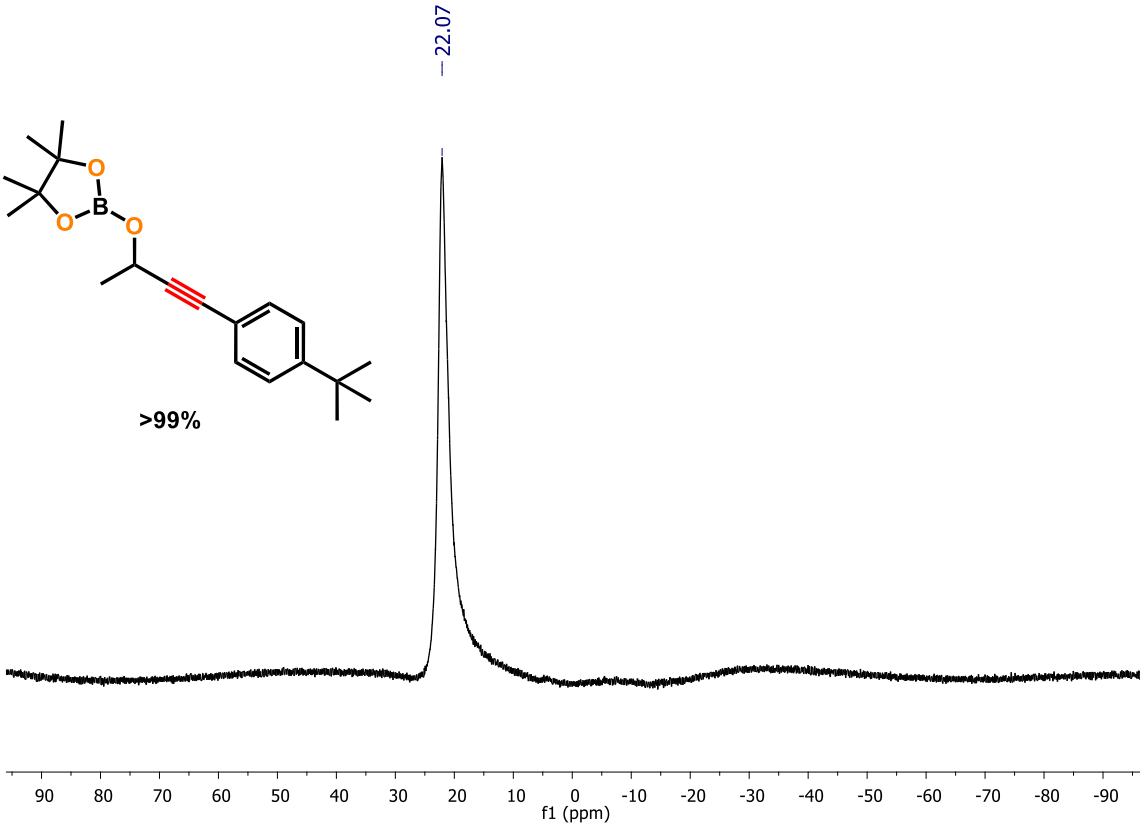

Figure S21. ^{11}B NMR spectrum of **2d** (128 MHz, $CDCl_3$, 298K).

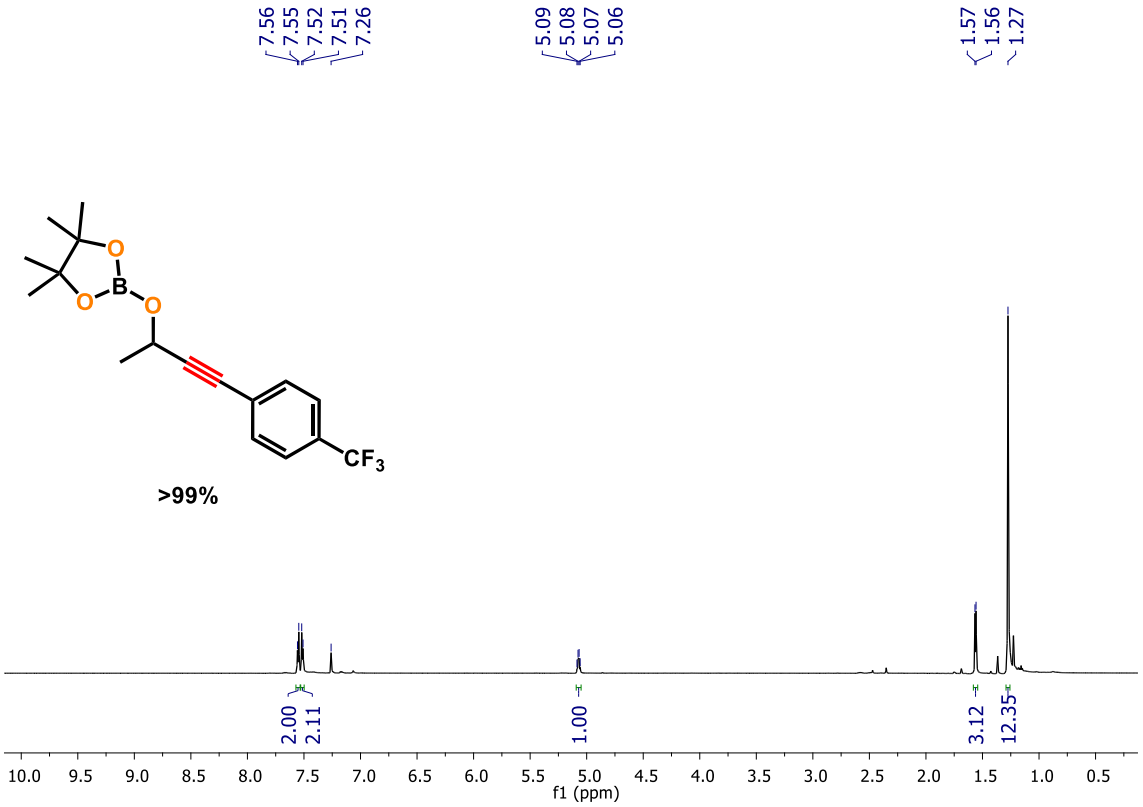

Figure S22. ^{1}H NMR spectrum of **2e** (700 MHz, $CDCl_3$, 298K).

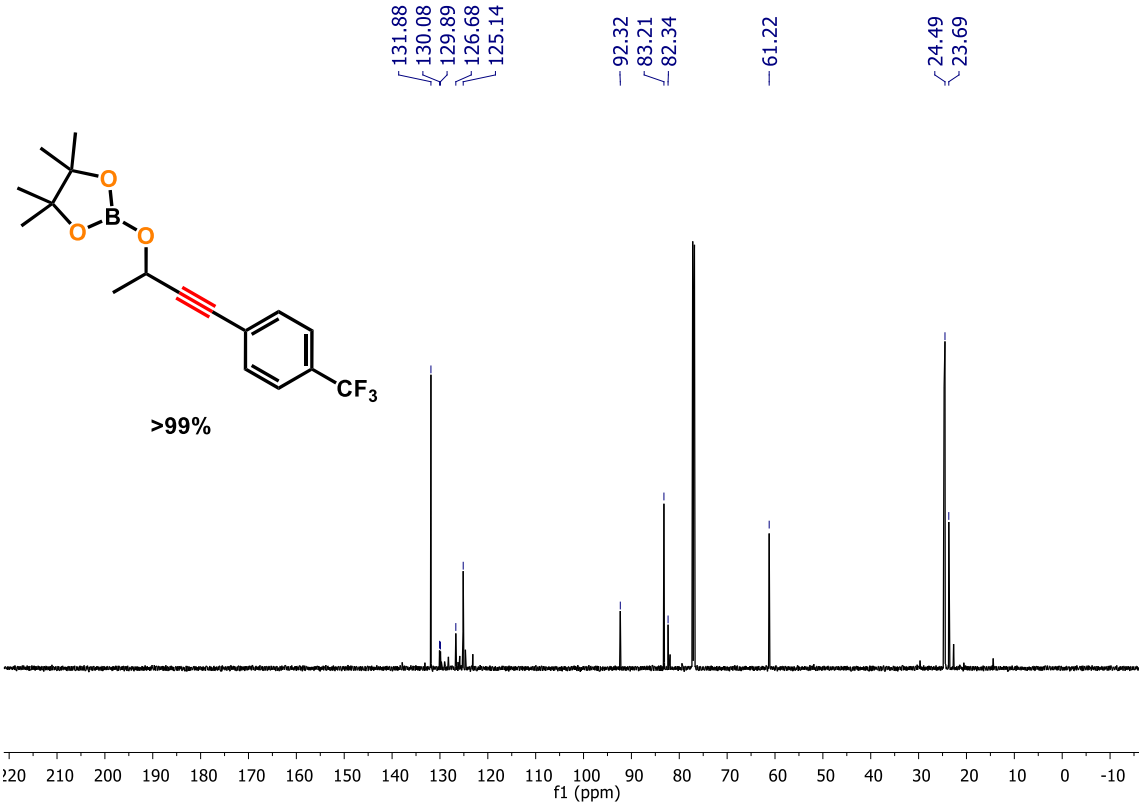

Figure S23. $^{13}C\{^{1}H\}$ NMR spectrum of **2e** (176 MHz, $CDCl_3$, 298K).

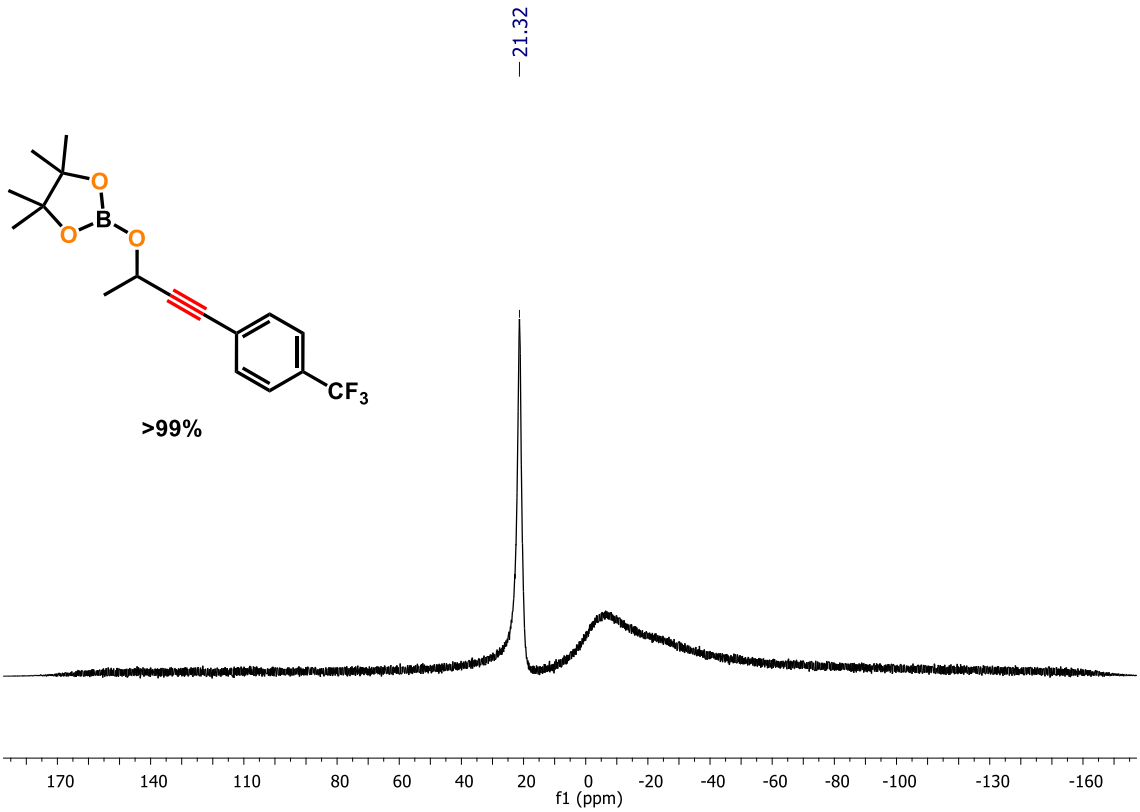

Figure S24. ^{11}B NMR spectrum of **2e** (128 MHz, $CDCl_3$, 298K).

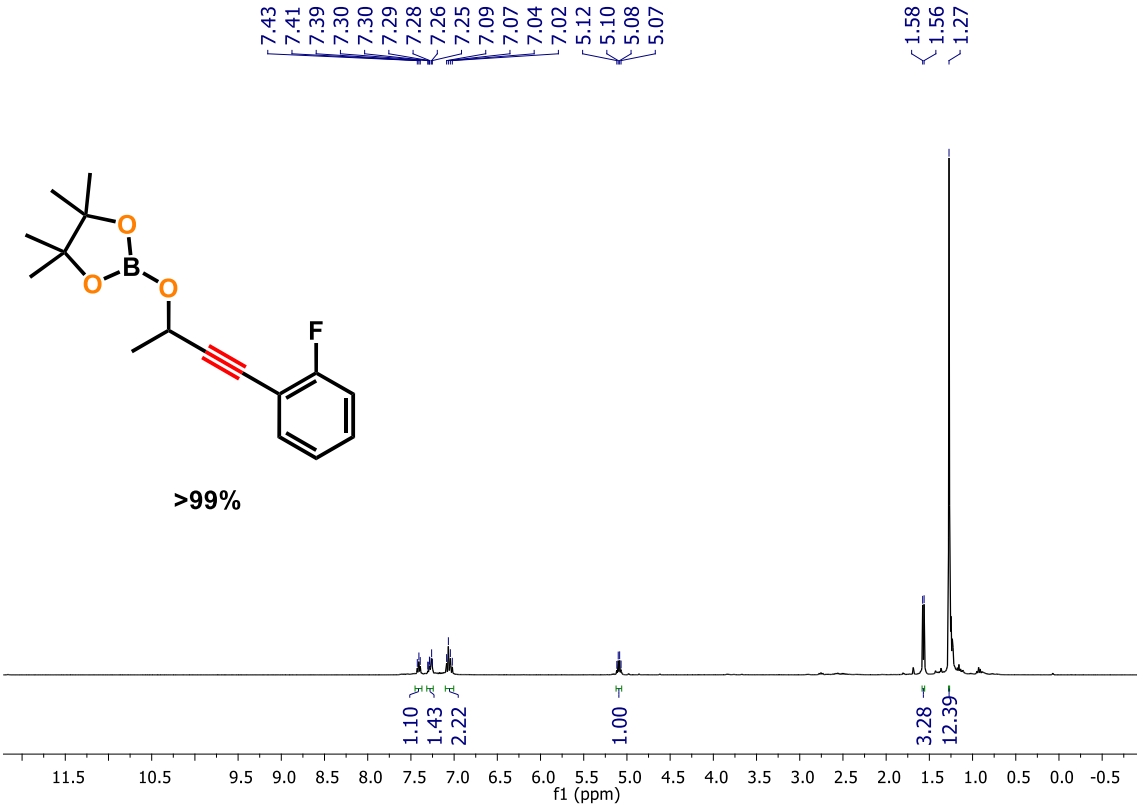

Figure S25. ^{1}H NMR spectrum of **2f** (400 MHz, $CDCl_3$, 298K).

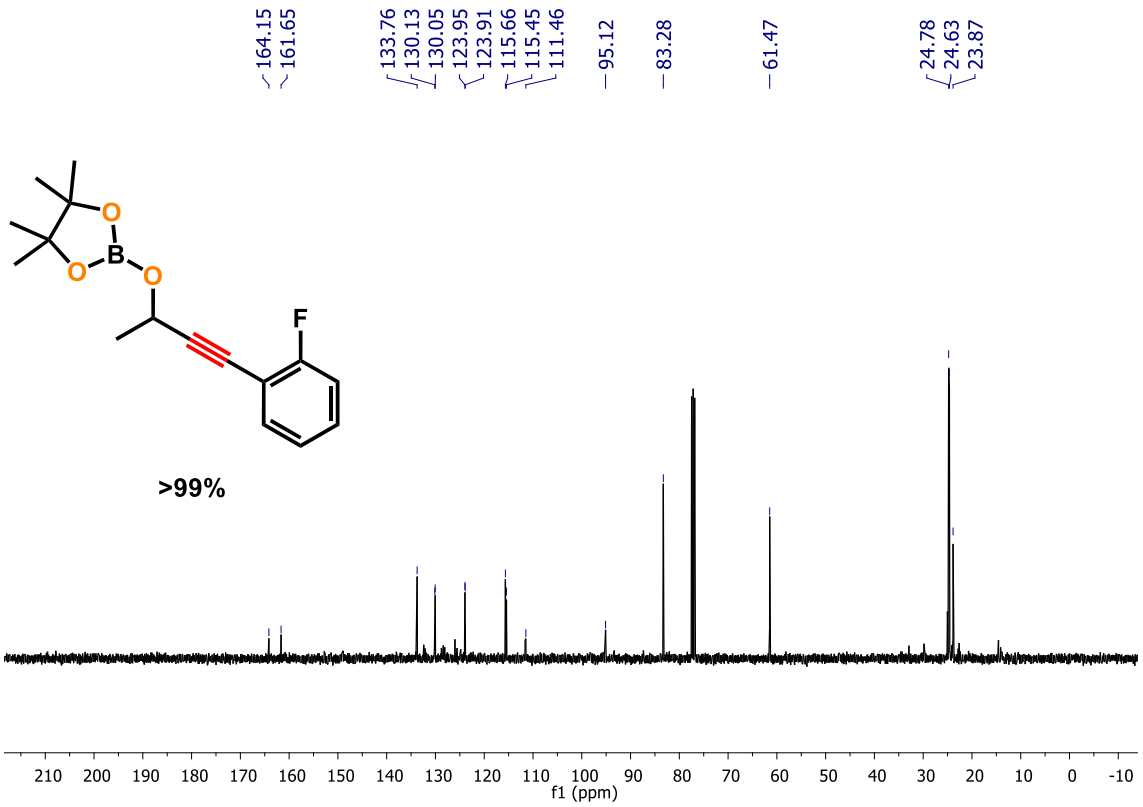

Figure S26. $^{13}C\{^{1}H\}$ NMR spectrum of **2f** (101 MHz, $CDCl_3$, 298K).

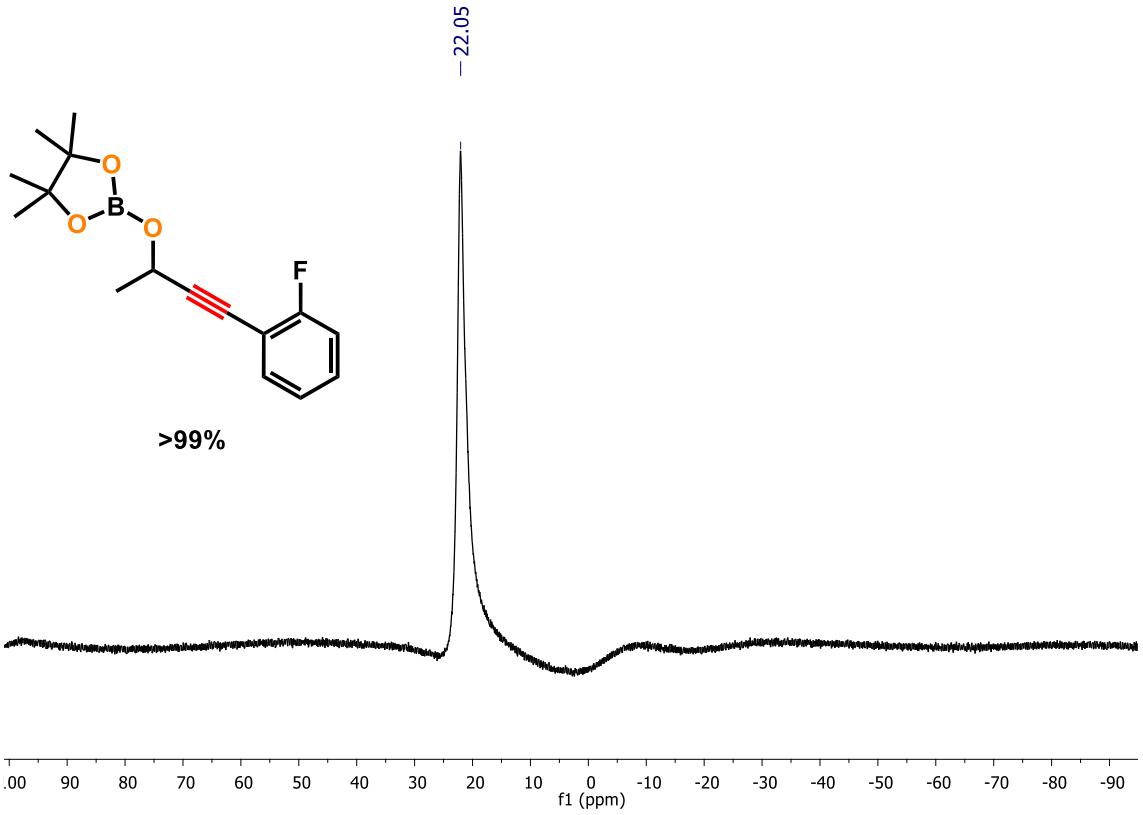

Figure S27. ^{11}B NMR spectrum of **2f** (128 MHz, $CDCl_3$, 298K).

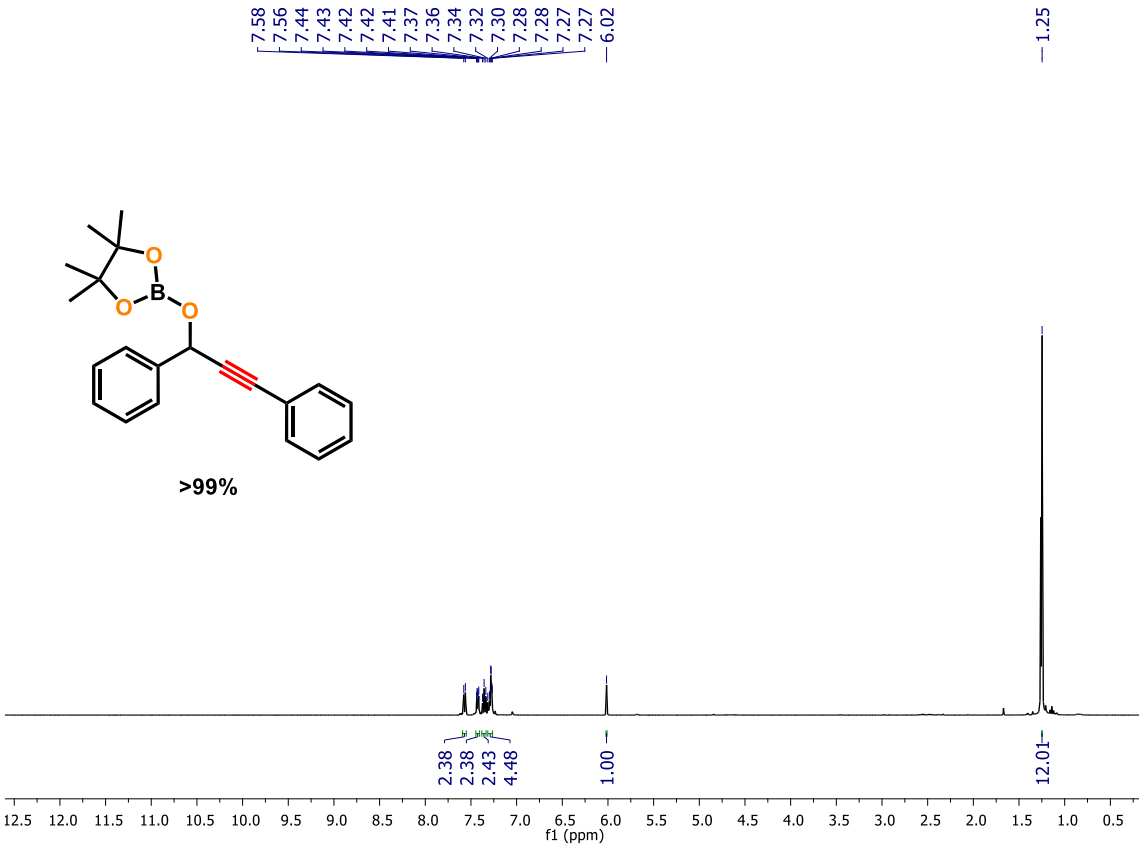

Figure S28. ^{1}H NMR spectrum of **2g** (400 MHz, $CDCl_3$, 298K).

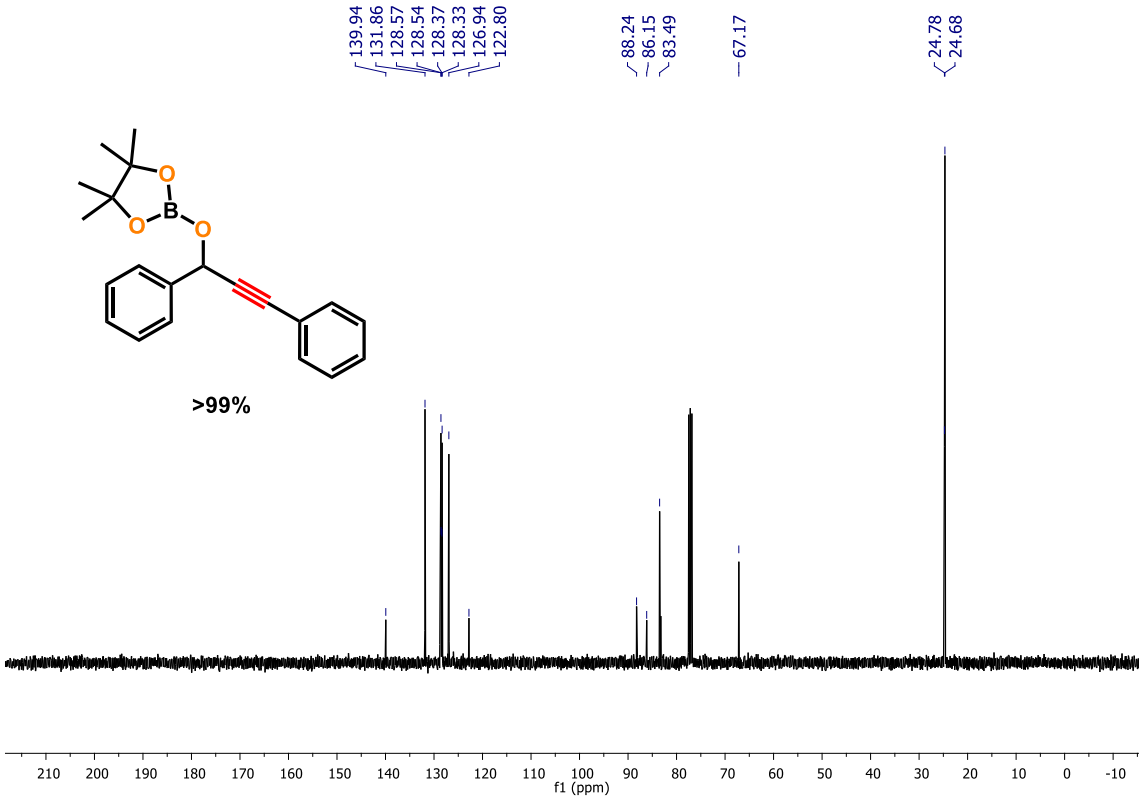

Figure S29. $^{13}C\{^{1}H\}$ NMR spectrum of **2g** (101 MHz, $CDCl_3$, 298K).

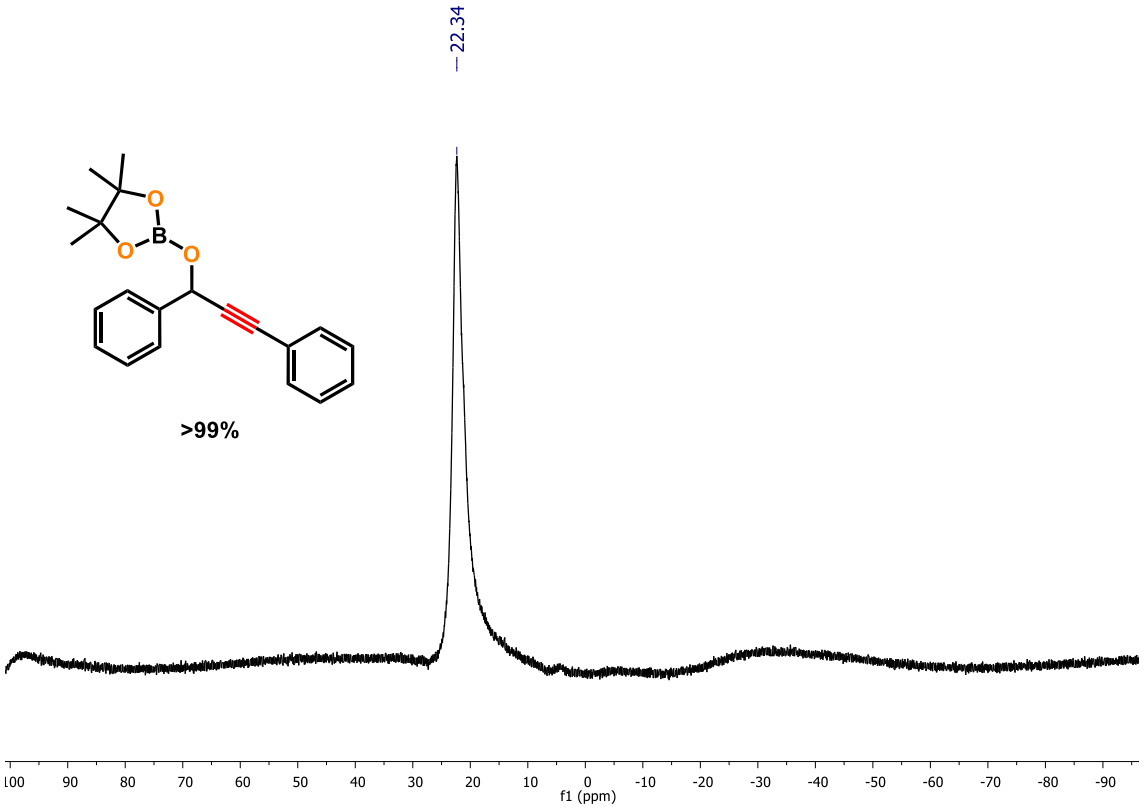

Figure S30. ^{11}B NMR spectrum of **2g** (128 MHz, $CDCl_3$, 298K).

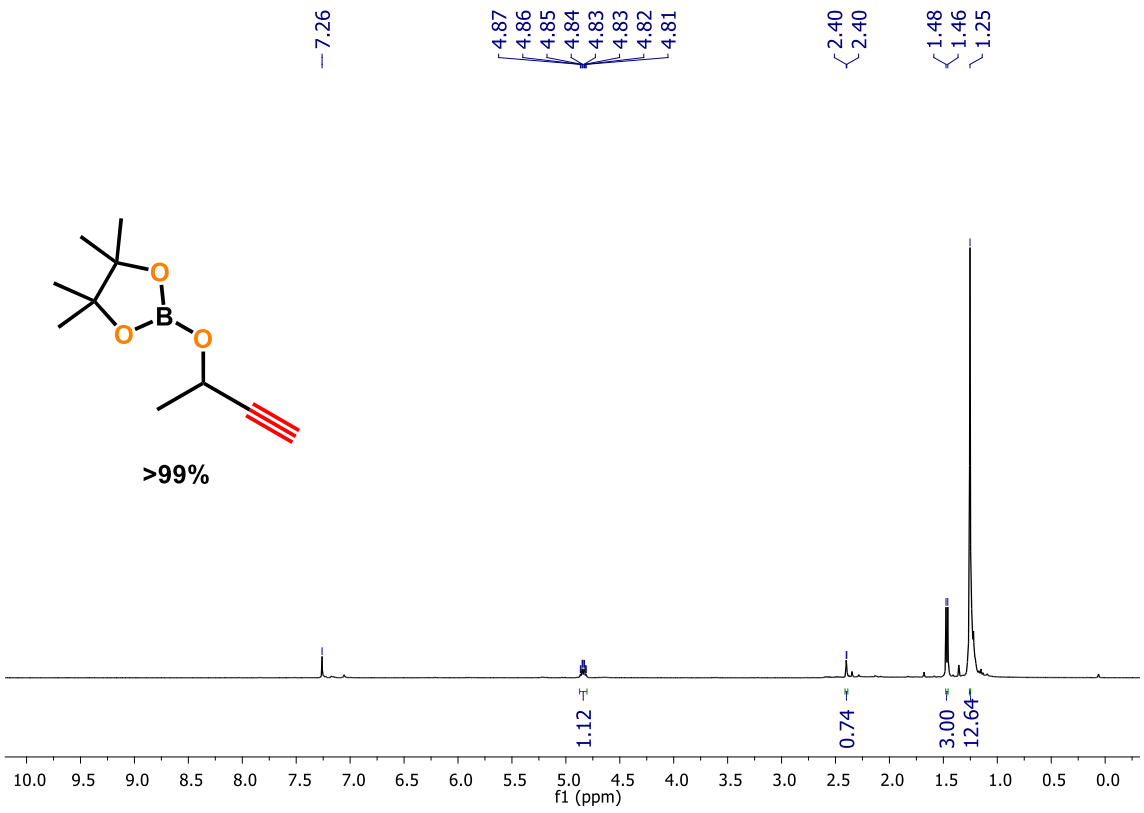

Figure S31. ^{1}H NMR spectrum of **2h** (400 MHz, $CDCl_3$, 298K).

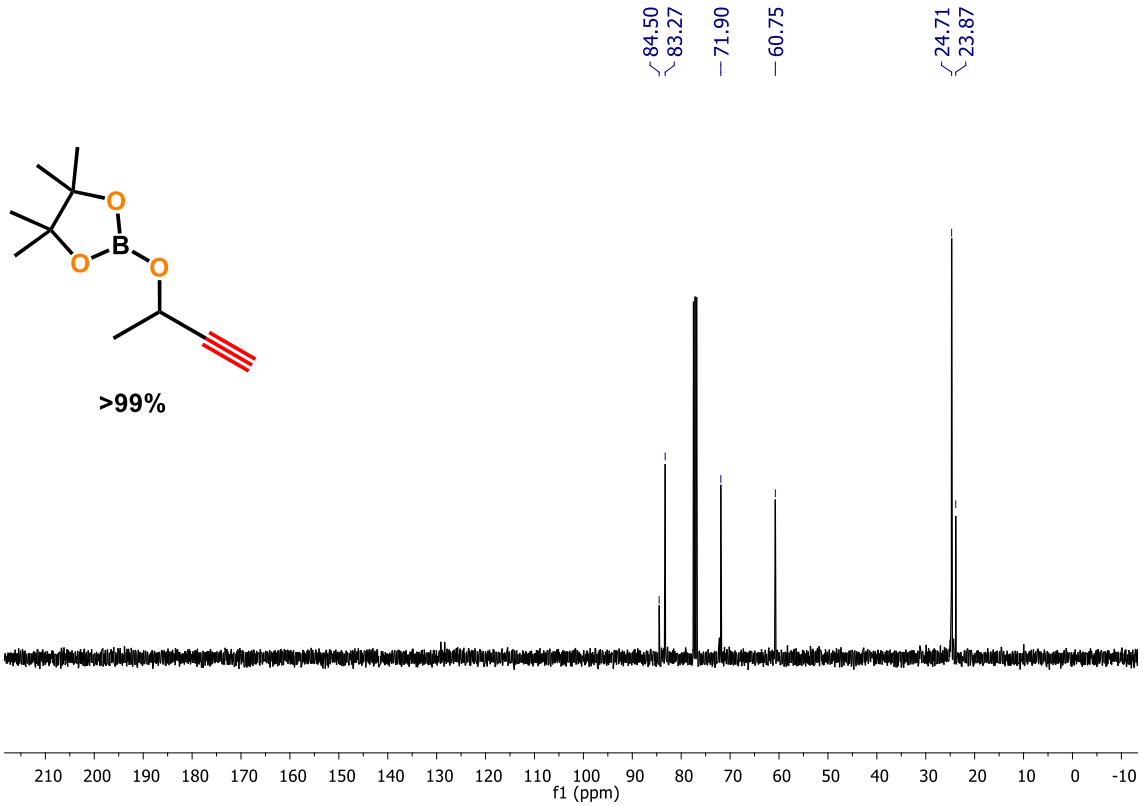

Figure S32. $^{13}C\{^{1}H\}$ NMR spectrum of **2h** (101 MHz, $CDCl_3$, 298K).

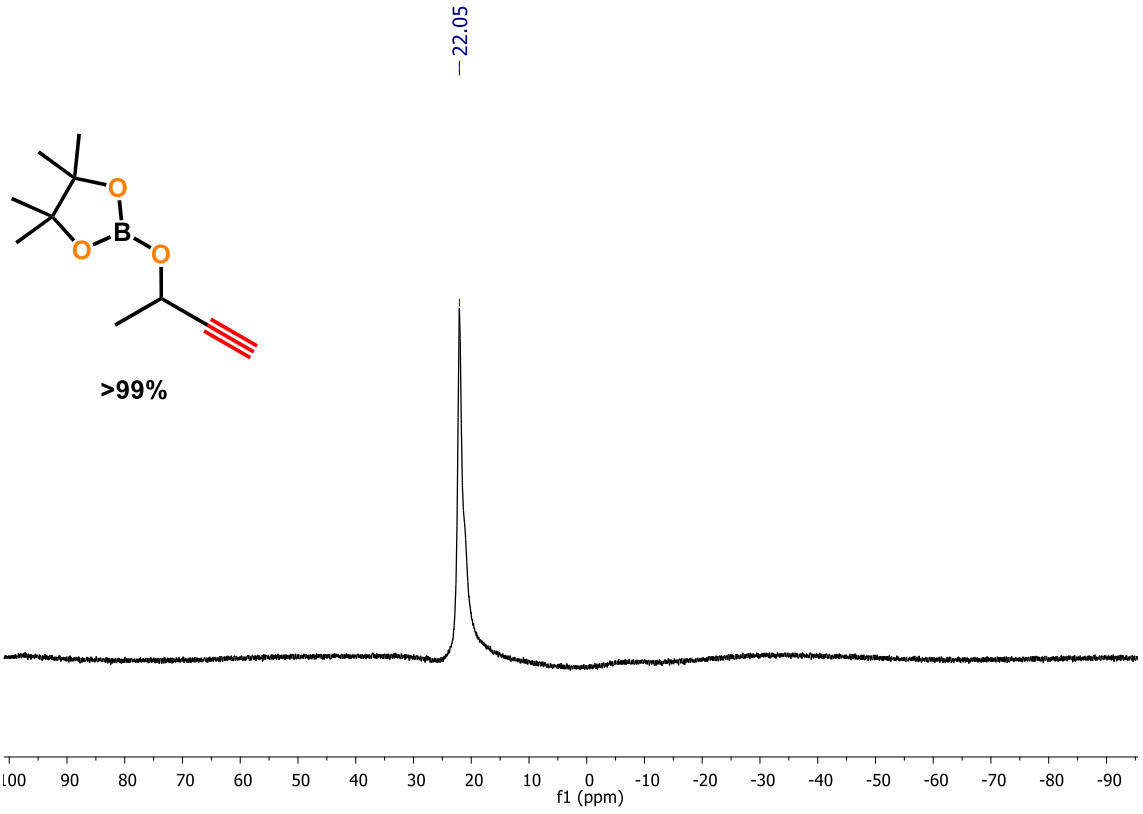

Figure S33. ^{11}B NMR spectrum of **2h** (128 MHz, $CDCl_3$, 298K).

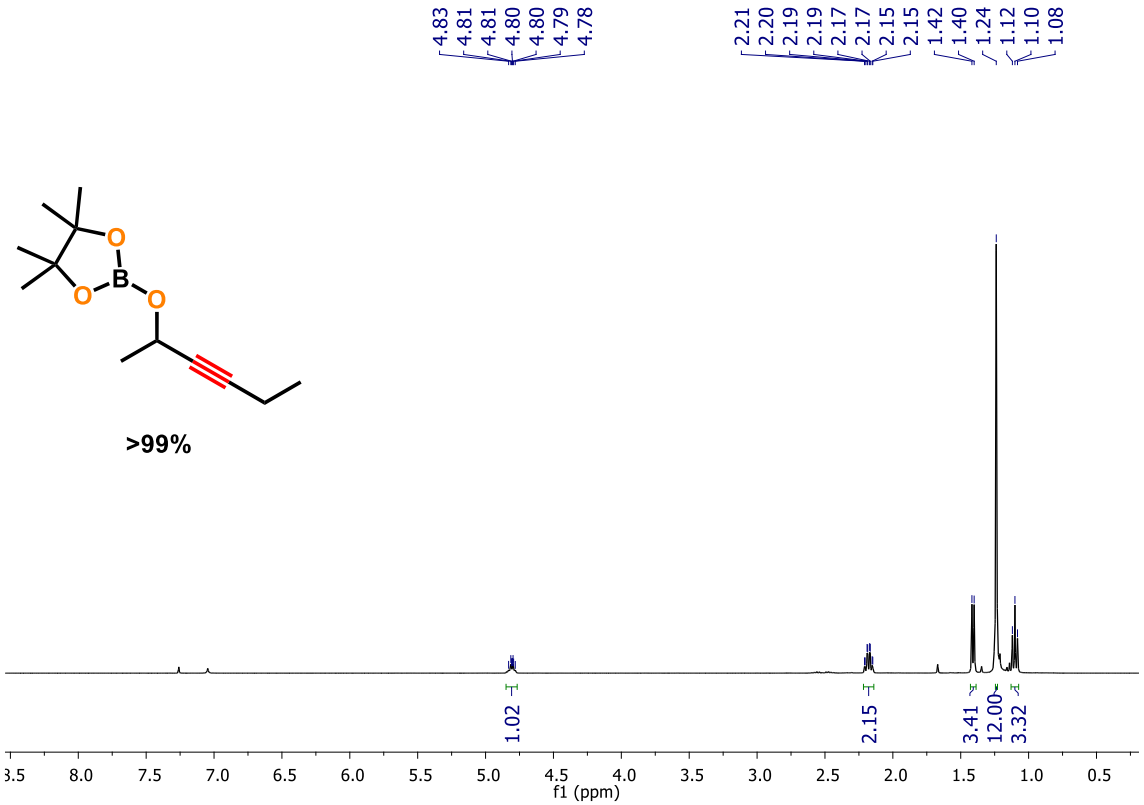

Figure S34. ^{1}H NMR spectrum of **2i** (400 MHz, $CDCl_3$, 298K).

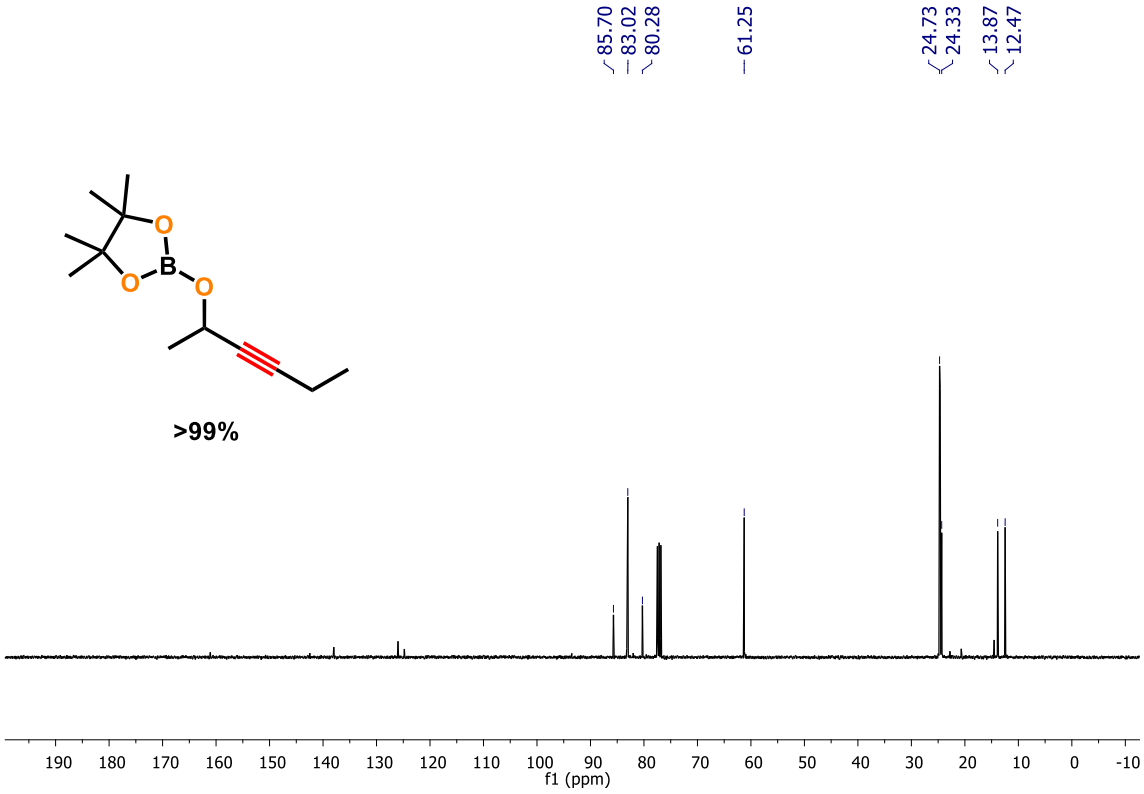

Figure S35. $^{13}C\{^{1}H\}$ NMR spectrum of **2i** (101 MHz, $CDCl_3$, 298K).

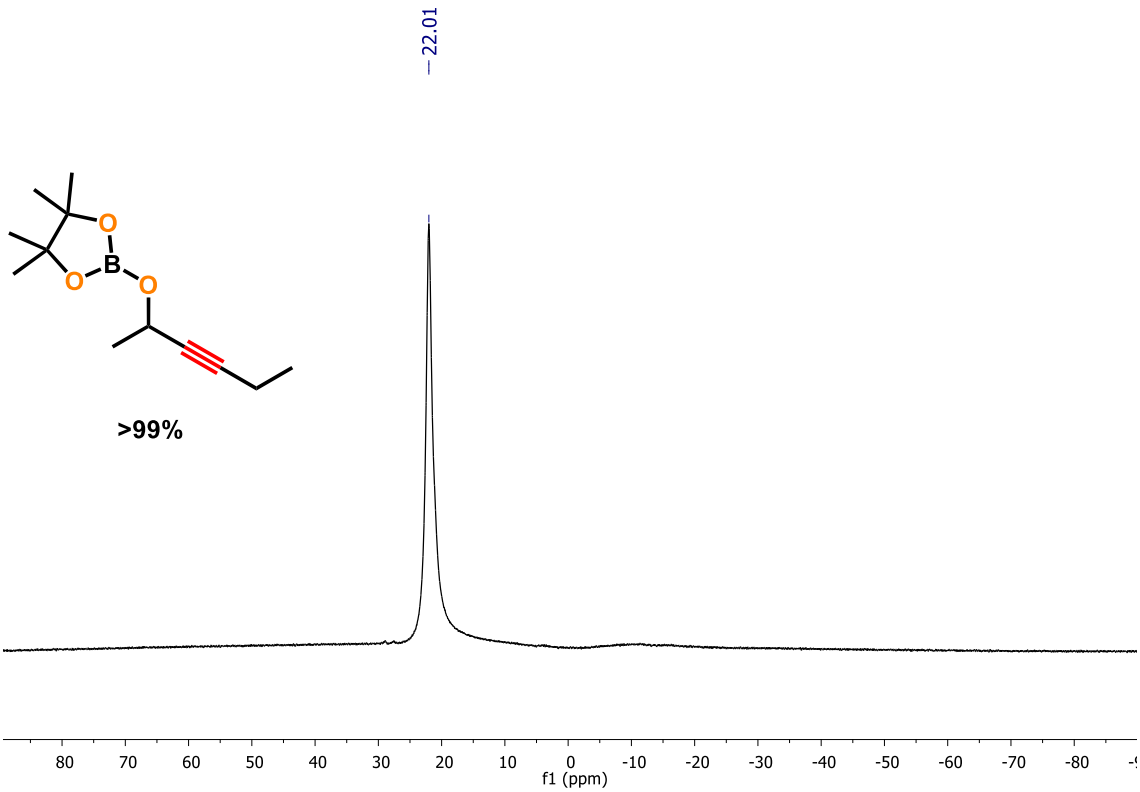

Figure S36. ^{11}B NMR spectrum of **2i** (128 MHz, $CDCl_3$, 298K).

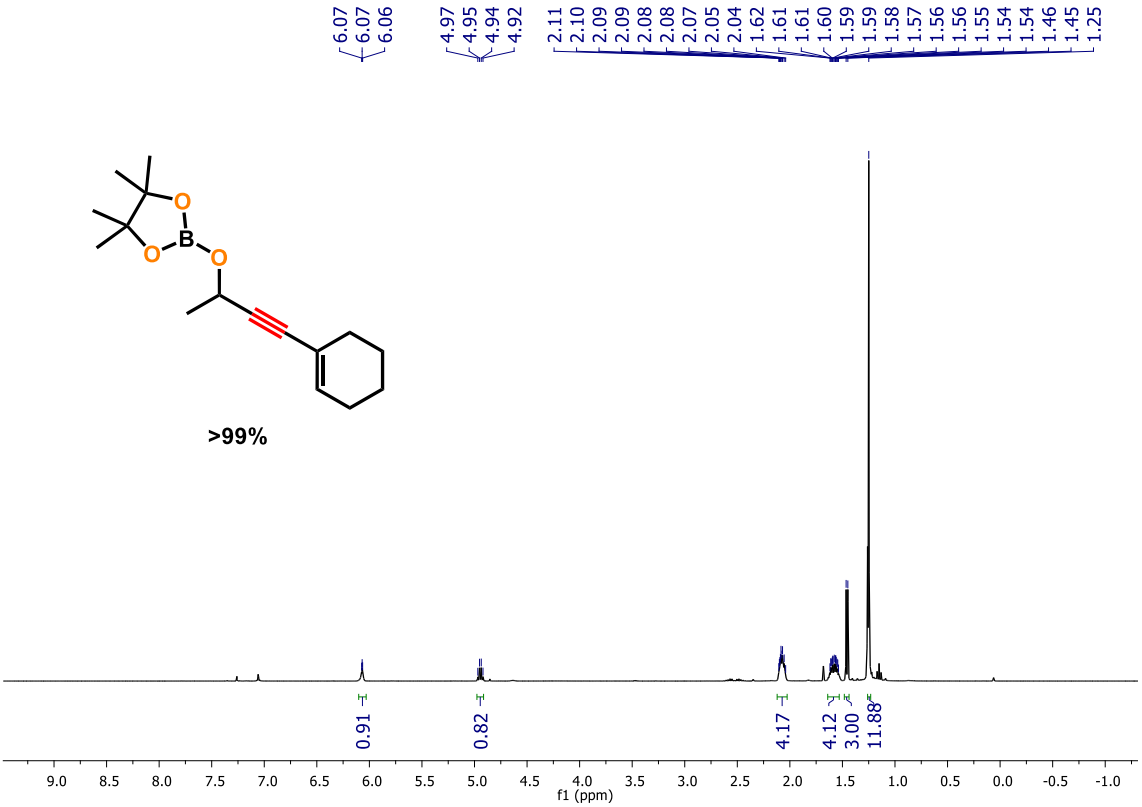

Figure S37. ^{1}H NMR spectrum of **2j** (400 MHz, $CDCl_3$, 298K).

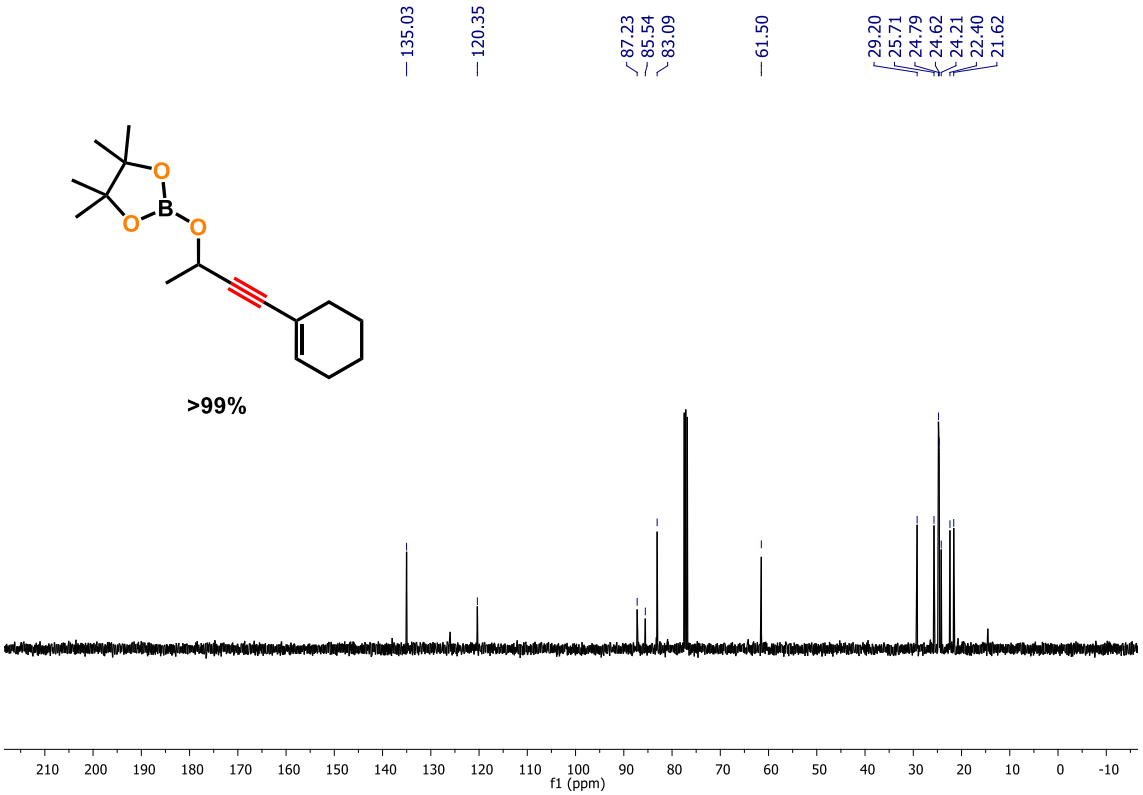

Figure S38. $^{13}C\{^{1}H\}$ NMR spectrum of **2j** (101 MHz, $CDCl_3$, 298K).

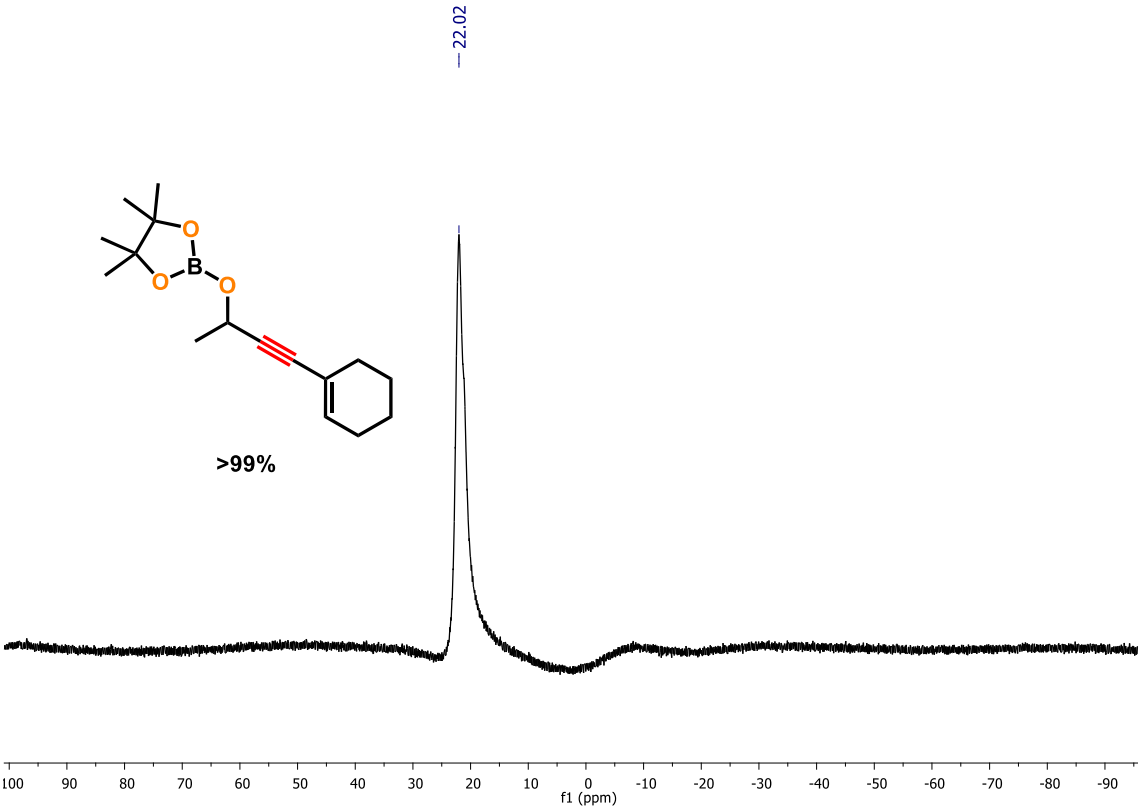

Figure S39. ^{11}B NMR spectrum of **2j** (128 MHz, $CDCl_3$, 298K).

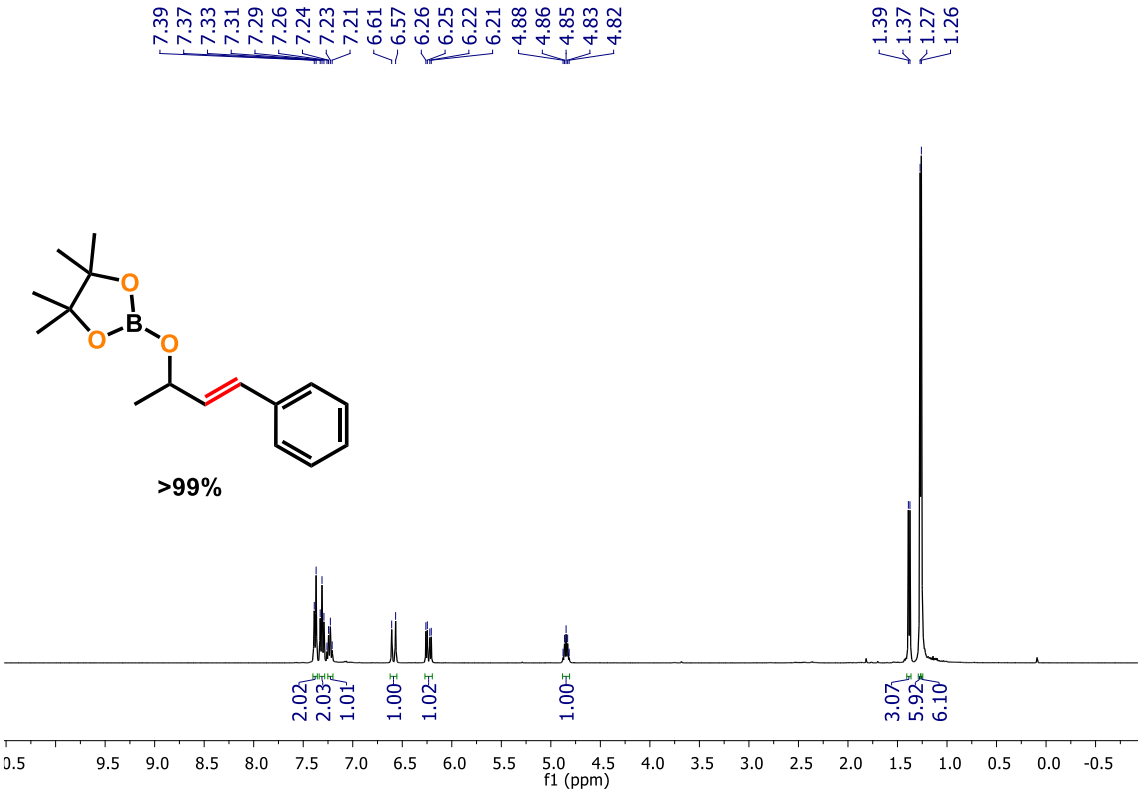

Figure S40. ^{1}H NMR spectrum of **4a** (400 MHz, $CDCl_3$, 298K).

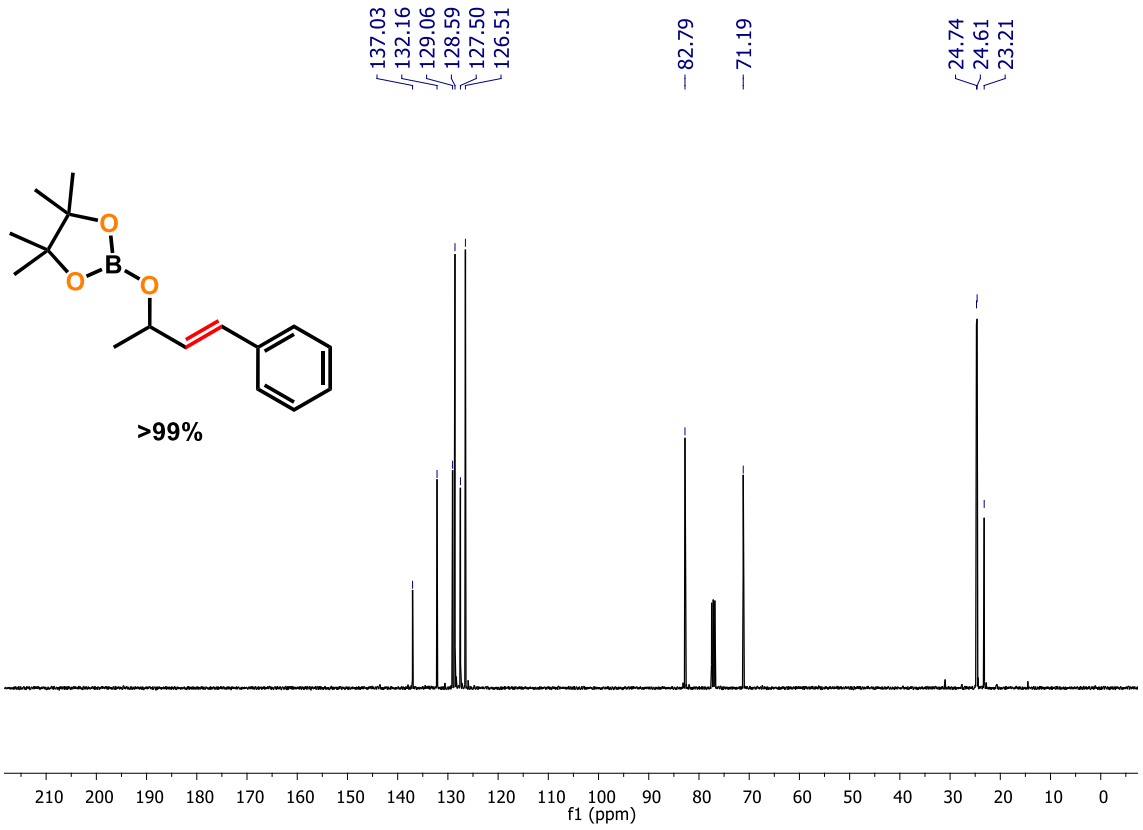

Figure S41. $^{13}C\{^{1}H\}$ NMR spectrum of **4a** (101 MHz, $CDCl_3$, 298K).

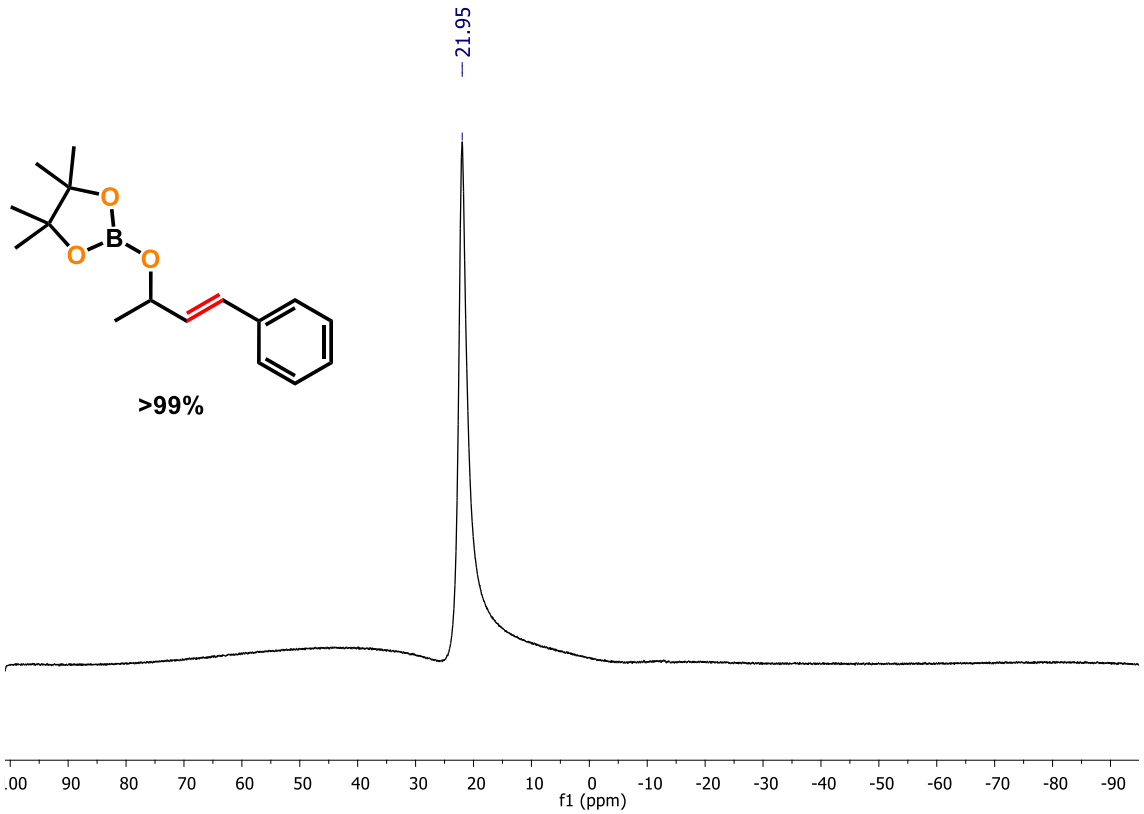

Figure S42. ^{11}B NMR spectrum of **4a** (128 MHz, $CDCl_3$, 298K).

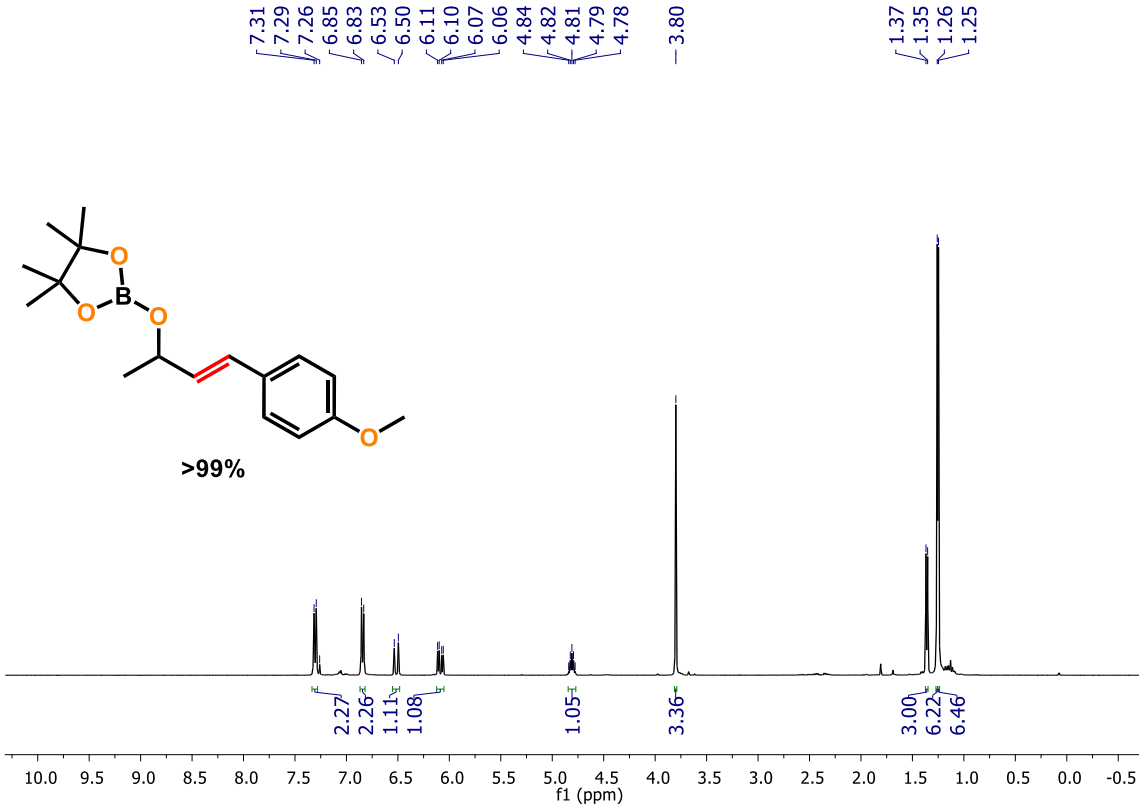

Figure S43. ^{1}H NMR spectrum of **4b** (400 MHz, $CDCl_3$, 298K).

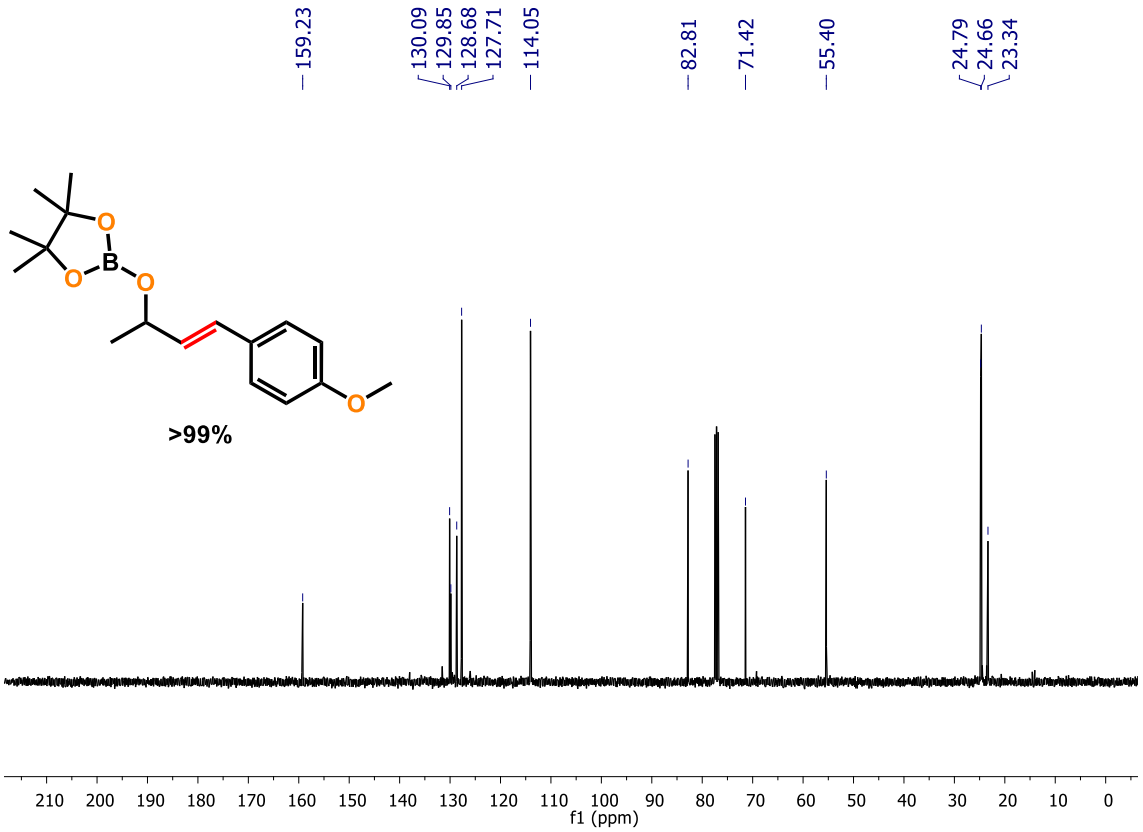

Figure S44. $^{13}C\{^{1}H\}$ NMR spectrum of **4b** (101 MHz, $CDCl_3$, 298K).

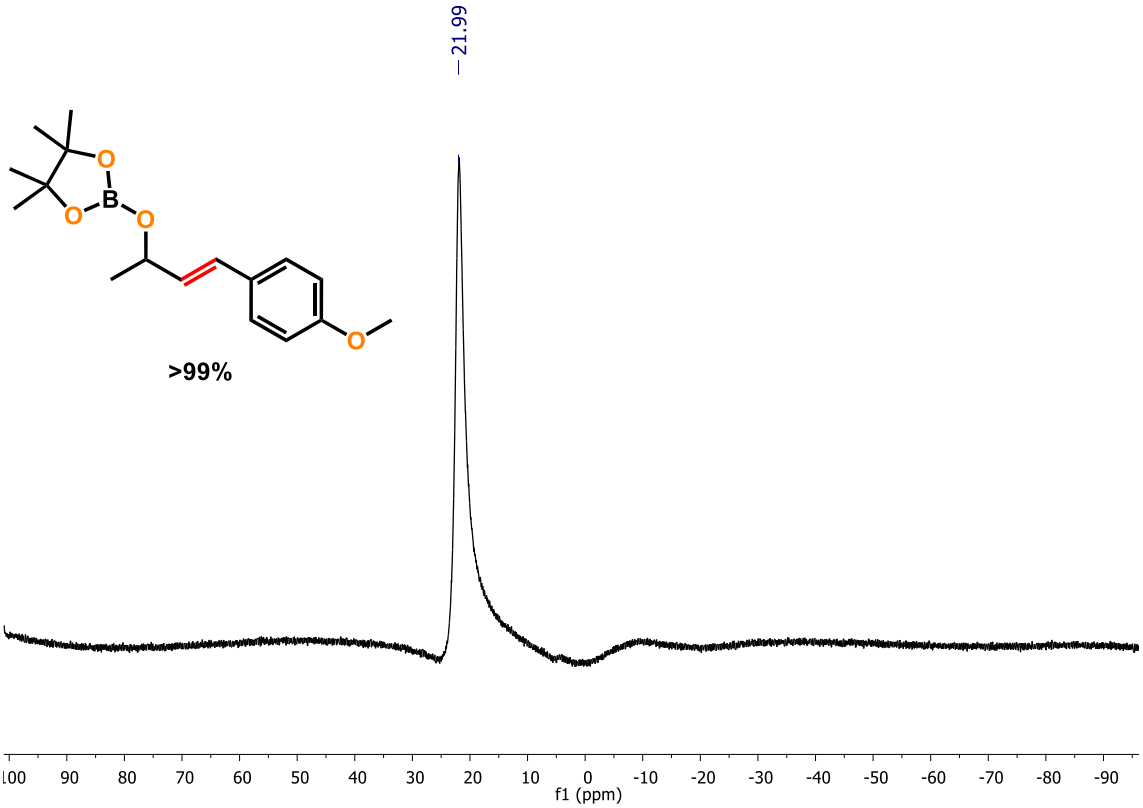

Figure S45. ^{11}B NMR spectrum of **4b** (128 MHz, $CDCl_3$, 298K).

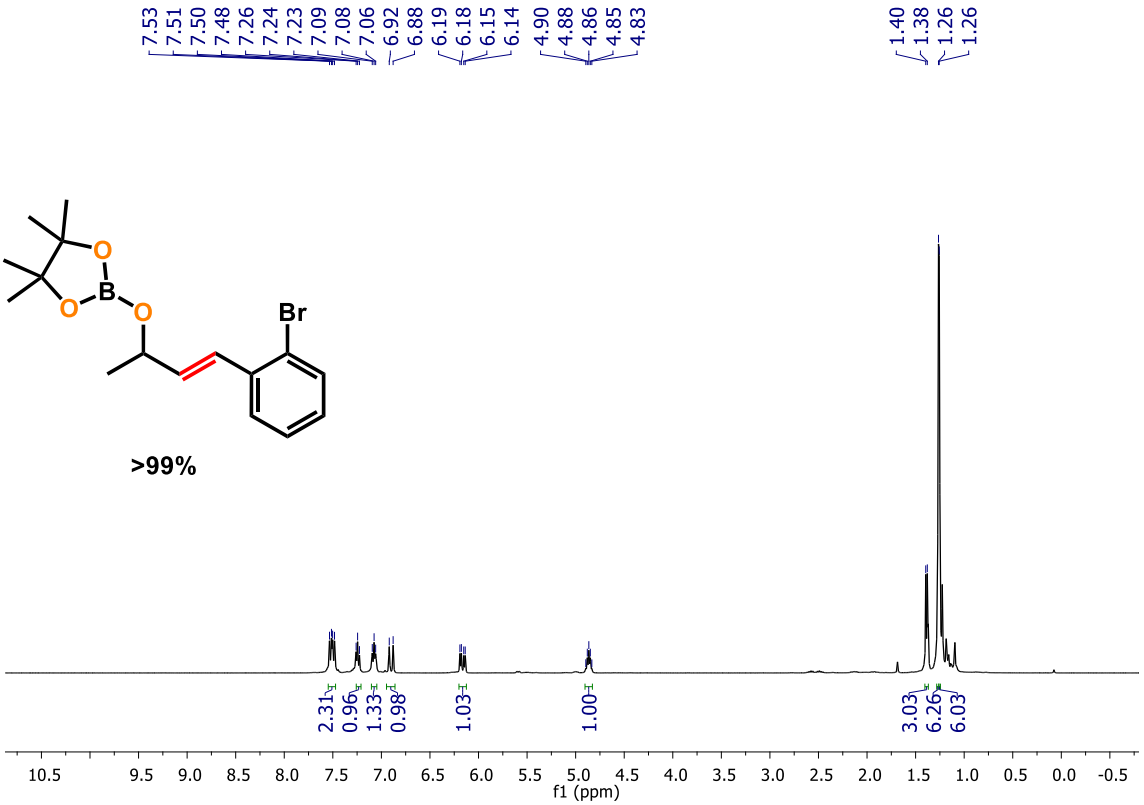

Figure S46. ^{1}H NMR spectrum of **4c** (400 MHz, $CDCl_3$, 298K).

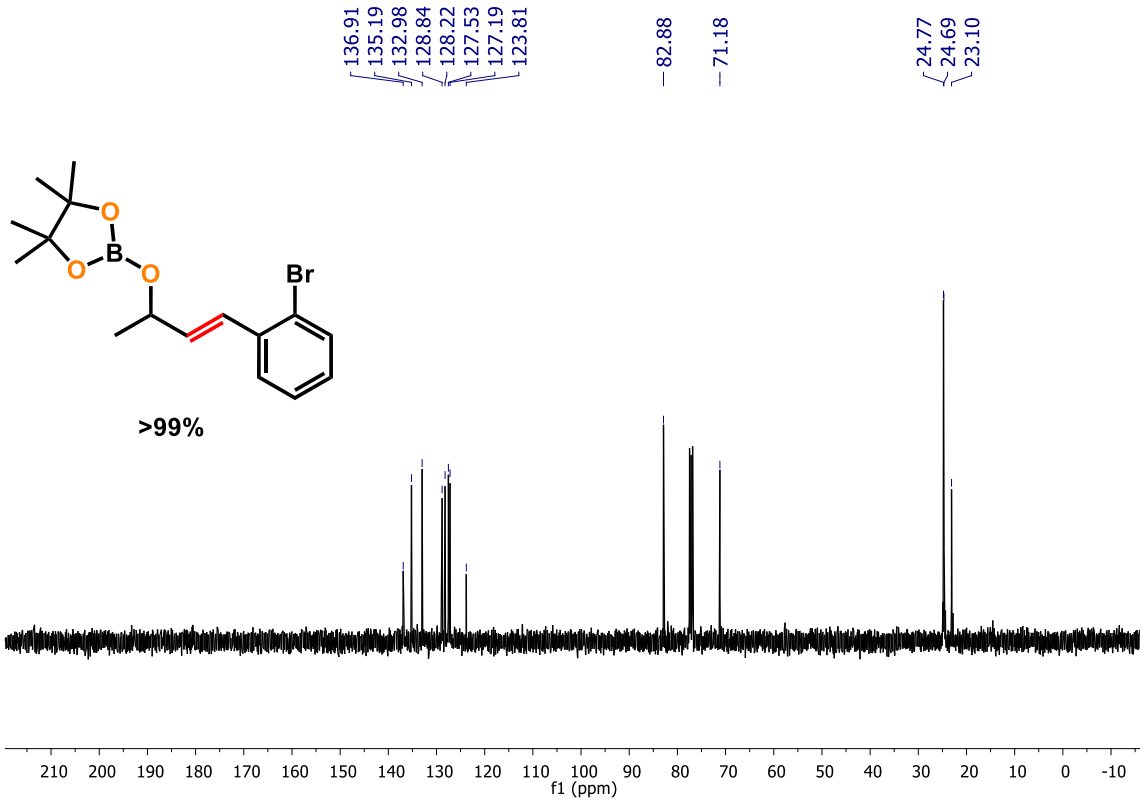

Figure S47. $^{13}C\{^{1}H\}$ NMR spectrum of **4c** (101 MHz, $CDCl_3$, 298K).

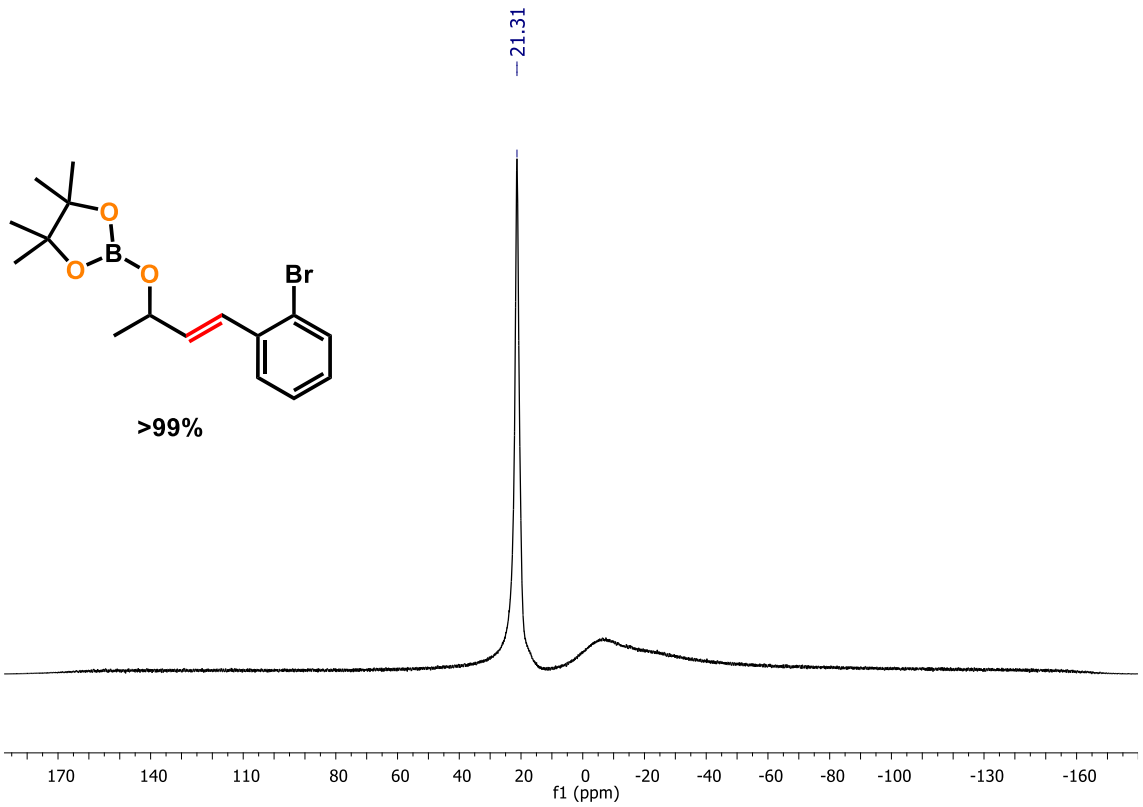

Figure S48. ^{11}B NMR spectrum of **4c** (128 MHz, $CDCl_3$, 298K).

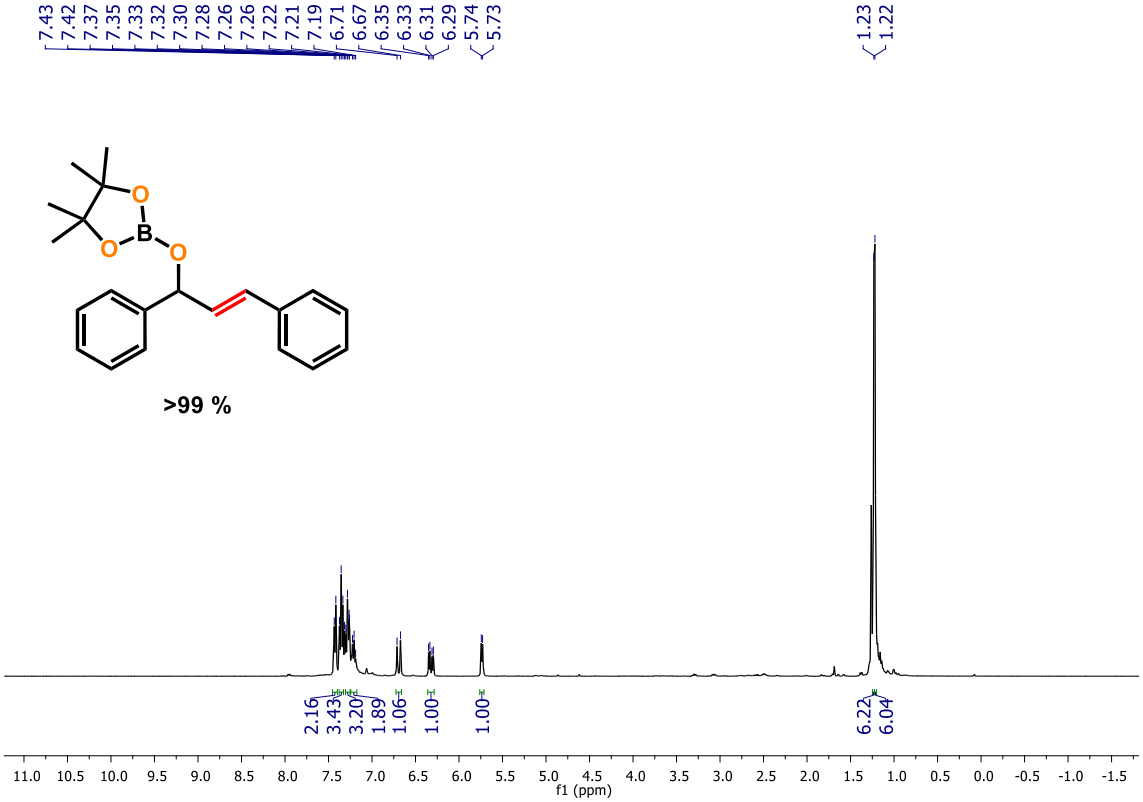

Figure S49. ^{1}H NMR spectrum of **4d** (400 MHz, $CDCl_3$, 298K).

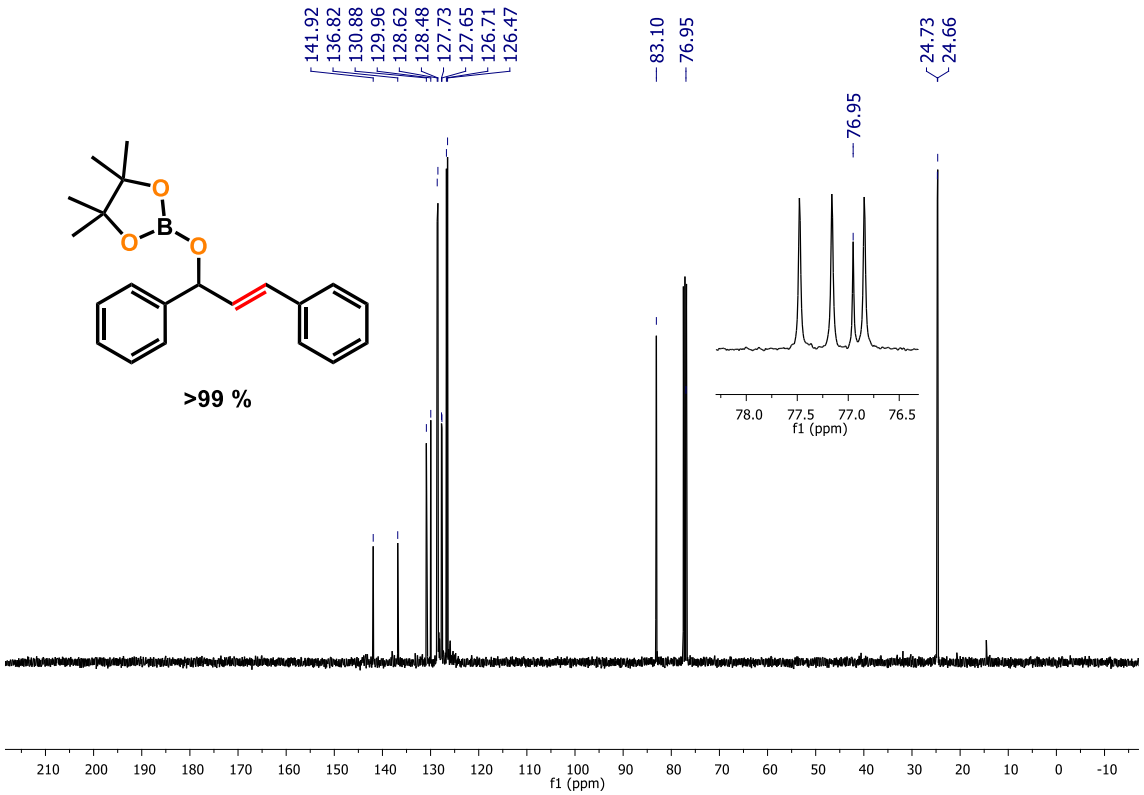

Figure S50. $^{13}C\{^{1}H\}$ NMR spectrum of **4d** (101 MHz, $CDCl_3$, 298K).

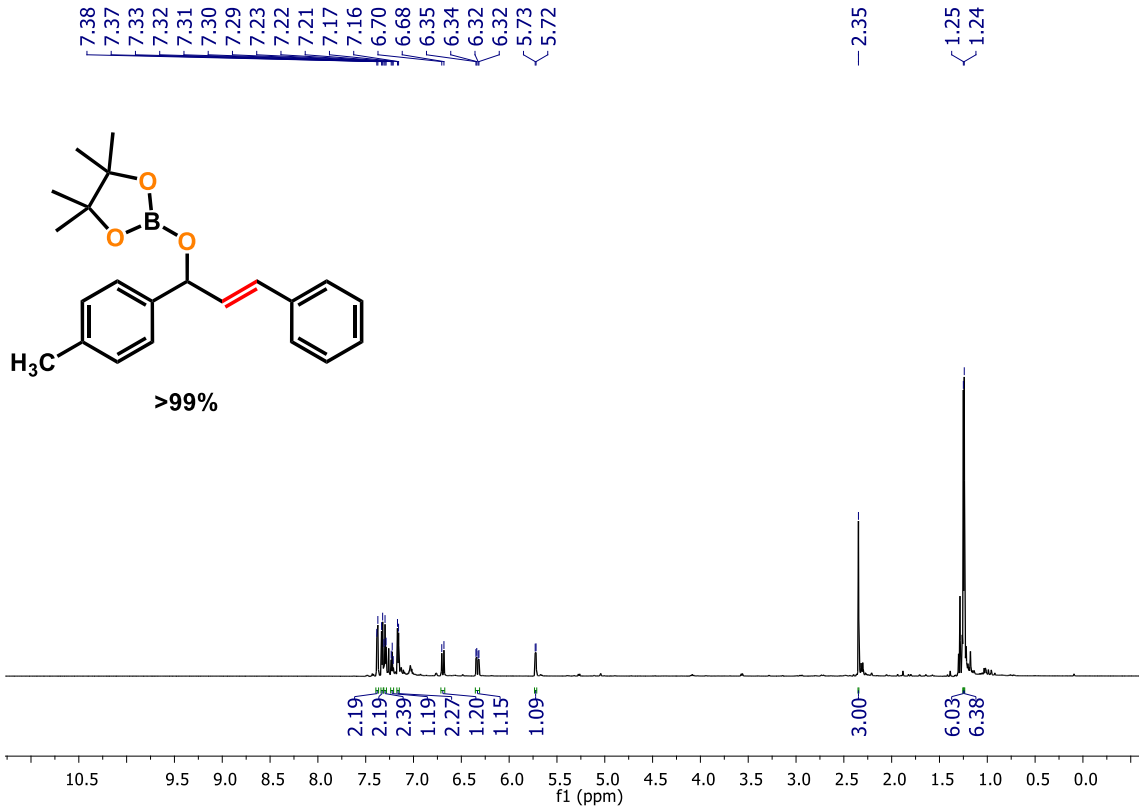

Figure S51. ^{1}H NMR spectrum of **4e** (700 MHz, $CDCl_3$, 298K).

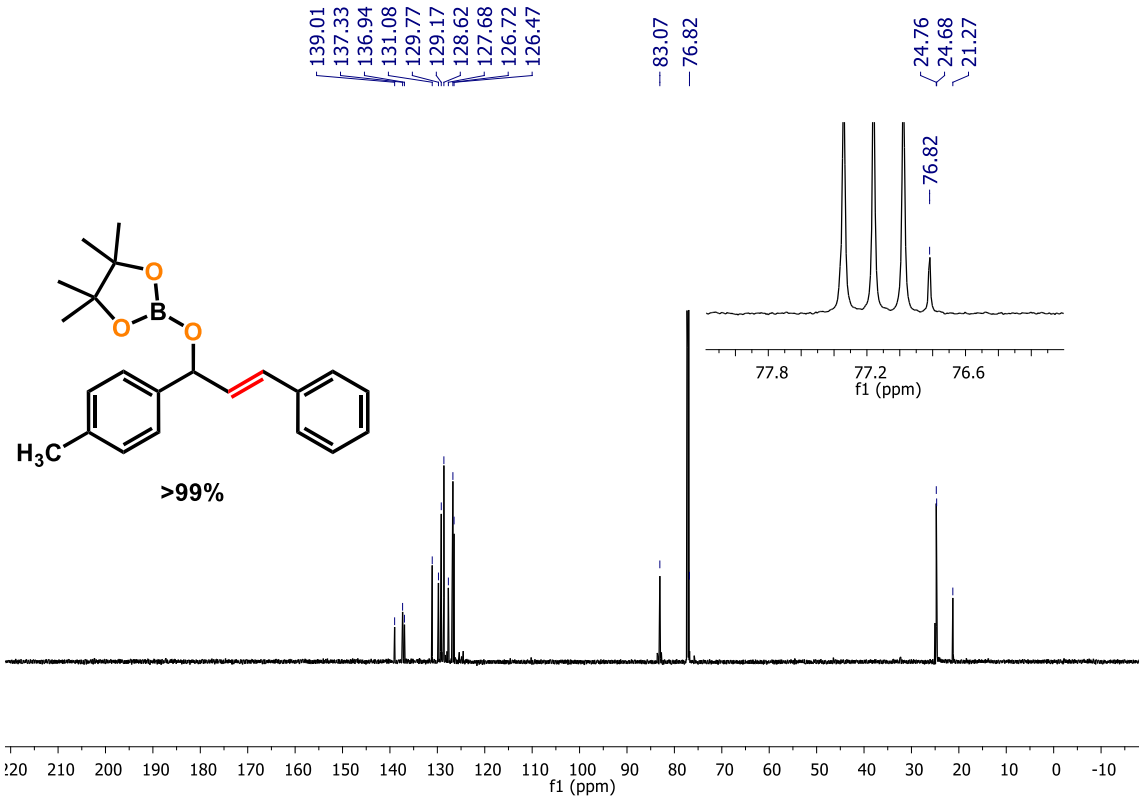

Figure S52. $^{13}C\{^{1}H\}$ NMR spectrum of **4e** (176 MHz, $CDCl_3$, 298K).

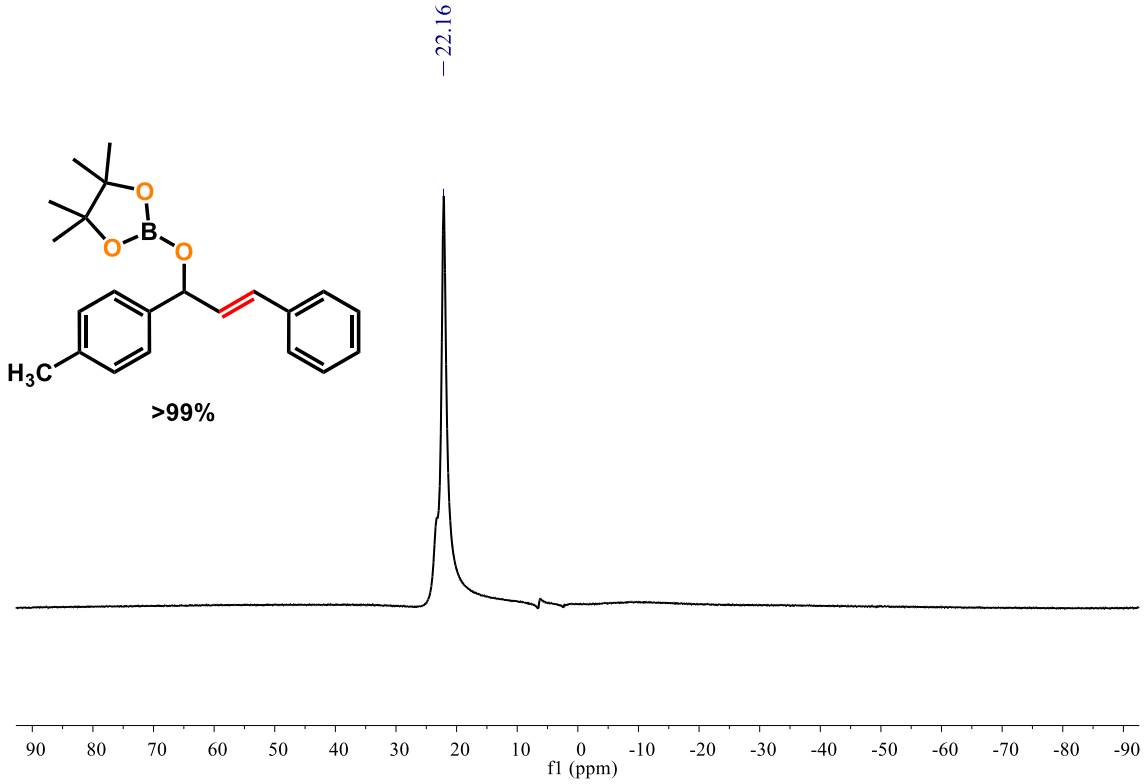

Figure S53. ^{11}B NMR spectrum of **4e** (128 MHz, $CDCl_3$, 298K).

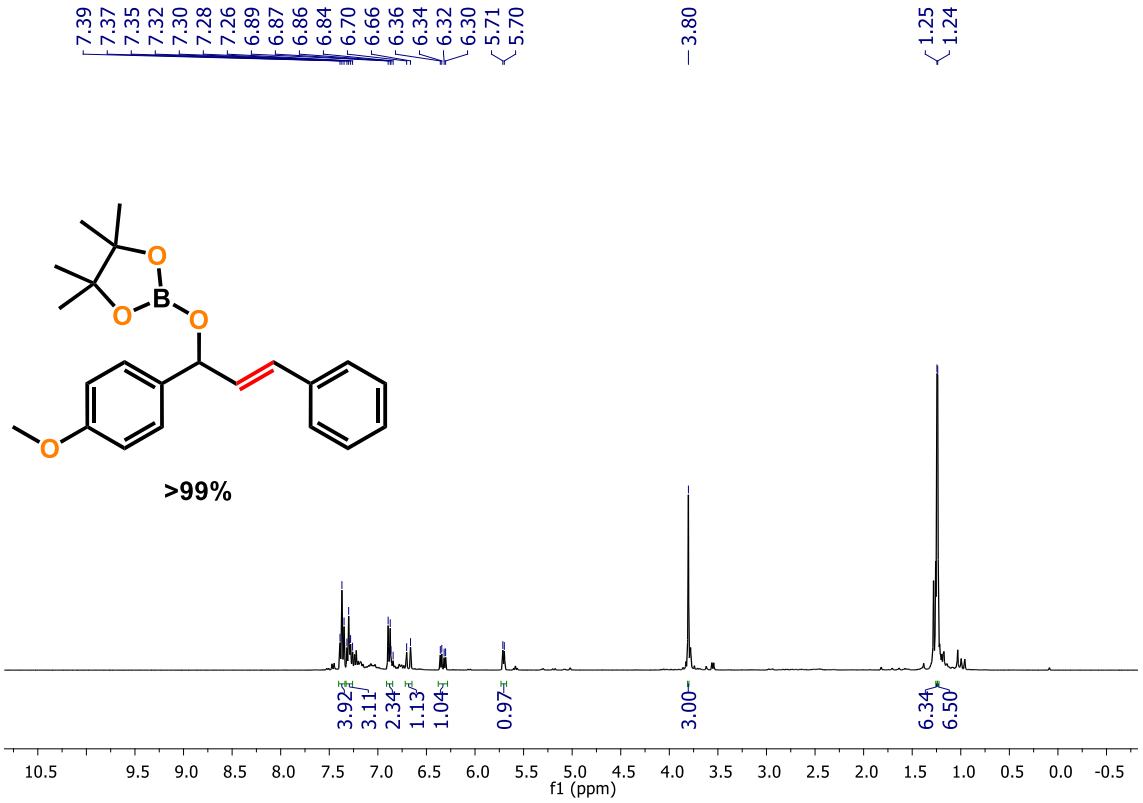

Figure S54. ^{1}H NMR spectrum of **4f** (400 MHz, $CDCl_3$, 298K).

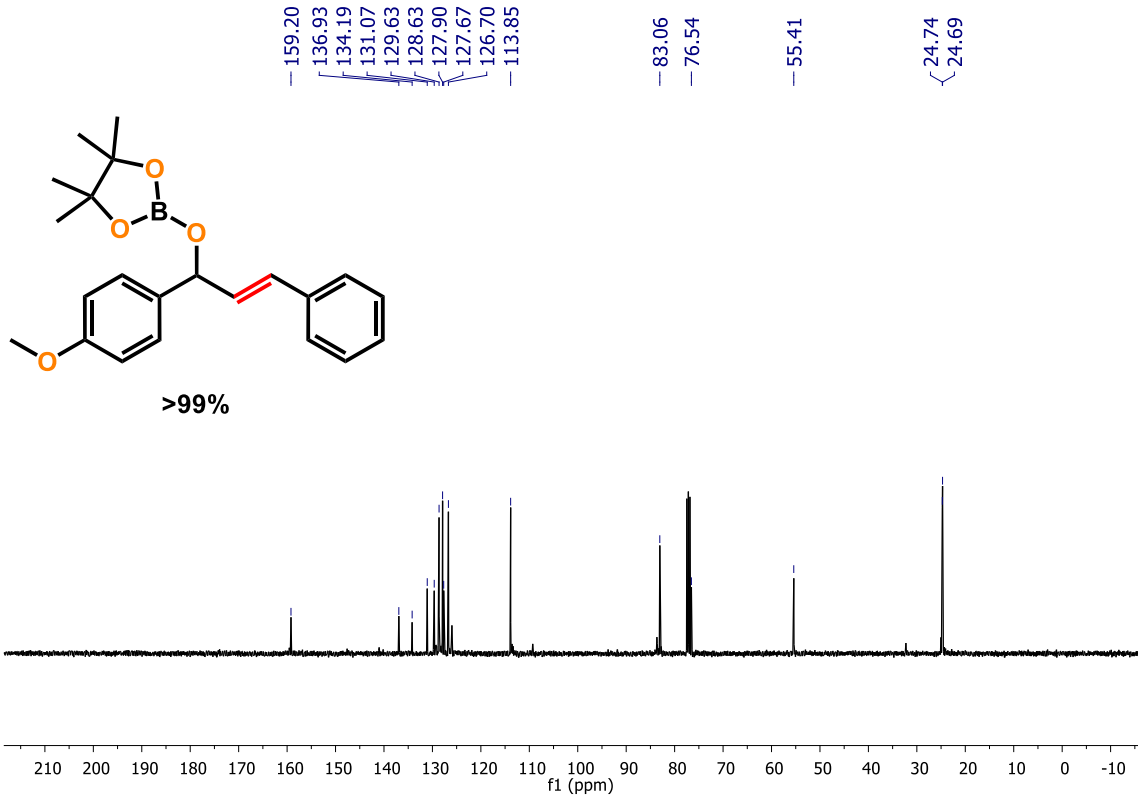

Figure S55. ^{13}C{^{1}H} NMR spectrum of **4f** (101 MHz, $CDCl_3$, 298K).

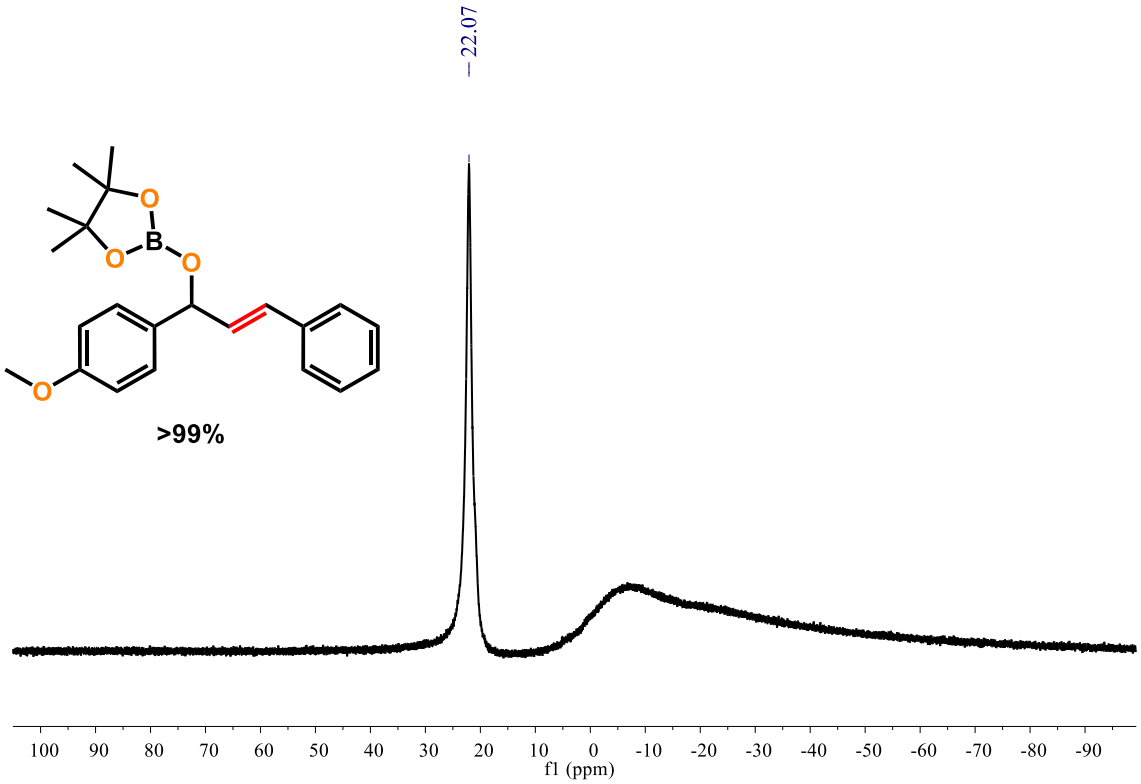

Figure S56. ^{11}B NMR spectrum of **4f** (128 MHz, $CDCl_3$, 298K).

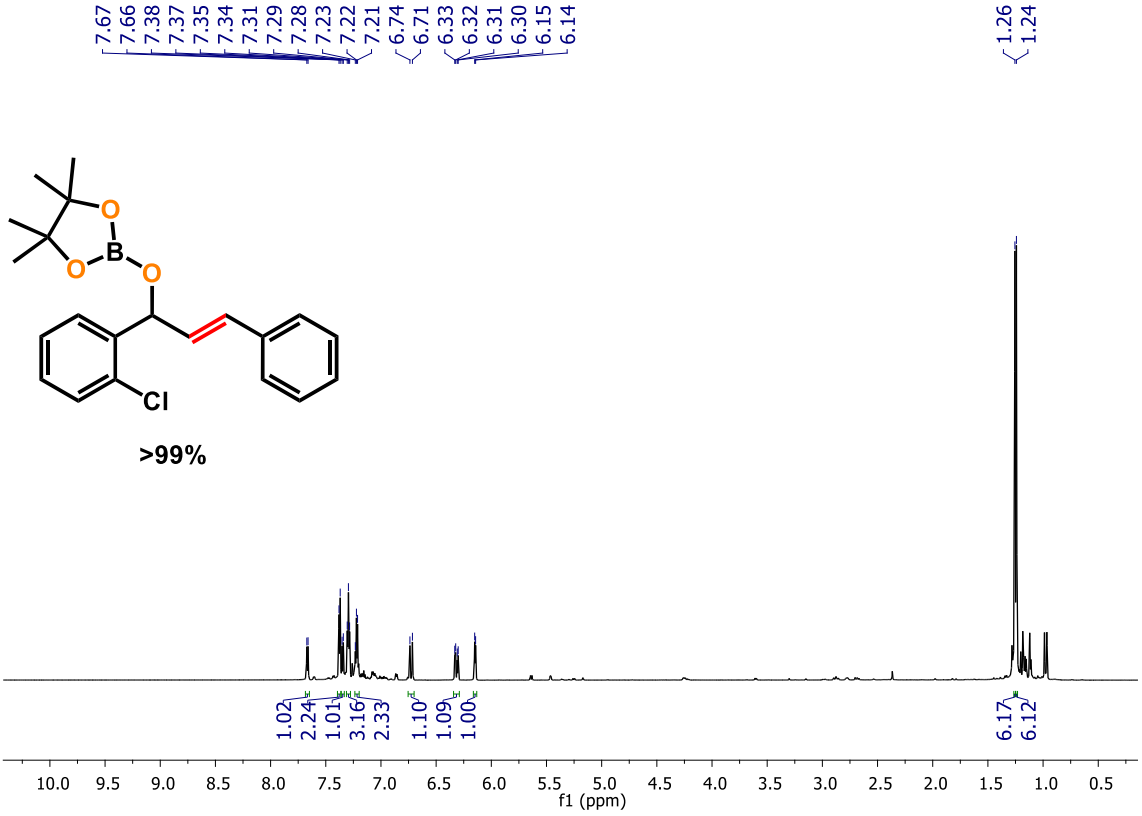

Figure S57. ^{1}H NMR spectrum of **4g** (700 MHz, $CDCl_3$, 298K).

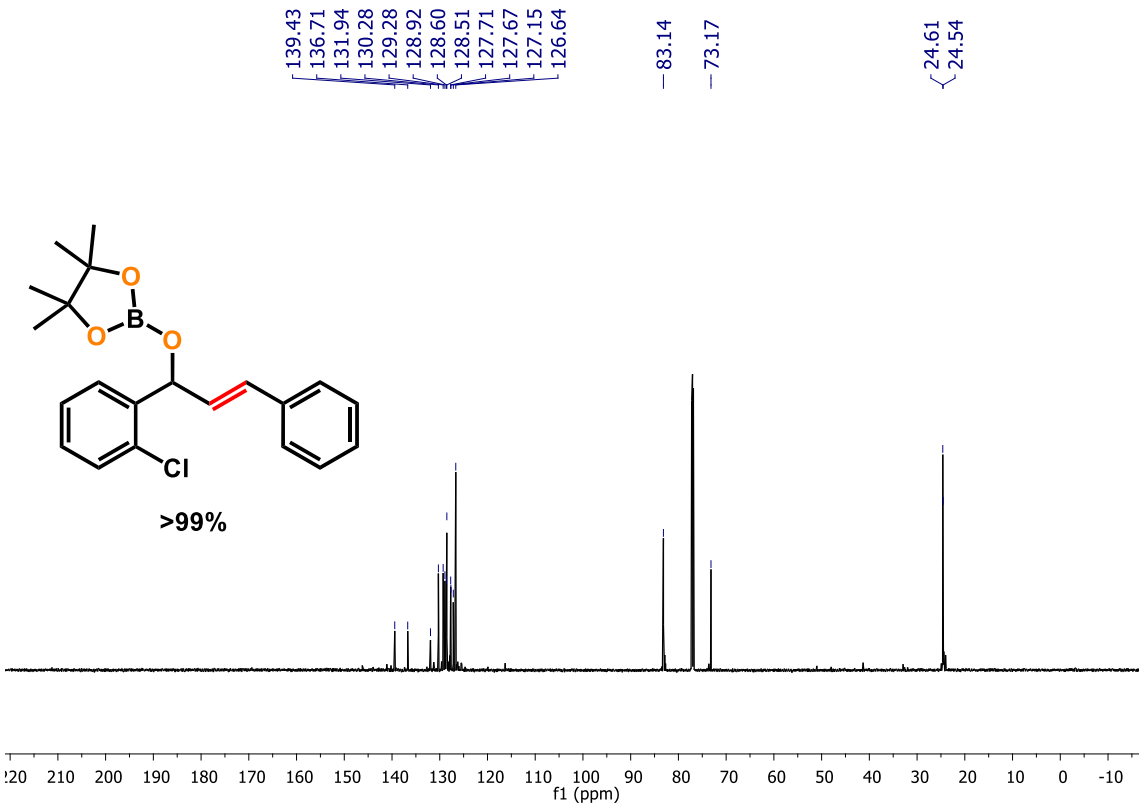

Figure S58. $^{13}C\{^{1}H\}$ NMR spectrum of **4g** (176 MHz, $CDCl_3$, 298K).

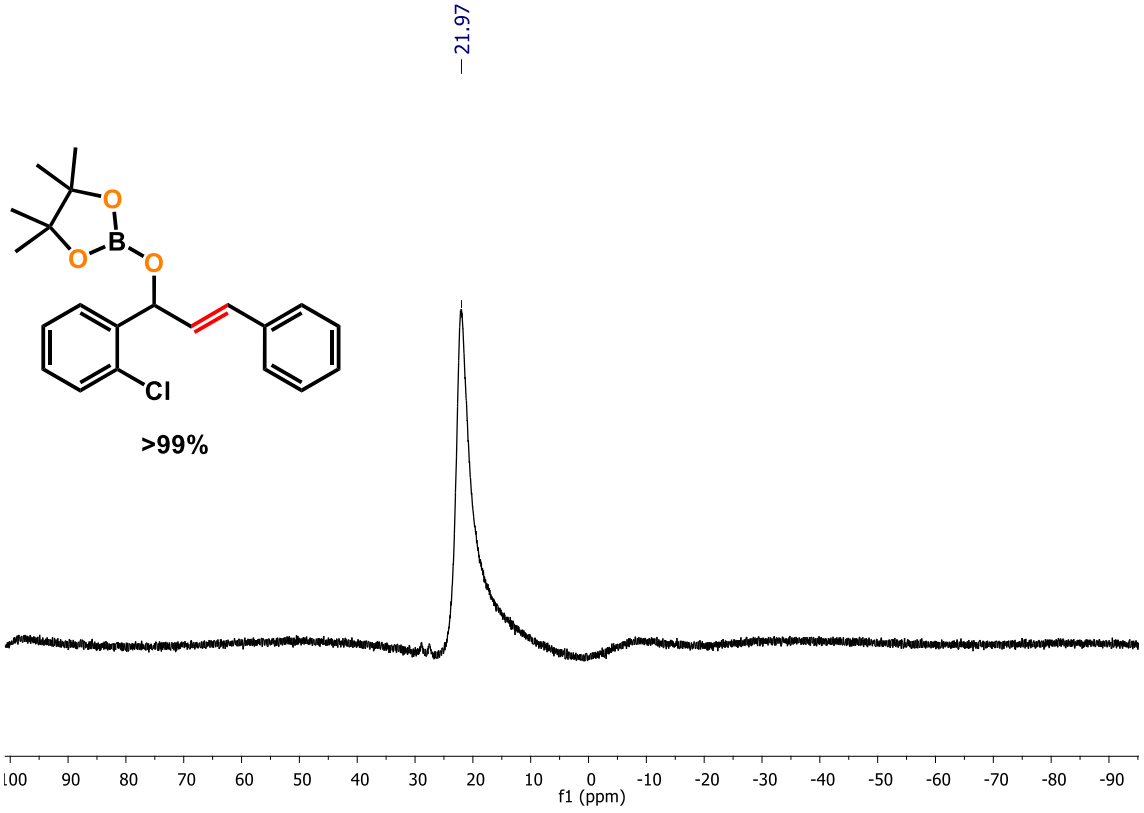

Figure S59. ^{11}B NMR spectrum of **4g** (128 MHz, $CDCl_3$, 298K).

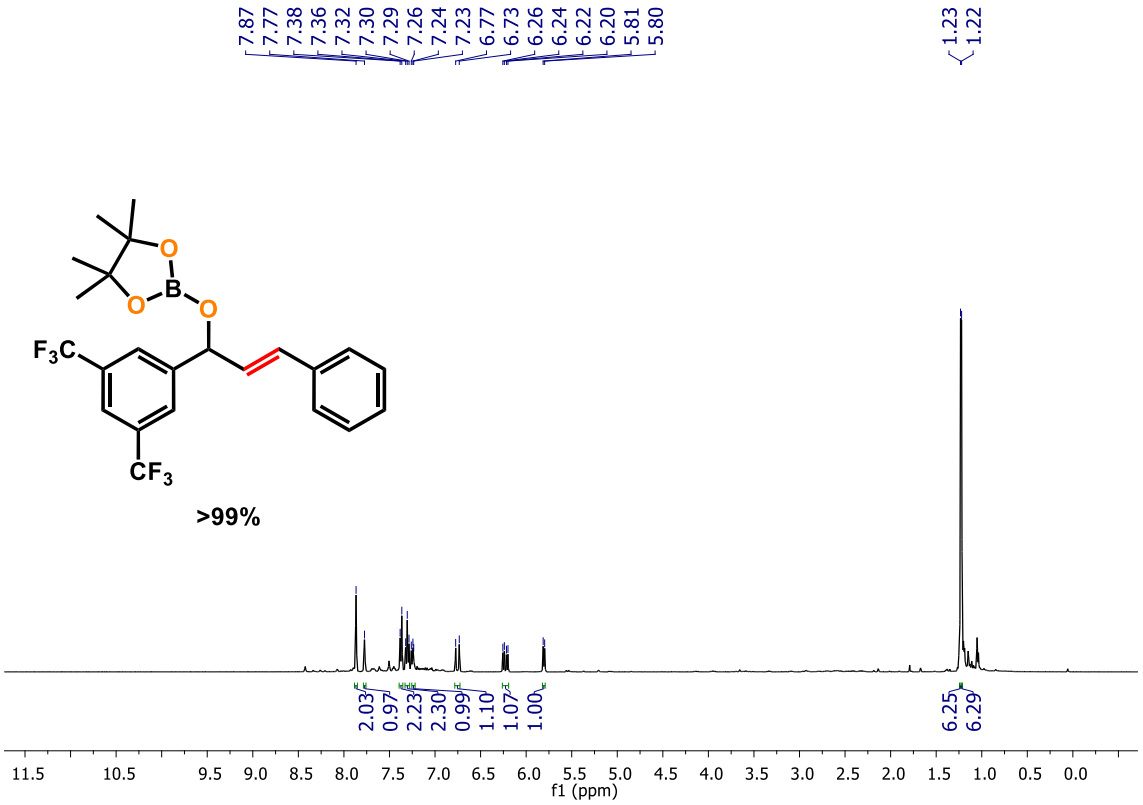

Figure S60. ^{1}H NMR spectrum of **4h** (400 MHz, $CDCl_3$, 298K).

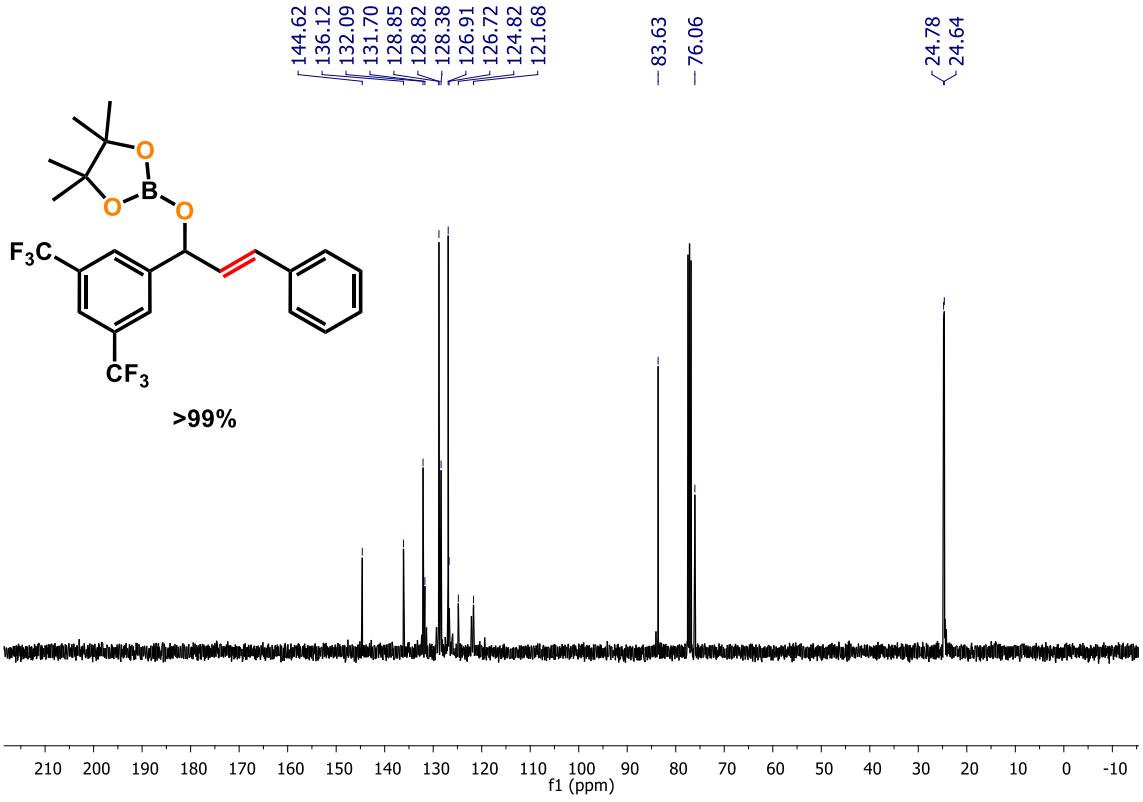

Figure S61. ^{13}C{^{1}H} NMR spectrum of **4h** (101 MHz, $CDCl_3$, 298K).

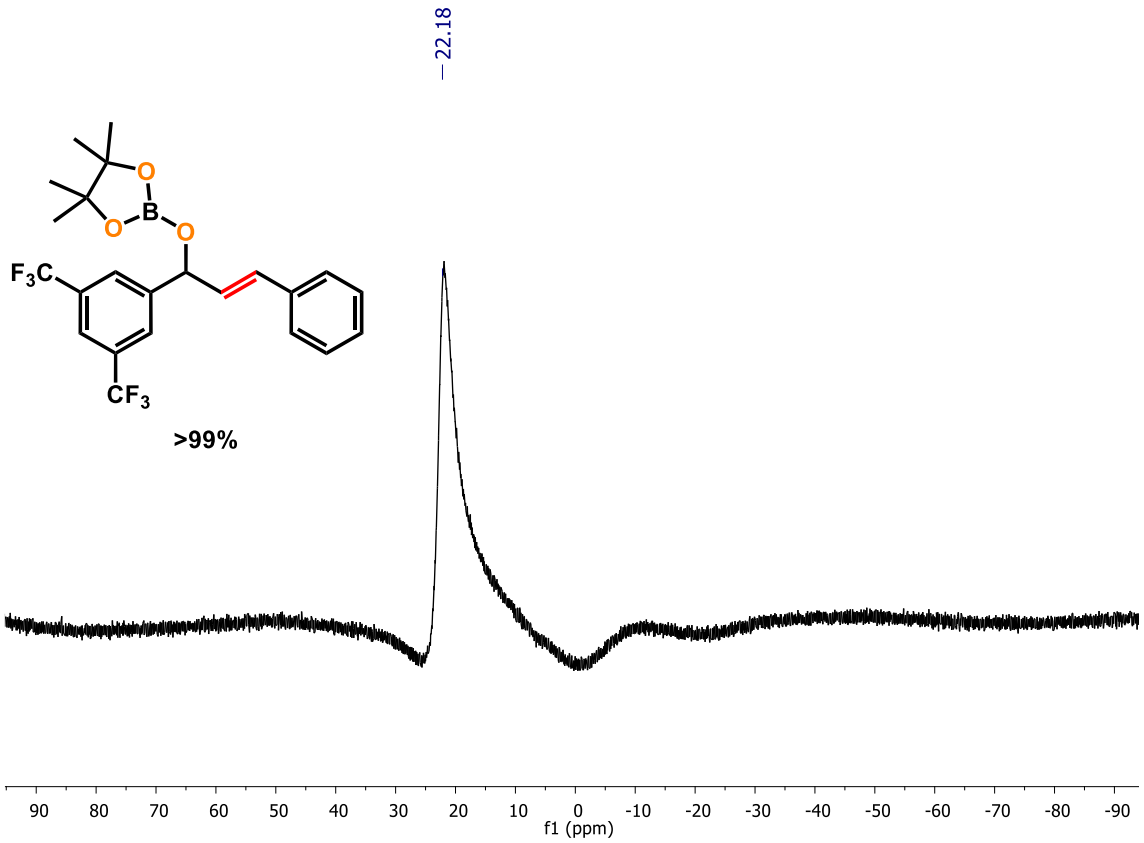

Figure S62. ^{11}B NMR spectrum of **4h** (128 MHz, $CDCl_3$, 298K).

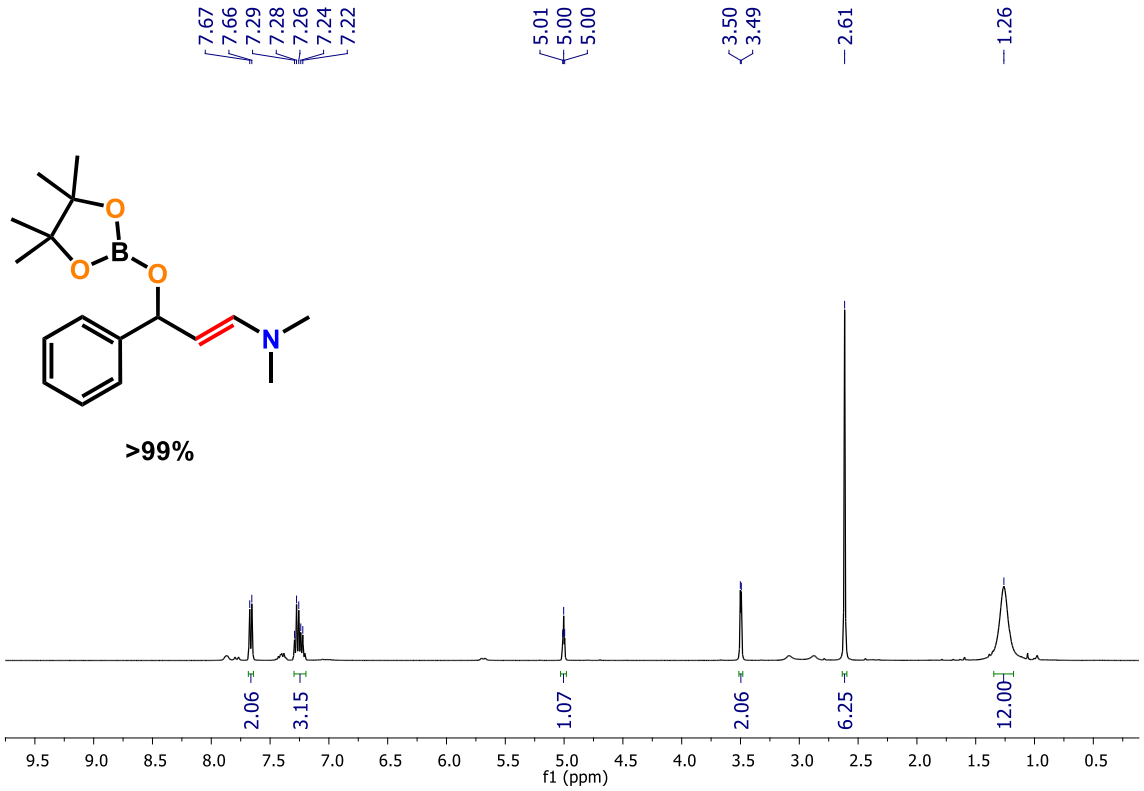

Figure S63. ^{1}H NMR spectrum of **4i** (400 MHz, $CDCl_3$, 298K).

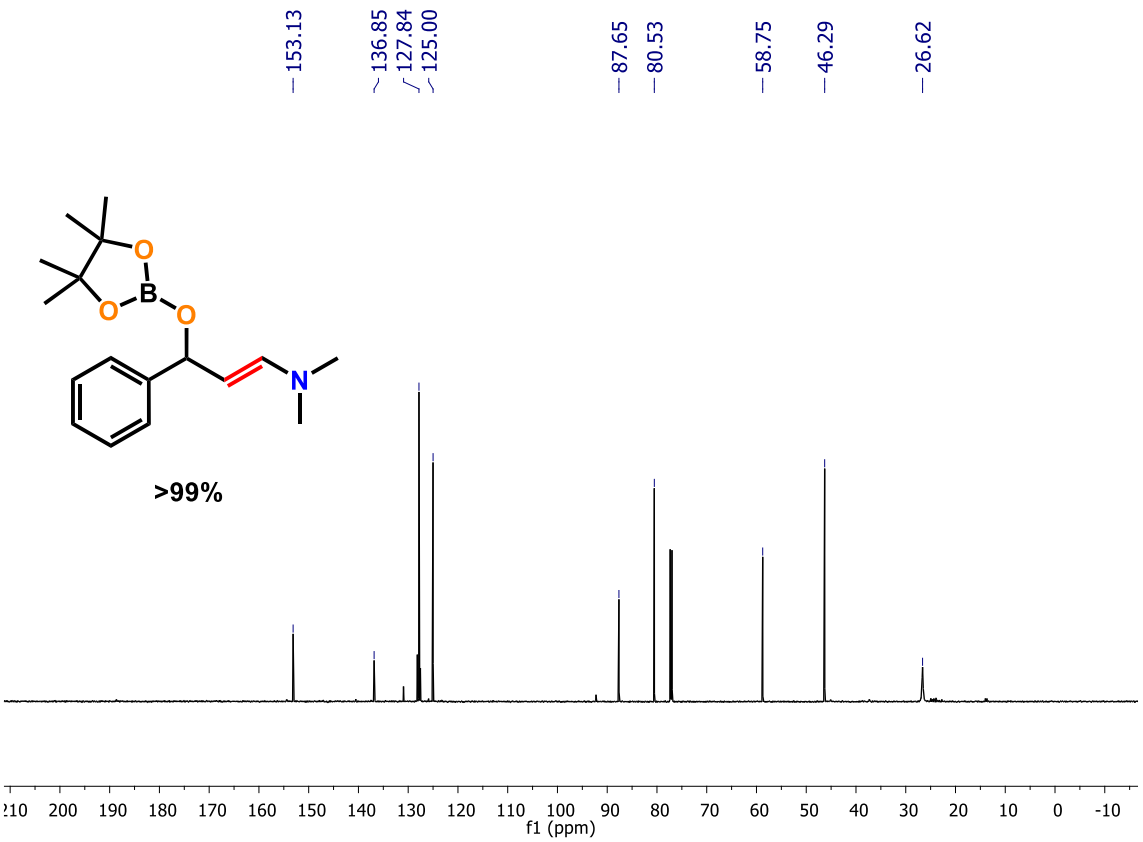

Figure S64. $^{13}C\{^{1}H\}$ NMR spectrum of **4i** (176 MHz, $CDCl_3$, 298K).

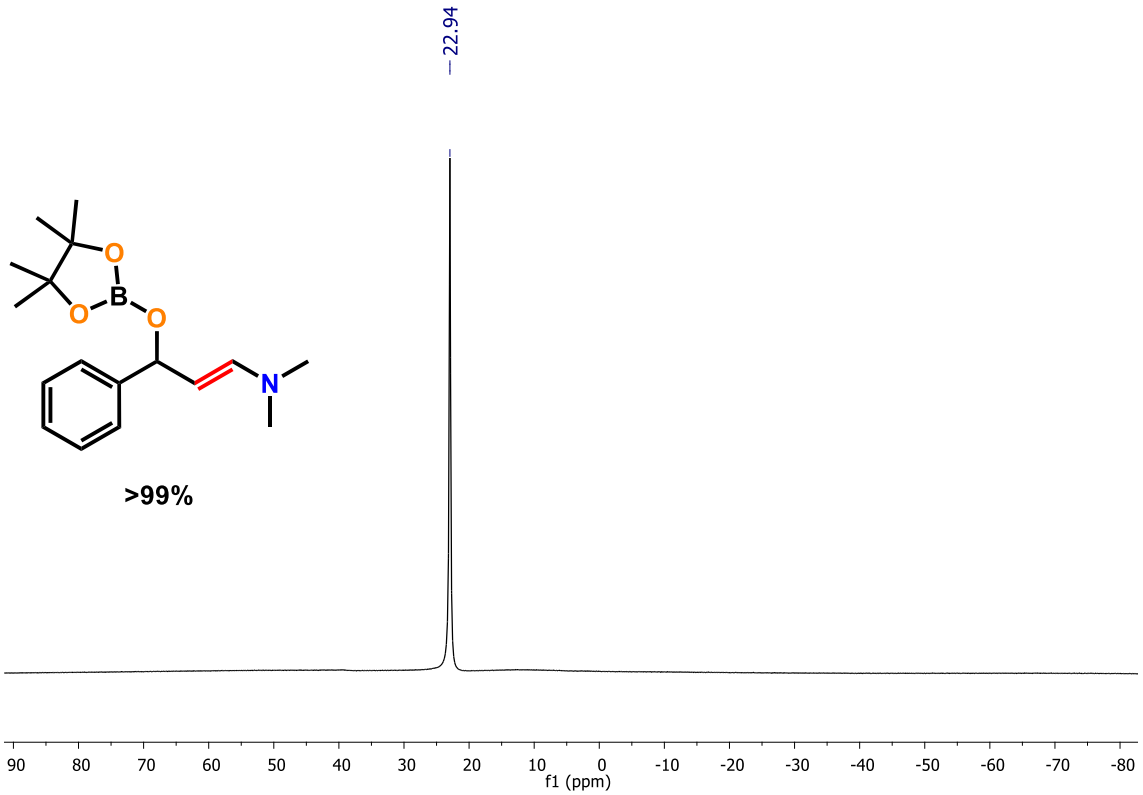

Figure S65. ^{11}B NMR spectrum of **4i** (128 MHz, $CDCl_3$, 298K).

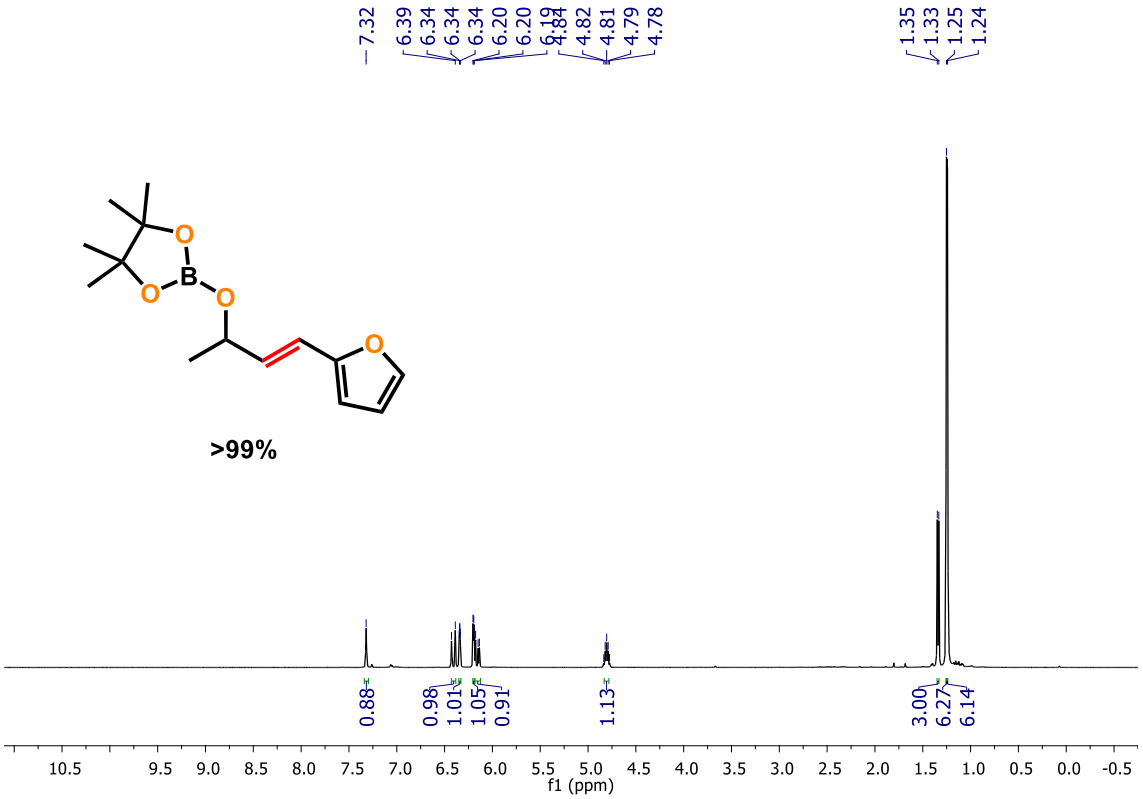

Figure S66. ^{1}H NMR spectrum of **4j** (400 MHz, $CDCl_3$, 298K).

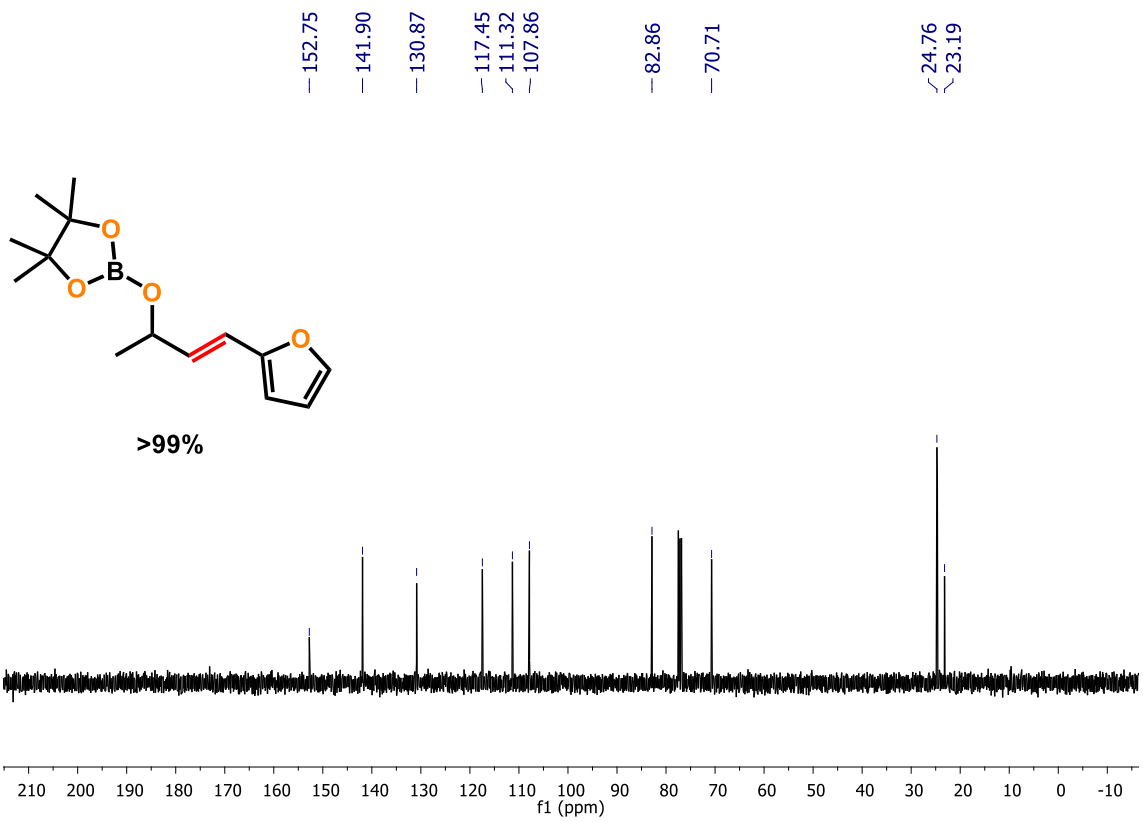

Figure S67. $^{13}C\{^{1}H\}$ NMR spectrum of **4j** (101 MHz, $CDCl_3$, 298K).

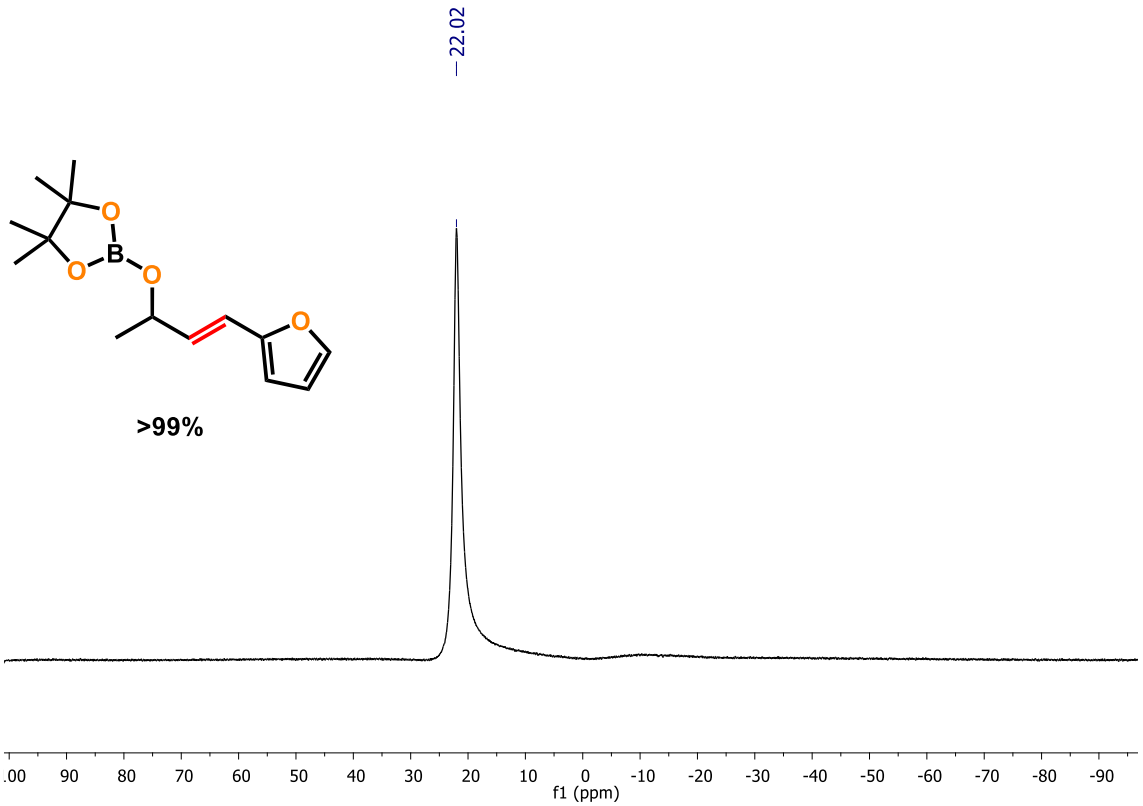

Figure S68. ^{11}B NMR spectrum of **4j** (128 MHz, $CDCl_3$, 298K).

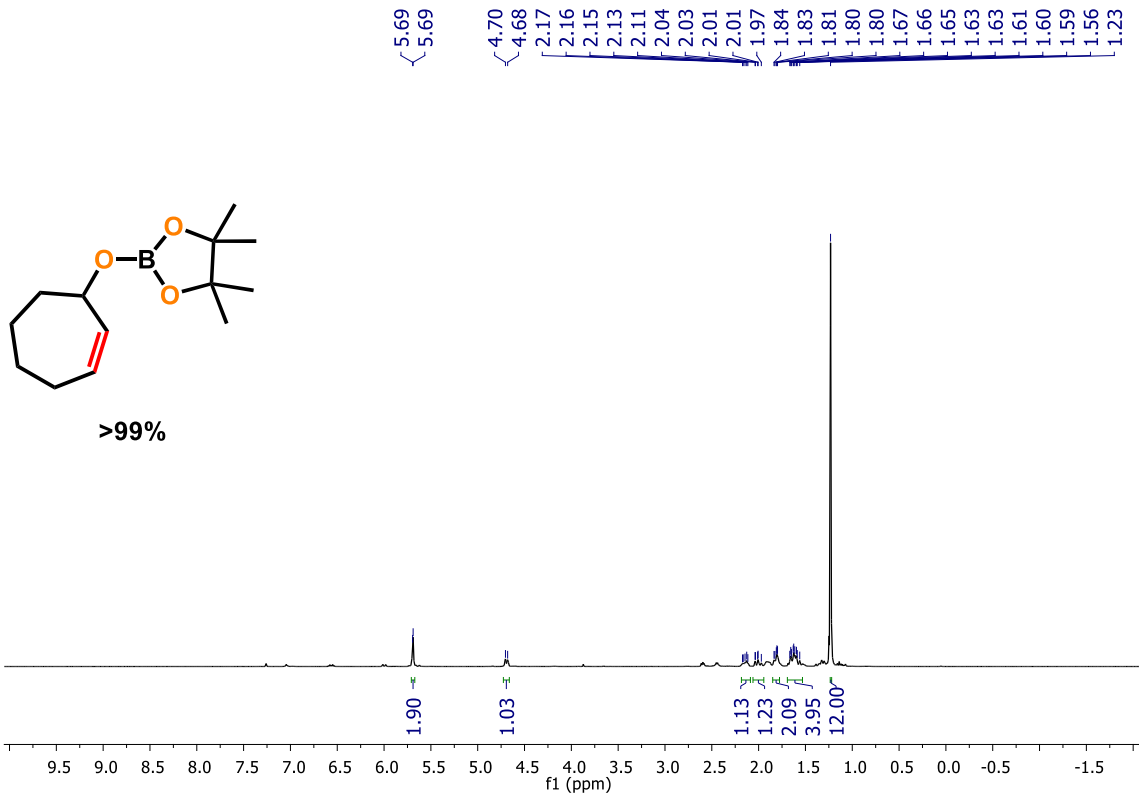

Figure S69. ^{1}H NMR spectrum of **4k** (400 MHz, $CDCl_3$, 298K).

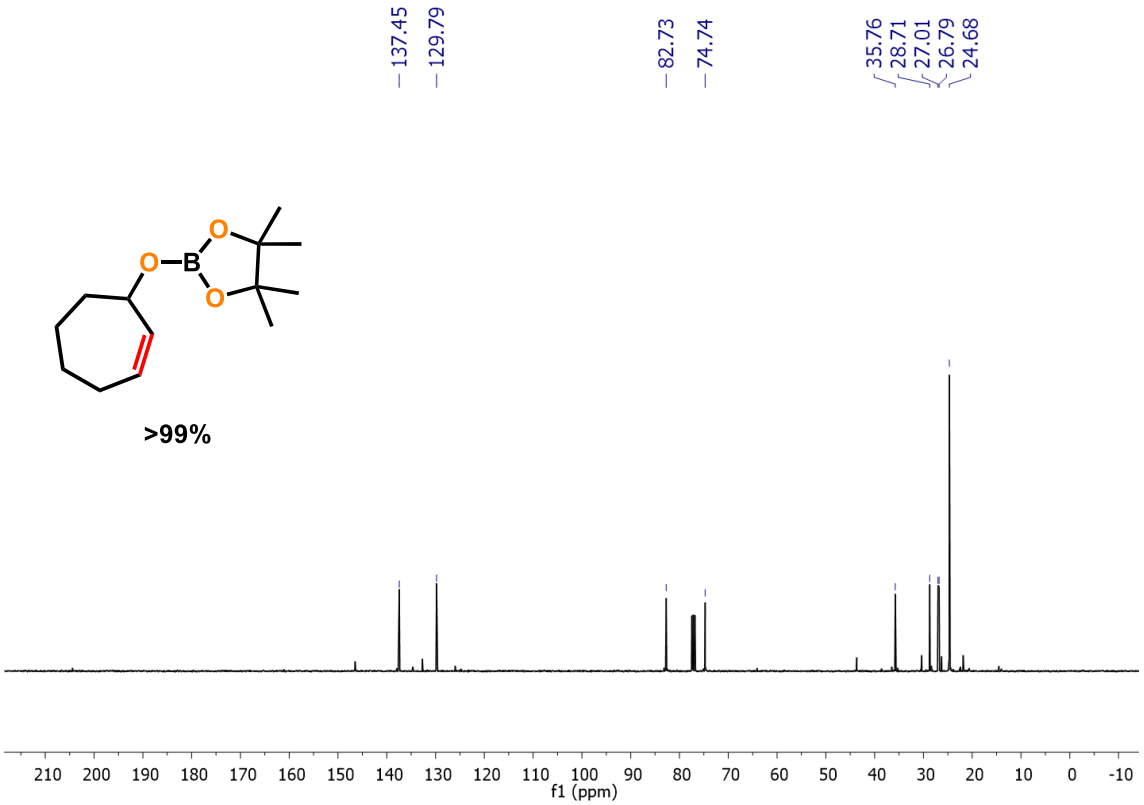

Figure S70. $^{13}C\{^{1}H\}$ NMR spectrum of **4k** (101 MHz, $CDCl_3$, 298K).

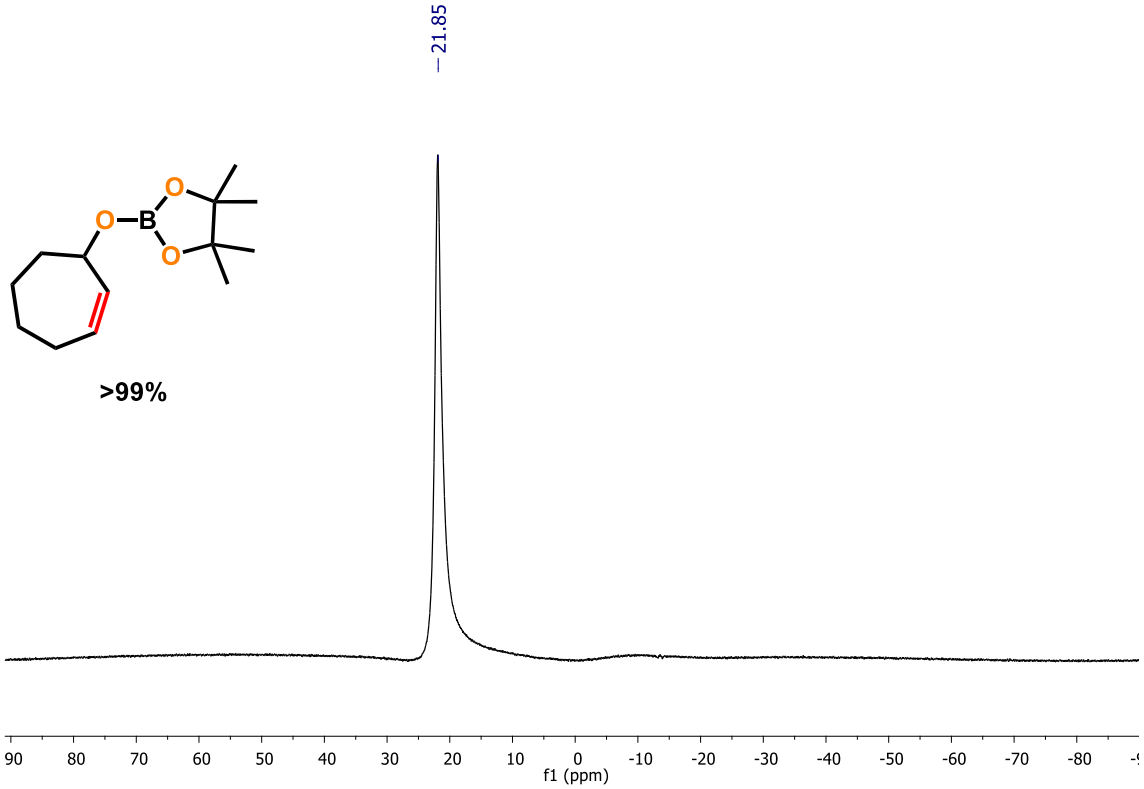

Figure S71. ^{11}B NMR spectrum of **4k** (128 MHz, $CDCl_3$, 298K).

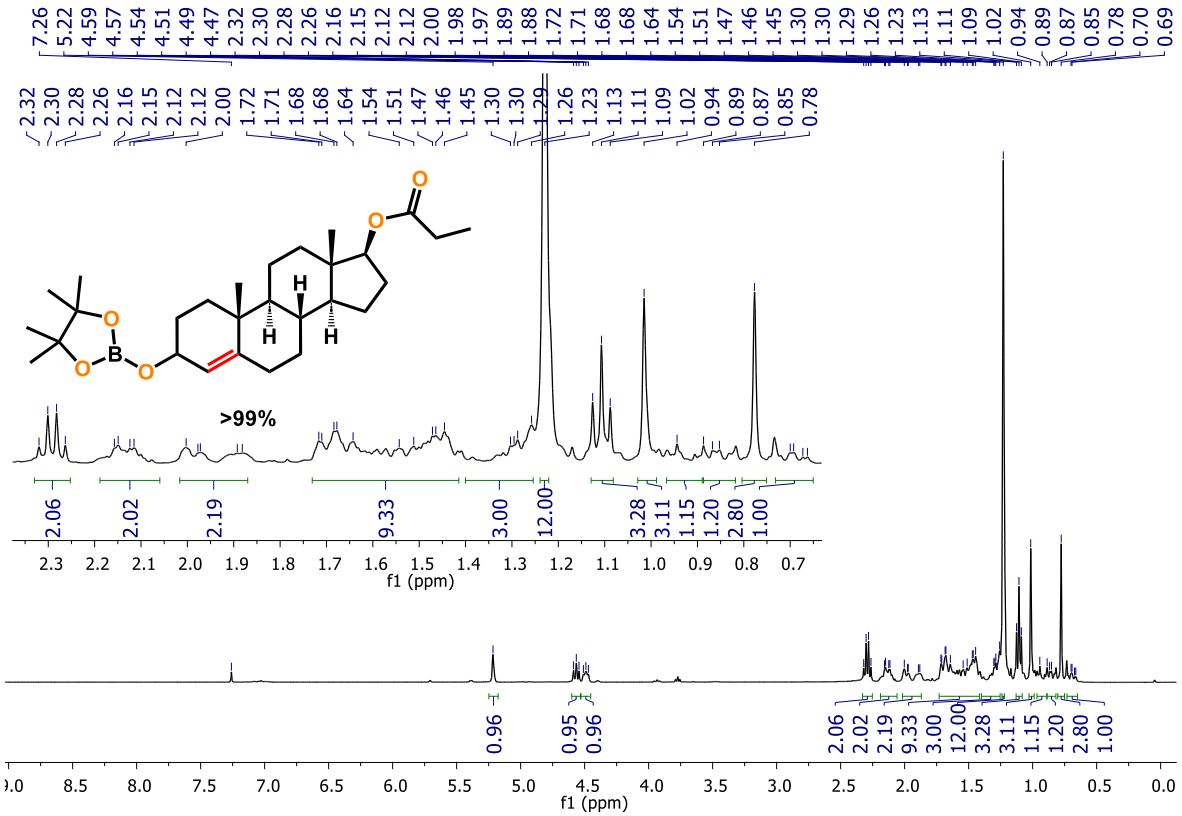

Figure S72. ^{1}H NMR spectrum of **4l** (400 MHz, $CDCl_3$, 298K).

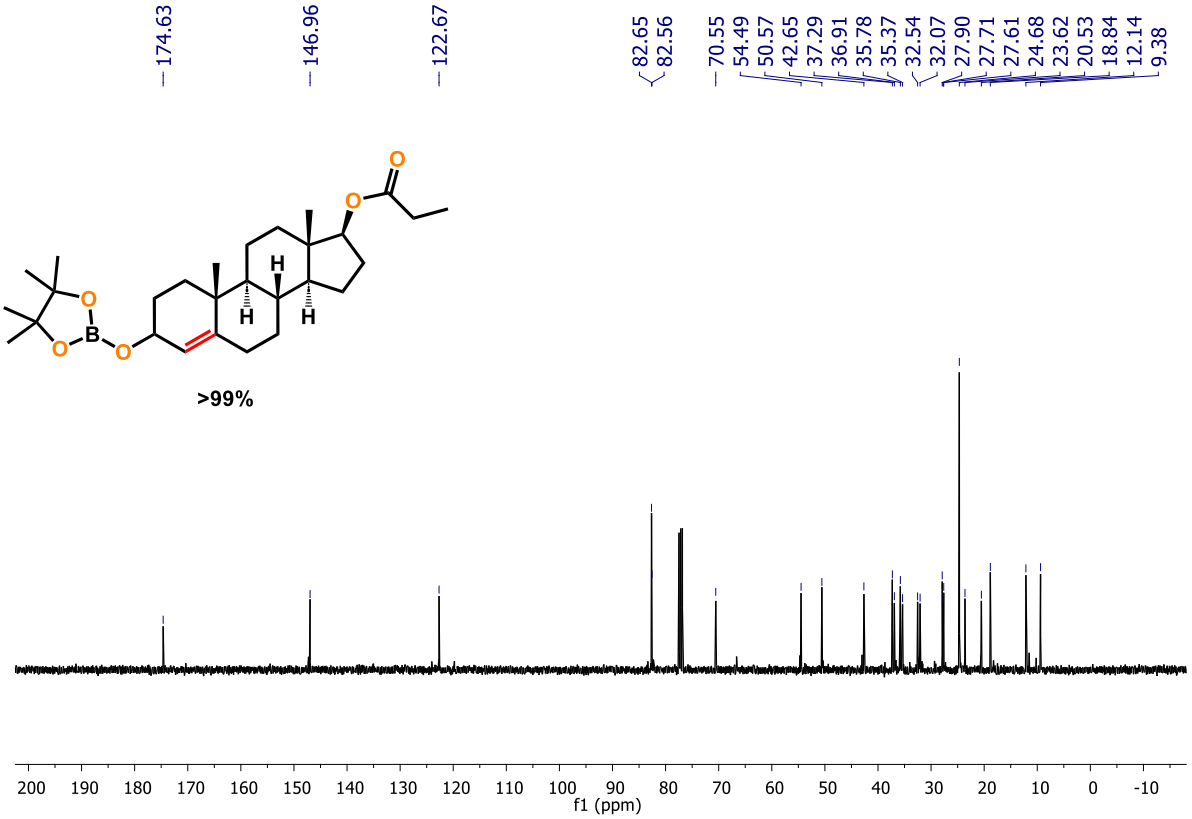

Figure S73. $^{13}C\{^{1}H\}$ NMR spectrum of **4l** (101 MHz, $CDCl_3$, 298K).

3. ^{1}H and $^{13}C\{^{1}H\}$ Spectra of Secondary Alcohols

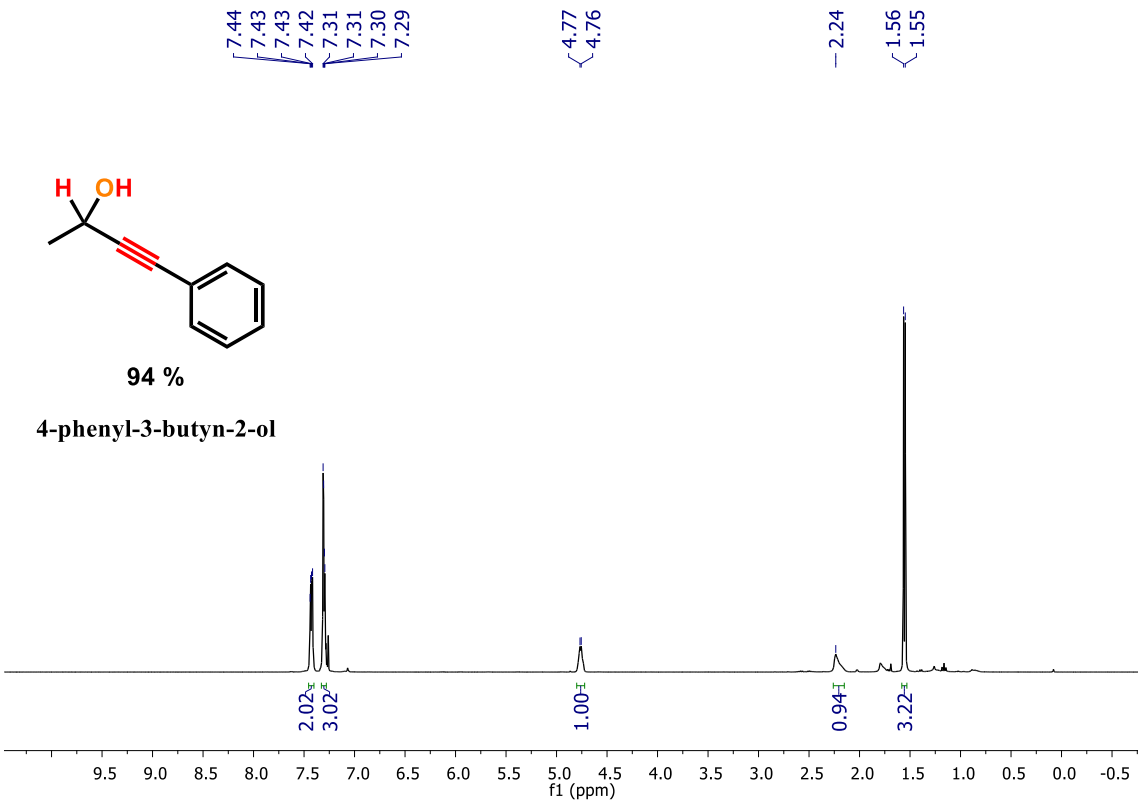

Figure S74. ^{1}H NMR spectrum of **2a'** (400 MHz, $CDCl_3$, 298K).

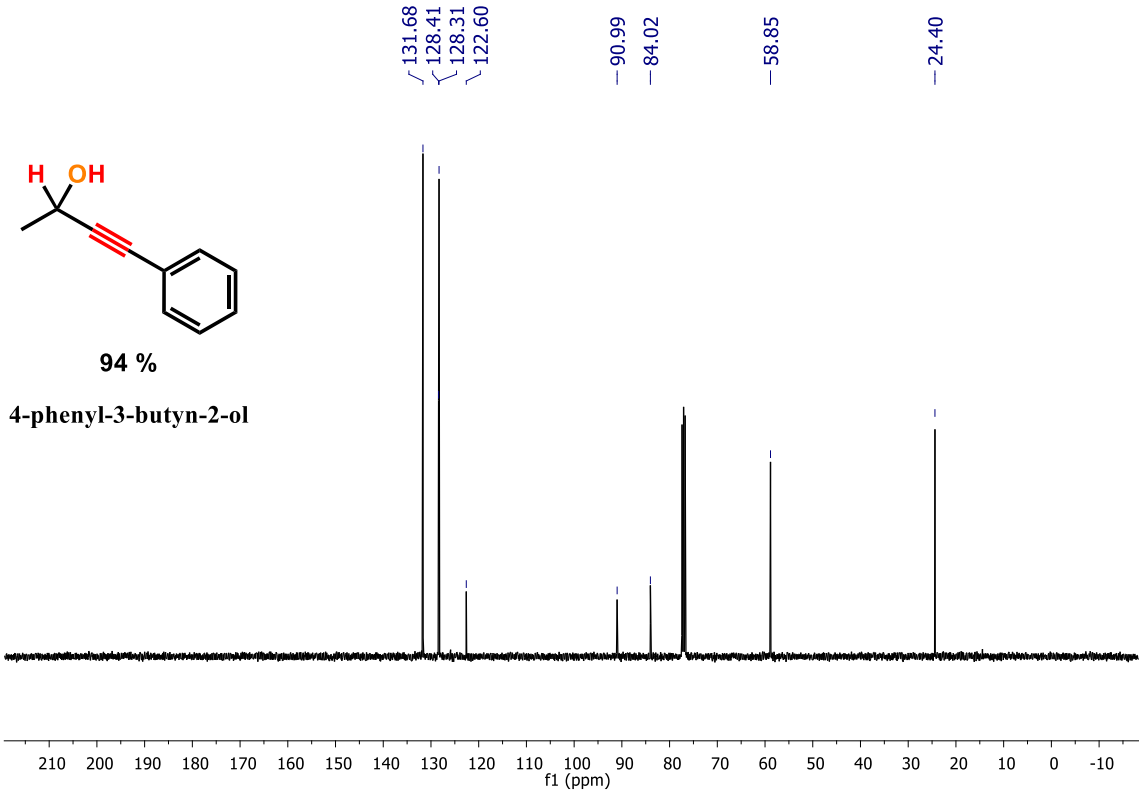

Figure S75. $^{13}C\{^{1}H\}$ NMR spectrum of **2a'** (101 MHz, $CDCl_3$, 298K).

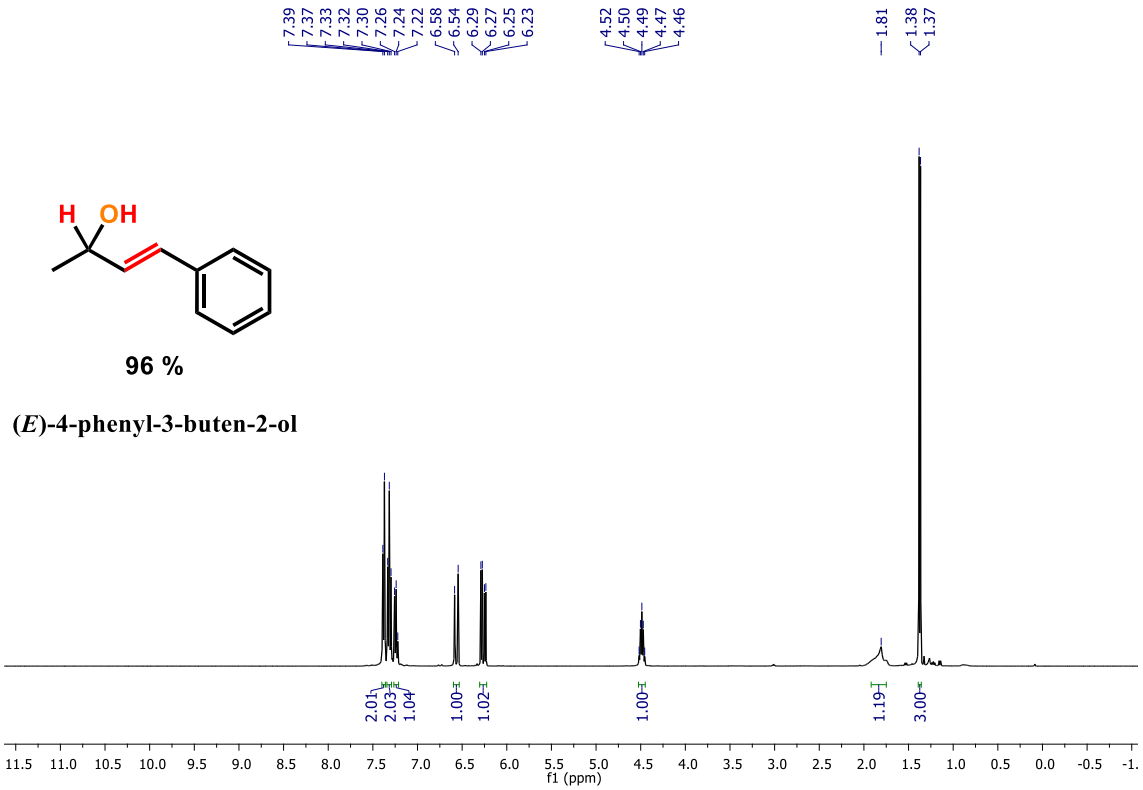

Figure S76. ^{1}H NMR spectrum of **4a'** (400 MHz, $CDCl_3$, 298K).

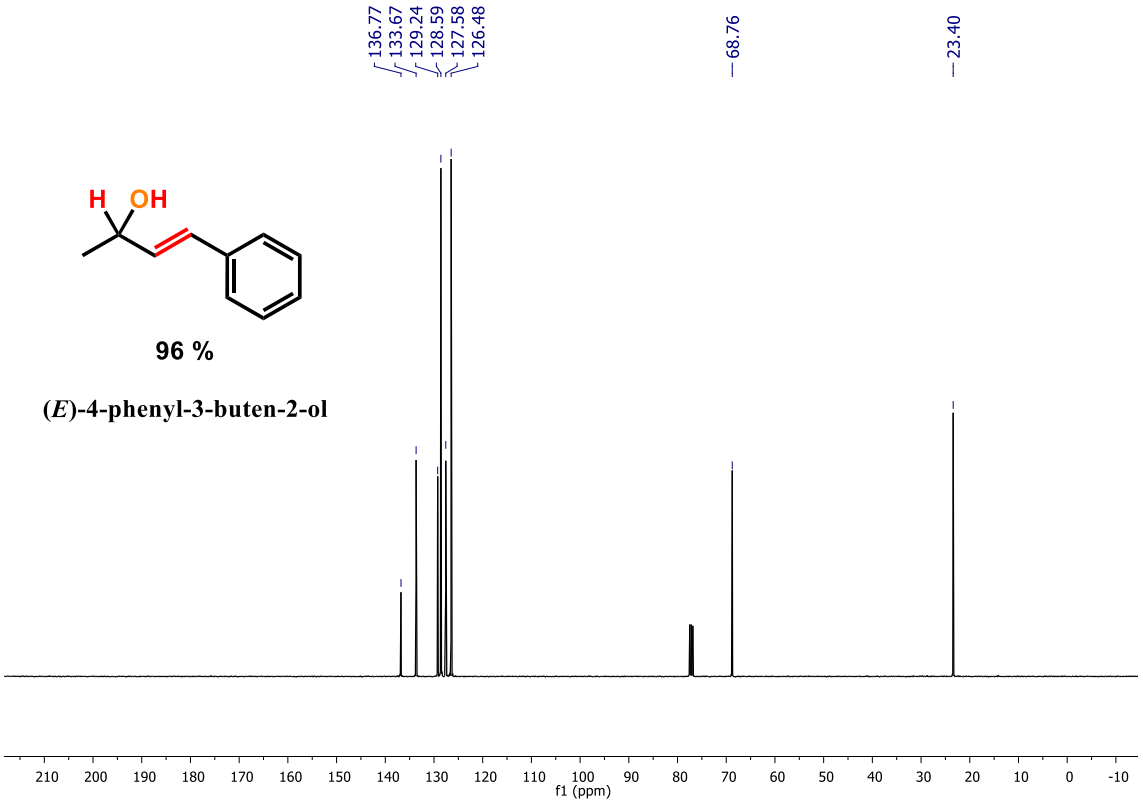

Figure S77. $^{13}C\{^{1}H\}$ NMR spectrum of **4a'** (101 MHz, $CDCl_3$, 298K).

4. ^{1}H and $^{13}C\{^{1}H\}$ Spectra for Intermolecular Chemoselectivity

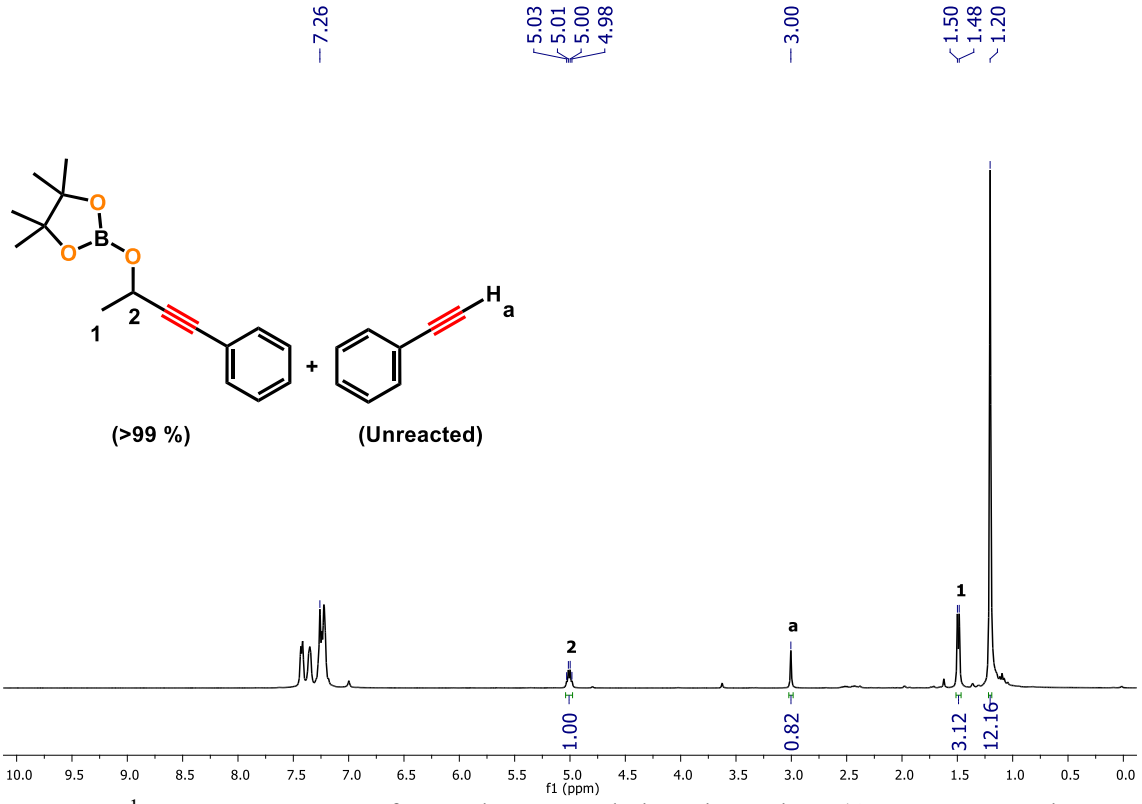

Figure S78. ^{1}H NMR spectrum of **2a** and unreacted phenylacetylene (400 MHz, $CDCl_3$, 298K).

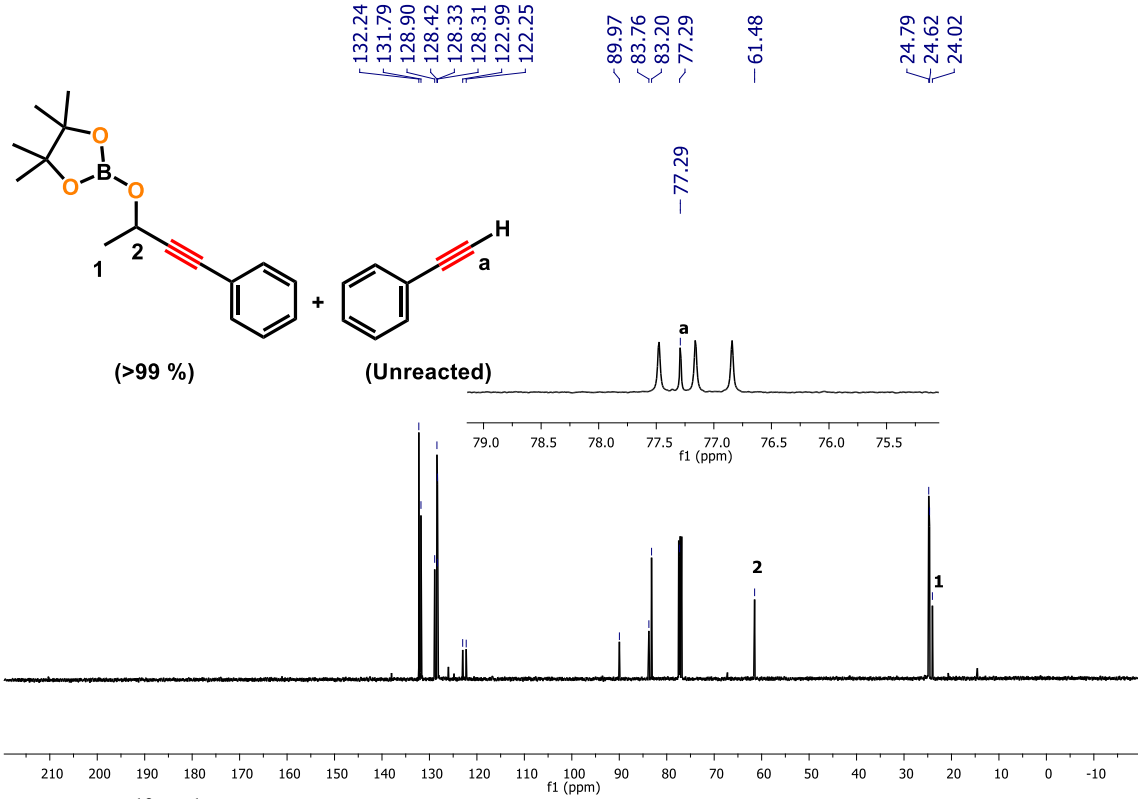

Figure S79. $^{13}C\{^{1}H\}$ NMR spectrum of **2a** and unreacted phenylacetylene (101 MHz, $CDCl_3$, 298K).

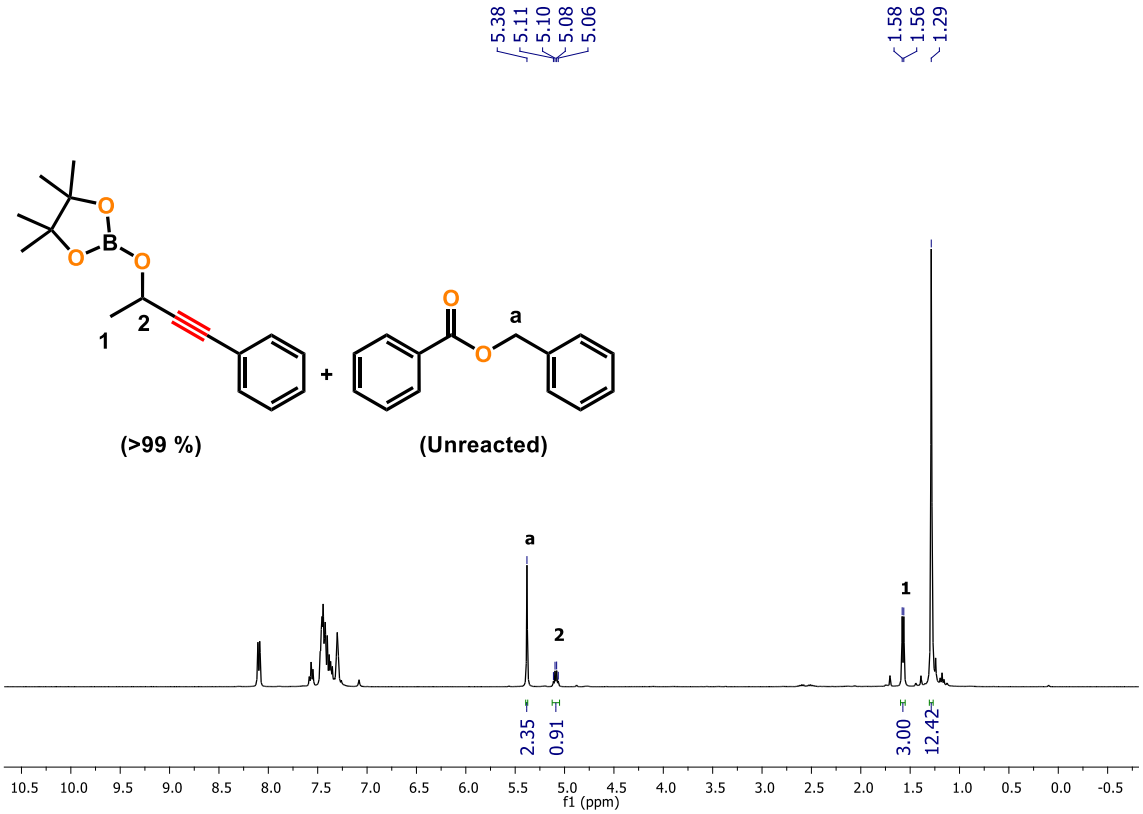

Figure S80. ^{1}H NMR spectrum of **2a** and unreacted benzyl benzoate (400 MHz, $CDCl_3$, 298K).

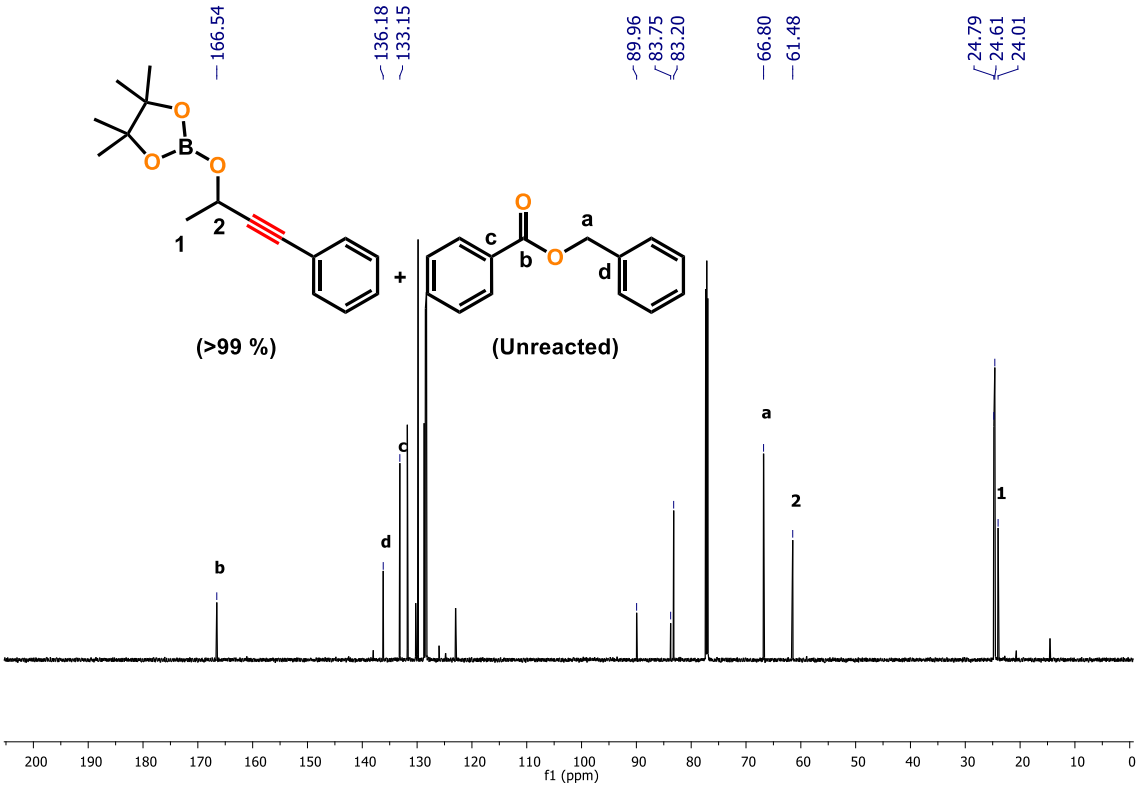

Figure S81. ^{13}C{^{1}H} NMR spectrum of **2a** and unreacted benzyl benzoate (176 MHz, $CDCl_3$, 298K).

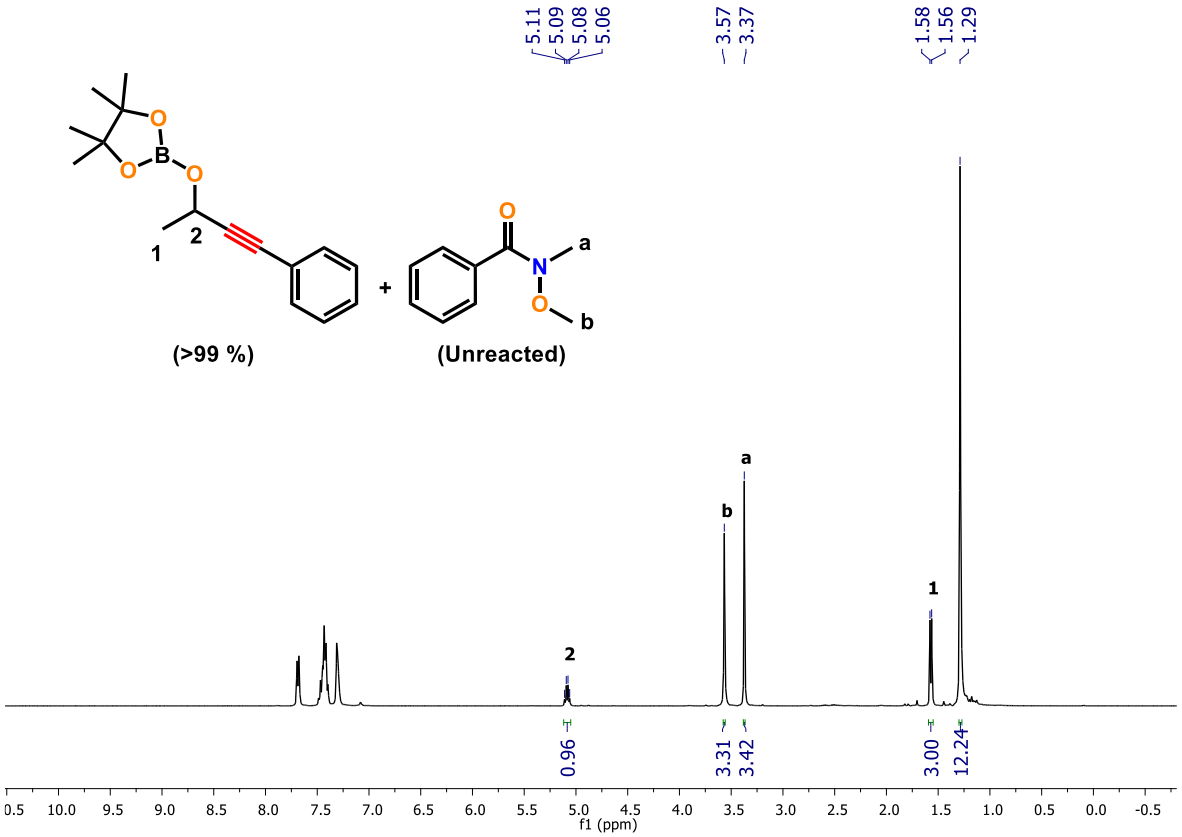

Figure S82. ^{1}H NMR spectrum of **2a** and N-methoxy-N-methylbenzamide (400 MHz, $CDCl_3$, 298K).

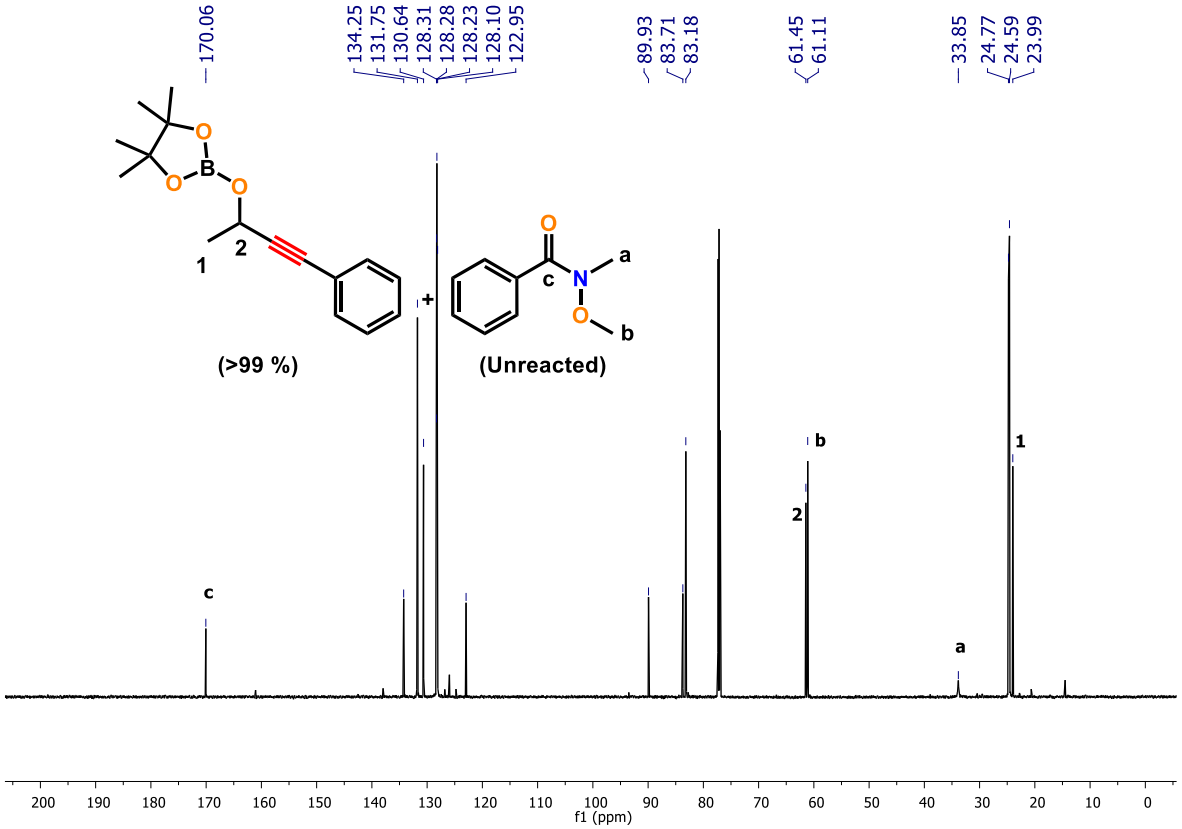

Figure S83. $^{13}C\{^{1}H\}$ NMR spectrum of **2a** and N-methoxy-N-methylbenzamide (176 MHz, $CDCl_3$, 298K).

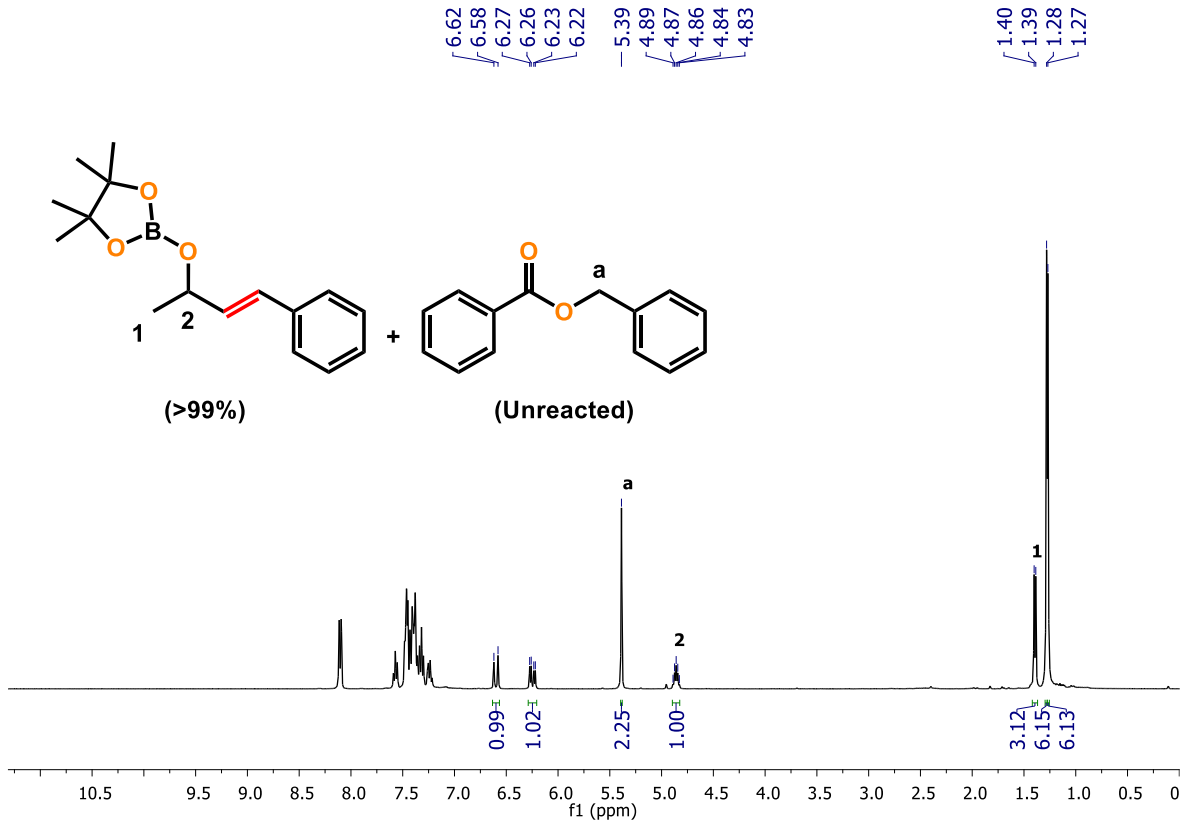

Figure S84. ^{1}H NMR spectrum of **4a** and unreacted benzyl benzoate (400 MHz, $CDCl_3$, 298K).

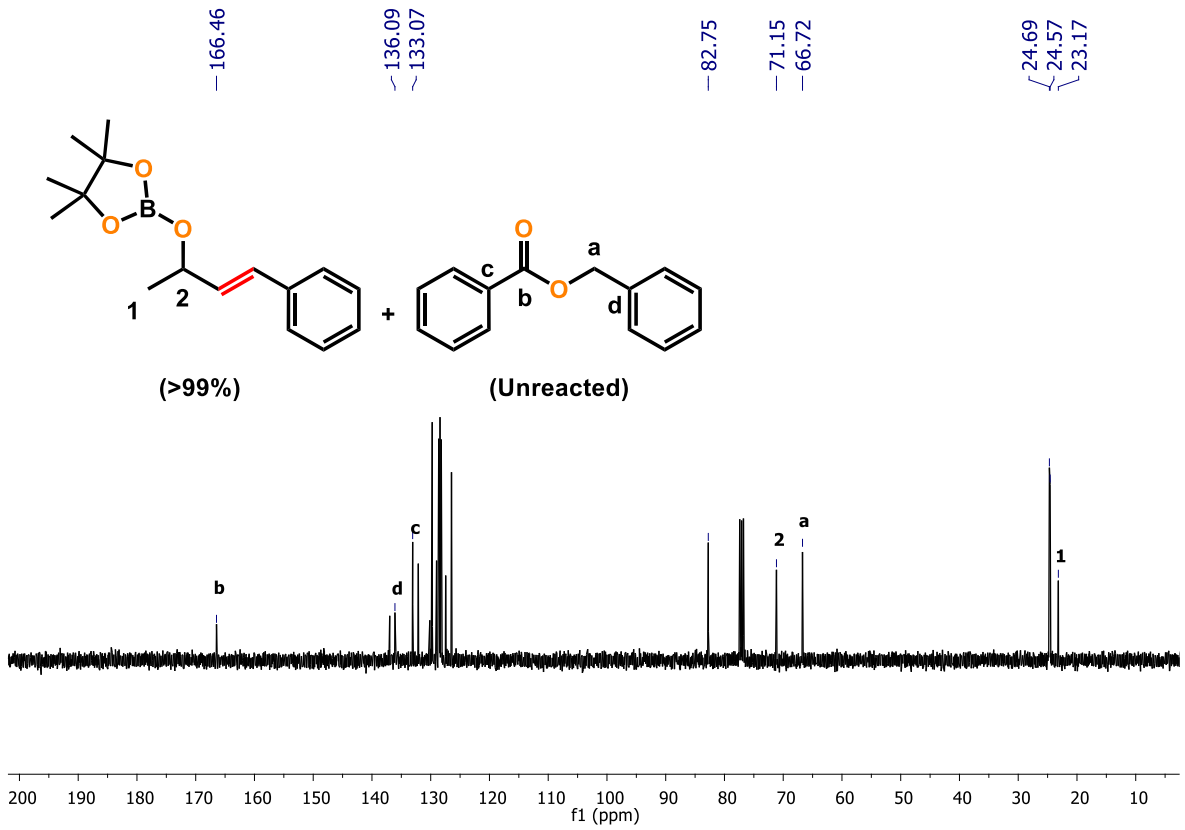

Figure S85. ^{13}C{^{1}H} NMR spectrum of **4a** and unreacted benzyl benzoate (101 MHz, $CDCl_3$, 298K).

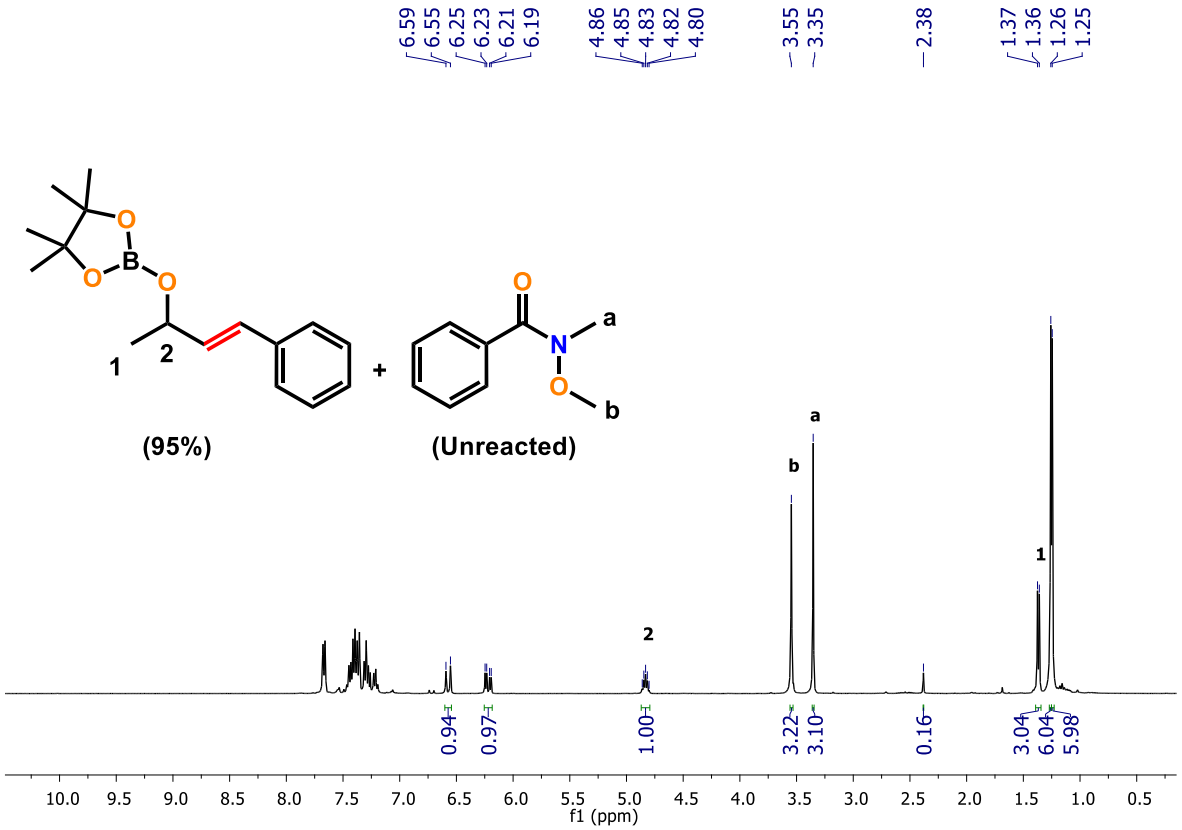

Figure S86. ^{1}H NMR spectrum of **4a** and N-methoxy-N-methylbenzamide (400 MHz, $CDCl_3$, 298K).

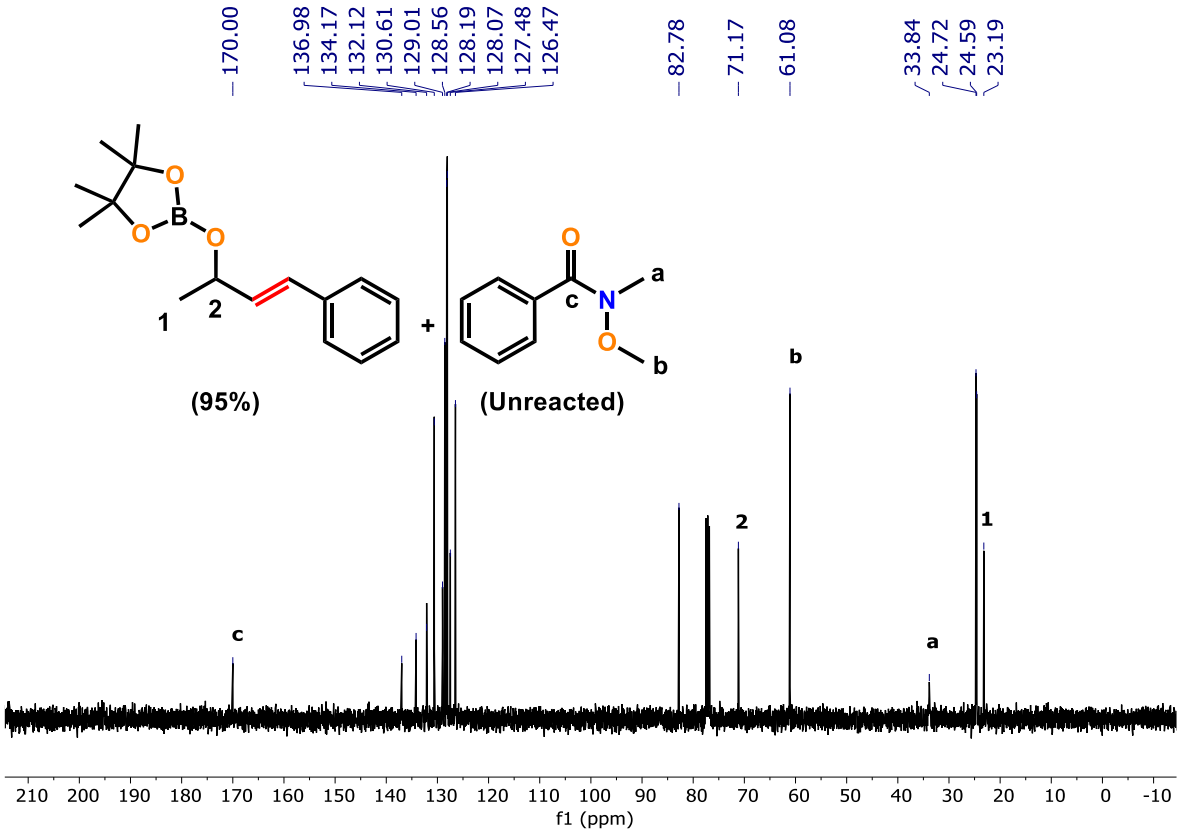

Figure S87. $^{13}C\{^{1}H\}$ NMR spectrum of **4a** and N-methoxy-N-methylbenzamide (101 MHz, $CDCl_3$, 298K).

5. Crystallographic Data of Mg-2

The single crystals of compound **Mg-2** were crystallized from C_6D_6 in a vial at room temperature as colorless blocks between 36 - 48 h inside the glovebox. The crystal data were collected on a Rigaku Oxford diffractometer with graphite-monochromated Cu-Kα radiation (λ = 1.54184 Å) at 100 K. Selected data collection parameters and other crystallographic results are summarized in Table S2. The structure was determined using direct methods employed in *ShelXT*,[1] *OleX*,[2], and refinement was carried out using least-square minimization implemented in *ShelXL*.[3] All non-hydrogen atoms were refined with anisotropic displacement parameters. Hydrogen atom positions were fixed geometrically in idealized positions and were refined using a riding model.

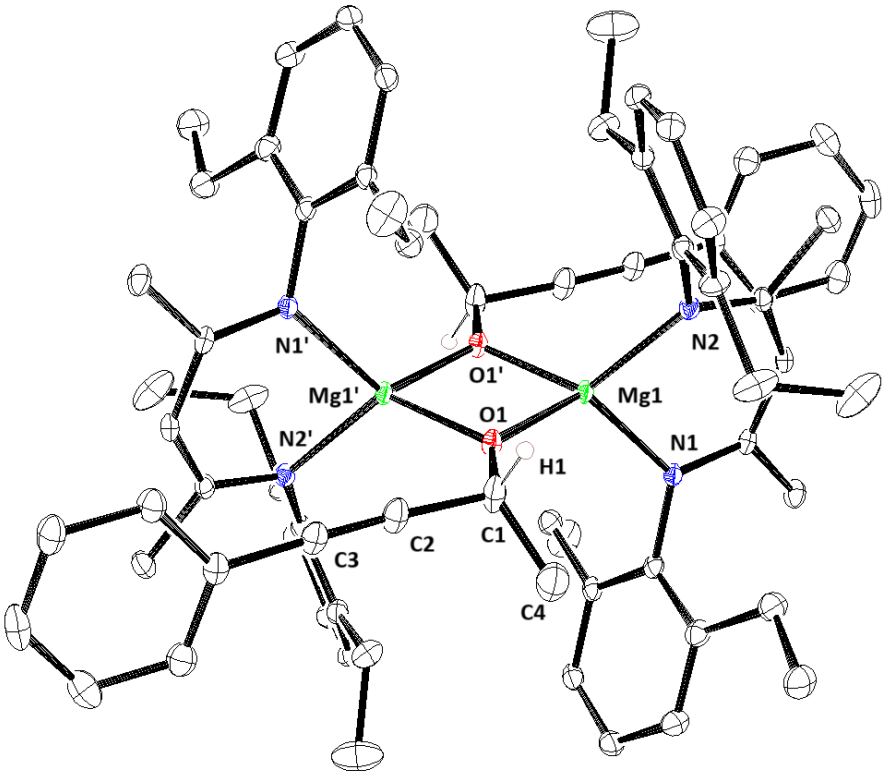

Figure S88. ORTEP representation of Mg-2 (Thermal ellipsoids are shown at 50% probability). Hydrogen atoms except H1 were omitted for clarity. The selected bond lengths (Å) and bond angles (°) are: N1-Mg1 2.0544 (13), N2-Mg1 2.0481 (12), Mg1-O1 1.9611 (11), Mg1-O1' 1.9753 (11), O1-C1 1.4096 (19), C2-C3 1.198 (2), N1-Mg1-N2 91.92 (5), N1-Mg1-O1 121.25 (5), N2-Mg1-O1 120.48 (5), Mg1-O1-Mg1' 97.53 (5), O1-Mg1-O1' 82.47 (5), Mg1-O1-C1 134.17 (9).

Table S2. Crystal data and structure refinement for **Mg-2**.

Identification code	**Mg-2**
CCDC	2494794
Empirical formula	$C_{70}H_{82.50}Mg_2N_4O_2$
Formula weight	1060.52
Temperature/K	100 K
Crystal system	triclinic
Space group	$P\bar{1}$
a/Å	10.6672(2)
b/Å	12.4690(2)
c/Å	13.4602(2)
α/°	70.3430(10)
β/°	68.974(2)
γ/°	72.7130(10)
Volume/Å^3	1541.70(5)
Z	1
ρ_{calc}g/cm^3	1.142
μ/mm^{-1}	0.705
F(000)	570.0
Crystal size/mm^3	0.2 × 0.18 × 0.17
Radiation	CuKα (λ = 1.54184)
2Θ range for data collection/°	7.282 to 150.512
Index ranges	$-12 \leq h \leq 13$, $-15 \leq k \leq 15$, $-16 \leq l \leq 16$
Reflections collected	29965
Independent reflections	6263 [R_{int} = 0.0436, R_{sigma} = 0.0255]
Data/restraints/parameters	6263/0/387
Goodness-of-fit on F^2	1.077
Final R indexes [I>=2σ (I)]	R_1 = 0.0481, wR_2 = 0.1297
Final R indexes [all data]	R_1 = 0.0502, wR_2 = 0.1313
Largest diff. peak/hole / e Å^{-3}	0.44/-0.32

References

1. G. Sheldrick, *Acta Crystallogr., A*, 2015, **71**, 3-8.
2. O. V. Dolomanov, L. J. Bourhis, R. J. Gildea, J. A. K. Howard and H. Puschmann, *J. Appl. Crystallogr.*, 2009, **42**, 339-341.
3. G. Sheldrick, *Acta Crystallogr., C*, 2015, **71**, 3-8.